ABSTRACT

Title of Thesis: ON-ORBIT SPACE SHUTTLE INSPECTION SYSTEM UTILIZING AN EXTENDABLE BOOM

Sadie Kathleen Michael, Master of Science, 2004

Thesis Directed By: Associate Professor David Akin
Department of Aerospace Engineering

An extension to the existing shuttle remote manipulator system (SRMS) on the space shuttle orbiter was developed to provide on-orbit inspection capabilities to survey the thermal protection system (TPS). Following the space shuttle *Columbia* tragedy, the ability to adequately inspect the orbiter TPS is required for every flight. The inspection system proposed here entails the design of a deployable boom extension to the SRMS that meets the system kinematic and structural requirements. Aiming for a compact and maneuverable system, an extendable boom was designed as an alternative to the boom system planned by NASA. Using requirements derived from of the inspection task, a preliminary design for the boom was developed using a lenticular extendable boom. The inspection system was designed to be compatible with existing orbiter systems while minimizing risk to the shuttle. This project confirmed the feasibility of an on-orbit extendable boom-based inspection system for the orbiter TPS.

ON-ORBIT SPACE SHUTTLE INSPECTION SYSTEM UTILIZING AN EXTENDABLE BOOM

By

Sadie Kathleen Michael

Thesis submitted to the Faculty of the Graduate School of the
University of Maryland, College Park, in partial fulfillment
of the requirements for the degree of
Master of Science
2004

Advisory Committee:

Associate Professor David Akin, Chair
Visiting Associate Professor Mary Bowden
Professor Anthony Vizzini

Dedication

In memory of the STS-107 *Columbia* astronauts:

Rick D. Husband, *Commander*

William C. McCool, *Pilot*

Michael P. Anderson, *Payload Commander*

David M. Brown, *Mission Specialist*

Kalpana Chawla, *Mission Specialist*

Laurel Blair Salton Clark, *Mission Specialist*

Ilan Ramon, *Payload Specialist*

for their heroic sacrifice.

Acknowledgements

I would like to thank my research advisors and thesis committee members: Dr. David Akin, Dr. Mary Bowden, and Dr. Anthony Vizzini, who have dedicated their time and effort towards this project. Thanks are extended to Dr. Akin for serving as chair of my thesis committee and for sharing my passion for the space program. To Dr. Bowden, I would like to thank you for the numerous hours you have spent with me discussing this project. I am grateful to Dr. Vizzini for introducing me to the wonderful world of aerospace engineering and composite materials. I enjoyed the years I spent working with composites in your laboratory on campus as an undergraduate student as well as the guidance you gave me as a graduate student. I would also like to thank Matthew Fox for his support throughout the years. I attribute many of my practical engineering skills to the hands-on training I received from Matt while working at the composites laboratory. Paul Wienhold also deserves to be recognized for his composites expertise relating to this project.

Funding for this project came from several fellowships and organizations. The Tau Beta Pi Astronauts fellowship awarded in memory of the *Columbia* commander, Rick Husband, funded the final stage of this project. The Minta Martin Fellowship from A. James Clark School of Engineering at the University of Maryland, College Park, funded the majority of this research and coursework related to this project during the past year. Funding for an earlier related project came from the Women in Engineering Fellowship program and the Composites Research Laboratory at the University of Maryland. Through this project, the idea of using an extendable boom for orbiter inspection was born. I would also like to thank the Society for the

Advancement of Material and Process Engineering (SAMPE) for their sponsorship over the past two years to present my research in the University Research Symposium at the annual international SAMPE conference held in Long Beach, California.

I would also like to recognize two teachers, who have helped me discover my talents. Through origami paper folding, my fourth grade teacher, Mr. Arlie Albeck, helped me find my confidence. Mr. Albeck, I thank you for keeping in touch with me all of these years. You will always have a special place in my heart. Secondly, I owe my steadfast determination to my high school calculus teacher, Ms. Linda Barnes. I will not soon forget the countless hours I spent solving calculus problems on the classroom chalkboard to the point where I would dream about math equations each night. Through this experience, I learned to never give up and to keep working towards a solution. This philosophy kept me focused on my goals and helped me complete this thesis research project over the past year.

My family has played an integral role in my graduate studies. I would like to thank my parents, Kurt and Kathleen Michael, for their support. I could always count on my parents to be there for me when I needed them. To my siblings Mary and David, I would like to thank you for putting up with my obsession with the space program for all of these years.

I am extremely fortunate to have my fiancé, Stephen Gant, who has given me nothing but unconditional love and support throughout the past year. I would like to thank Steve for spending countless hours listening to me babble on about my research, while understanding very little of it over the phone. This thesis is informally dedicated to him as a thank you for making me the person I am today.

Lastly, I would like to thank my grandparents, Donald and Cleone Michael for giving me the gift of space for my thirteenth birthday. After the five days I spent in the Future Astronaut Training Program in Hutchinson, Kansas, my life changed forever. I began a life obsession with the space program that has guided me to where I am today. I often catch myself looking up towards the stars hoping to one day fly amongst them. Grandma and grandpa, thank you for showing me the stars.

As I begin a new phase of my life, I would like to leave you with my favorite quote from the father of modern rocketry, Robert Goddard, “It is difficult to say what is impossible, for the dream of yesterday is the hope of today and the reality of tomorrow.” I would like to thank my family, friends, teachers, and co-workers again for teaching me not to be afraid to dream big.

Table of Contents

List of Tables

List of Figures

List of Acronyms and Abbreviations

CAIB	*Columbia* Accident Investigation Board
CTM	collapsible tube mast
D-H	Denavit-Hartenberg
DLR	German Aerospace Center
DOF	degree(s) of freedom
EB	extendable boom
EE	end effector
EGF	electrical grapple fixture
EP	SRMS elbow pitch joint
ESA	European Space Agency
EVA	extra-vehicular activity
FEM	finite element modeling
GF	grapple fixture
ISS	International Space Station
NASA	National Aeronautics and Space Administration
OBAS	orbiter body axis system
OBSS	orbiter boom sensor system
ORAS	orbiter rotational axis system
RCC	reinforced carbon-carbon
RTF	return to flight
SP	SRMS shoulder pitch joint

SRMS	shuttle remote manipulator system
SSRMS	space station remote manipulator system
SY	SRMS shoulder yaw joint
TML	total mass loss
TPS	thermal protection system
VCM	volatile condensable material
WLE	wing leading edge
WP	SRMS wrist pitch joint
WR	SRMS wrist roll joint
WY	SRMS wrist yaw joint

Measurement Units

°C	degree Celsius
cm	centimeter
deg or °	degree
°F	degree Fahrenheit
ft	foot
hr	hour
in	inch
kg	kilogram
lb	pound-force
lb_m	pound-mass
m	meter

psi	pounds per square inch
s	second
slug	English gravitational mass unit

List of Symbols

A	cross-sectional area
a	center offset
a_i	link length (D-H parameter)
a_{SRMS}	SRMS de/acceleration applied to boom
A(x,y)	equation representing flange segment of boom quarter-profile
b	flange width
b_a	flange bond width
B(x,y)	equation representing fillet segment of boom quarter-profile
c	expanded width
C(x,y)	equation representing curve segment of boom quarter-profile
d	tangential point between fillet and curve segments
d_i	link offset (D-H parameter)
E	elastic (Young's) modulus
f	distributed boom load
G	shear modulus
H	flattened thickness
h	expanded thickness
I	area moment of inertia
J	polar moment of inertia
L	total boom length
M_{tip}	tip mass

m	boom mass per length
P	boom tip load
P_{cr}	critical axial buckling load
${}^{OBAS}\vec{p}_{tip}$	position vector of boom tip in OBAS coordinates
$\vec{q}$	joint parameter vector
R	shape radius
r	fillet radius
${}^{ORAS}R_{tip}$	orientation matrix for boom tip in ORAS coordinates
T	internal torque
t	profile thickness
t_a	flange bond thickness
t_{SRMS}	SRMS stopping time
u	boom tip deflection in x-direction
v	boom tip deflection in y-direction
v_{SRMS}	maximum SRMS velocity
w	flattened width
${}^{OBAS}(X,Y,Z)_{tip}$	position of boom tip in OBAS coordinates
x,y,z	local boom coordinates
α_i	link twist (D-H parameter)
ε_{max}	maximum strain
ϕ	boom twist angle
ϕ_R	shape angle

ϕ_r	fillet angle
λ	natural frequency
θ_i	joint angle (D-H parameter)
ρ_{min}	minimum boom stowage radius

Chapter 1: Introduction

After the loss of NASA's space shuttle orbiter, *Columbia*, and its crew on February 1, 2003, efforts have focused on safely returning the vehicle to flight. Following the tragedy, the importance of developing an on-orbit inspection system capable of viewing all external surfaces of the orbiter thermal protection system (TPS) became a focal point. This study was aimed at examining the feasibility of a deployable boom-based inspection system capable of surveying the orbiter TPS. First, the *Columbia* accident is discussed along with its cause, followed by subsequent recommendations for returning to flight. The focus of this research was to select and develop an orbiter inspection system. Future research efforts may continue to develop the system design through further definition of hardware possibly extending the system capabilities to include repair tasks. Some methodologies used to meet the inspection requirements are presented, focusing on deployable boom systems. A basic overview of deployable booms appears herein, ultimately leading to the selection of a closed-section extendable boom.

1.1 *Columbia* Accident and Investigation

On January 16, 2003, the space shuttle, *Columbia*, was launched from Cape Canaveral, Florida. At the end of the mission, sixteen days later, the orbiter broke up during atmospheric re-entry killing all seven astronauts onboard. The *Columbia* Accident Investigation Board (CAIB), established to find the cause of the disaster, concluded that the *Columbia* orbiter suffered structural damage to the left wing leading edge (WLE). NASA launch-site footage of the shuttle launch showed that a

piece of insulation foam separated from the external tank of the shuttle shortly after launch. This piece of insulation foam collided with the left WLE reinforced carbon-carbon (RCC) paneling of the orbiter [1]. Consequently, it is hypothesized that this foam impact created a hole with an approximate diameter of 6in to 10in (15cm to 25cm) [1]. This hole left the wing structure vulnerable to the hot gases encountered during atmospheric re-entry subsequently destroying the orbiter electronics and structural members causing it to become unstable and uncontrollable, ultimately leading to its destruction.

Due to the poor resolution of the launch film and the limited viewing capabilities on-board the orbiter, the extent of the damage to the RCC paneling was unknown. Insulation foam impacts on the orbiter TPS during launch were an almost routine occurrence; however, none of these impacts resulted in damage to the extent that was suffered by *Columbia*. The piece of insulation foam that collided with *Columbia* was unusually large and it happened to strike a particularly sensitive part of the wing. Due to a false sense of security resulting from numerous previously successful debris-strike missions, NASA management was unaware of the life-threatening damage that had occurred. The severity of the impact became apparent during the investigation when the CAIB replicated the impact scenario and found that a piece of insulation foam fired at the same momentum in a variety of possible trajectories resulted in significant damage to the RCC flight hardware panels. Damage observed in the panels tested included a 16in by 17in (41cm by 43cm) hole and 10in (25cm) long cracks [1].

The extent and size of the damage to *Columbia* resulting from the insulation foam impact will never be known. Efforts to obtain enhanced images of the orbiter from space were stifled by NASA management and the capability to image the suspected impact region from the orbiter was insufficient. For example, images taken from inside the orbiter were unable to view the left WLE where the impact had occurred because it was obscured by the orbiter payload bay doors. *Columbia* did not have a shuttle remote manipulator system (SRMS) onboard, so attempting to view the damaged region obstructed by the payload bay doors using the robotic arm was not an option. The damage probably could have been observed and assessed via an unscheduled extra-vehicular activity (EVA) performed by the crew; however, at the time this option presented too much risk to the crew, who were unaware of the consequences of the panel damage. If damage had been found, it is unknown if a rescue mission could have been set in motion in time to save the *Columbia* crew. Attempts to repair the damage using materials found onboard the orbiter was considered too risky with no guarantee of a safe re-entry. Alternatively, the International Space Station (ISS) could not provide a safe haven for the crew because *Columbia* was in a different orbit and it lacked the necessary fuel to reach the ISS. Furthermore, the orbiter was not equipped to dock with the ISS because the station docking mechanism had not been installed in the payload bay due to the scientific experiment laboratory that was onboard.

1.2 Inspection Recommendations and Methodologies

As a result of the investigation, the CAIB made several recommendations for NASA to consider before returning the space shuttle to flight. Among these

recommendations, the CAIB requested that NASA "develop a comprehensive autonomous (independent of Station) inspection and repair capability to cover the widest possible range of damage scenarios" [1]. This recommendation, CAIB recommendation 6.4-1, sets forth the requirements for returning the shuttle to flight with regard to on-orbit inspection and repair procedures. In sum, on-orbit inspection strategies must be able to survey all regions of the orbiter TPS at the resolution requirements set by NASA.

Inspection and repair of the orbiter TPS is one of the most challenging and extensive return to flight tasks. In approaching this problem, the existing orbiter systems were first evaluated for their capability to meet the inspection requirements. Relying on current orbiter systems, the orbiter TPS cannot be adequately inspected without the aid of the ISS. This restricts all remaining shuttles to ISS missions; consequently, non-ISS missions such as the servicing of the Hubble Space Telescope can no longer be performed by the orbiter. Additionally, if the orbiter fails to achieve the correct orbit, fails to dock successfully, or is damaged during or after undocking with the ISS, the current inspection capabilities of the orbiter alone do not meet the established criteria [2]. To prepare for these scenarios, a new inspection system that meets the inspection criteria must be devised to operate independently of the ISS. In the interest of returning the shuttle to flight as soon as possible, the new inspection system should utilize and impose minimal limitations on the existing orbiter systems.

Inspection system methodologies range from creating extensions to the orbiter robotic manipulator, free-flying robots, erectable trusses, and jetpack-assisted space walks. The NASA return to flight (RTF) plan incorporates several different inspection

methodologies to provide a comprehensive system capable of meeting the inspection and repair requirements [3]. The NASA plan relies heavily on the ISS; therefore, all remaining shuttle flights are scheduled to perform ISS missions until the station assembly is complete, at which point the shuttle will be retired from flight. As a result, NASA decided to focus on ISS resources in the development of orbiter TPS inspection and repair methodologies. Additional risks associated with creating and implementing an autonomous inspection capability independent of the ISS was considered unnecessary; however, NASA plans to continue analyzing the merit of different methodologies, which addresses these scenarios. For NASA's explanations of the identified risks associated with non-ISS missions, please see reference [3].

To avoid developing new hardware for additional inspection and repair systems, NASA is working to mitigate risks associated with scenarios that would leave the ISS capabilities unavailable. Near-term plans to mitigate TPS risks are [3]:

- to make modifications to the space shuttle vehicle to eliminate liberation of critical debris;
- to employ improved ground and vehicle-based cameras and impact sensors for debris detections and damage assessment;
- to perform on-orbit TPS surveys using the SRMS and space station remote manipulator system (SSRMS) cameras;
- to enlist ISS crew to make observations during shuttle approach and docking;
- to develop techniques for extra-vehicular activity (EVA)-based TPS tile and RCC repair tasks.

Through these activities, the probability of damage occurring to the orbiter TPS is decreased. Furthermore, these objectives increase the probability that if damage does occur, it can be promptly detected and its consequences can be mitigated in flight.

The NASA RTF inspection plan can be divided into three phases. The first phase occurs after launch during the beginning stages of the rendezvous procedure between the orbiter and the ISS. During this phase, the most critical areas of the orbiter TPS, the RCC WLE and nose cap, are scanned by the Orbiter Boom Sensor System (OBSS). The OBSS is composed of a rigid fixed-boom extension to the SRMS made from two SRMS spare arm booms with a camera and sensor package located at one end of the boom. This boom has two grapple fixtures, so it can be grasped at two locations as a means of adjusting the reach capability of the system. This boom will be stowed on the starboard sill of the payload bay, similarly to the SRMS itself, which is on the port sill. This boom system will also be used to inspect and measure the depth of any critical TPS damage that may have been detected by other inspection methods. The OBSS is also planned to have the capability to support an EVA crewmember if repairs are needed.

The next phase of the NASA RTF inspection plan occurs as the orbiter nears the ISS during the rendezvous maneuver. The orbiter performs a turnabout maneuver to orient the orbiter underbelly towards the ISS, so station crewmembers can digitally image the orbiter TPS surface from approximately 600ft (180m). The rendezvous and docking procedure was modified to facilitate this phase of the inspection plan. As the orbiter continues its rendezvous and docking procedure with the ISS, the station crew

continues taking digital images and making observations to assess the condition of the orbiter TPS.

The last phase of the NASA RTF plan takes place after the orbiter is docked to the ISS. This part of the inspection plan includes further examination of the orbiter TPS using both the shuttle and space station robotic manipulators (SRMS and SSRMS). After docking with ISS, the OBSS will be used to further inspect any suspect areas on the orbiter TPS. Currently, TPS repair strategies planned by NASA must be carried out at the ISS, where the SSRMS can be used to stabilize an EVA crewperson. As the ISS construction progresses, the accessibility of the SSRMS will be limited by a Japanese module. Approximately halfway through the remaining ISS construction missions, the SSRMS will become unusable for inspection tasks; therefore, a system that can fully inspect the orbiter in addition to the ISS-based imagery is highly desirable.

The SRMS alone cannot adequately meet the inspection criteria laid out by NASA [2]; therefore, an extension to the SRMS is one way to provide the necessary reach capability. The reach capability of the SRMS is dependent on the location and orientation of its end effector. For detailed diagrams of the SRMS reach envelopes see reference [4]. The addition of a boom to the existing SRMS was selected as the basis of the on-orbit inspection system due to its simplicity compared to designing an entirely new system. NASA is developing the OBSS, an instrumented boom extension that relies on the orbiter robotic manipulator for maneuverability [3]. Likewise, this research focused on a variation of the NASA boom extension concept, addressing the feasibility of using a deployment-based inspection system.

A simple method to provide the required extension to the SRMS is to use a fixed-boom. In essence, the NASA RTF OBSS design is a fixed-boom concept. This type of boom is rigid and therefore its length cannot be adjusted. It has good structural properties; however, it is difficult to maneuver and can be massive. To inspect using this type of boom on orbit, the SRMS will grab the fixed-boom and survey the orbiter TPS using the camera and sensor package located at the tip of the boom. To conduct the TPS survey, the SRMS is positioned such that the tip of fixed-boom is brought across the orbiter surface. Figure 1-1 shows a line representing the location of the boom tip as the fixed-boom system is used to inspect the orbiter TPS. One major concern with the fixed-boom inspection system is avoiding contact with the orbiter as the SRMS with the fixed-boom attachment takes on many different configurations. Although this type of boom extension allows for increased reach, alternatively, a deployable boom extension may alleviate many of the logistical concerns associated with a fixed boom system.

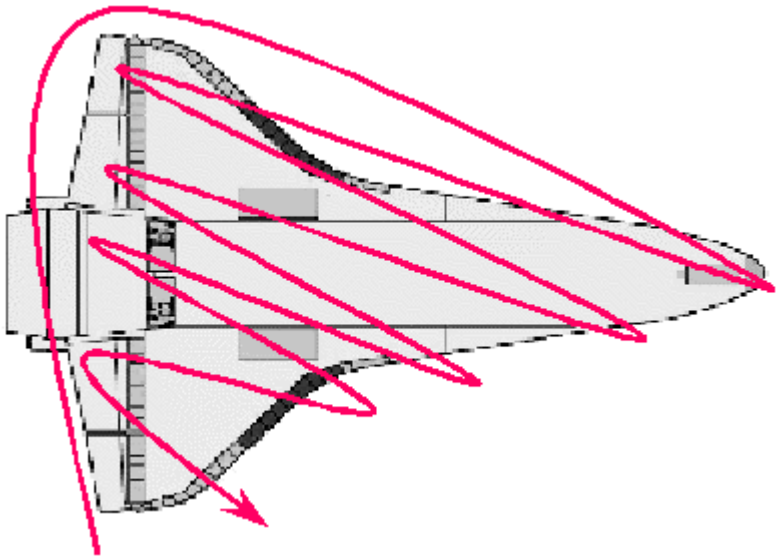

Figure 1-1: Fixed-boom inspection scheme

The idea behind the SRMS extension is that it will provide full inspection capability without the aid of ISS. Although this particular inspection system is not currently under development at NASA, it may serve as an alternative to the OBSS or as a supplemental inspection system. This project aims to address the possibility that the ISS cannot be relied upon for inspection purposes.

1.3 Deployable Boom Technology

Aiming for a compact maneuverable system, a deployable-boom system was studied as an alternative to the fixed-boom system planned by NASA. Deployable booms are a type of transformable beam-like structures that are capable of executing large extensions and retractions in an autonomous way. In most cases, the boom configuration changes between a compact, packaged state and a large, deployed state. The boom transforms between these two configurations through deployment extension and retraction. This transformation process should be reliable and should not cause damage to the boom structure. The current trend is towards simpler deployable structures that are cheaper and more reliable. Fixed booms do not have the ability to transform through deployment action.

In general, deployable booms have reduced overall mass and small packaged volumes for launch. Reducing payload mass and volume, allows flexibility for the shuttle payload, imposing less restrictions on planned ISS assembly missions. In particular, the reduced volume and possibly mass of the deployable system could prevent the need for additional shuttle missions to the ISS due to the lost payload capacity.

Deployment is essential to the success of a deployable boom-based inspection system; therefore, the type of boom extension selected must be chosen carefully. Linearly deployed booms have a long heritage of use in various spacecraft applications such as increasing instrument resolution, reducing cross-contamination, protecting extremely sensitive equipment, and providing remoteness from the spacecraft [5],[6]. In the case of this design, the primary purpose of the boom is to provide an increased reach capability while maintaining structural integrity throughout all phases of deployment.

The four main types of linearly deployed booms considered were: telescoping, inflatable, articulated or coiled, and tubular extendable booms. After considering these types of booms, tubular extendable booms were selected based on the imposed system requirements. The imposed boom system requirements are discussed later in section 2.2. For the inspection boom system, the boom must have good stiffness characteristics for all deployed lengths.

Telescoping booms consist of several sections stacked within one section [7],[8]. When deployed, the series of sections are pushed outward forming the boom structure like a common radio or television antenna. Major problems associated with telescoping booms are that they tend to be much heavier than other types of comparable booms and are limited in length [5]. This type of boom was not selected for the inspection boom system; instead, lighter weight booms options were explored.

Inflatable booms depend on inflation pressure for deployment and must be rigidized for long-term missions. Maintaining proper inflation pressure of the boom throughout the inspection process would be too demanding on orbiter systems;

therefore, the boom should be rigidized. Rigidization causes problems because the deployment length cannot be readjusted and the now fixed-boom must be stowed or jettisoned before returning to Earth. The inflatable boom concept has the initial stowage features of a deployable boom, but for use it becomes a fixed-boom that leads to the same logistical concerns that the deployable boom was designed to overcome.

Articulated or coiled booms are often stowed in a folded or coiled configuration and deployed using a motor-driven lanyard or the stored strain energy of the boom [9]-[13]. Benefits of these types of booms are that they can be stowed in a tight volume and can include elements tailored for a particular application. A major disadvantage of these booms are that the transition region, where the boom unfolds or uncoils to its deployed configuration, has considerably less stiffness than the fully deployed sections. To overcome this weakness in the transition region, the boom stowage canister can be extended to offer additional stiffness past the transition region. This adds considerable weight and volume to the system, so articulated or coiled booms were not selected.

Tubular extendable booms are stowed on reels where by transitioning from a flattened to a curved geometry the boom stiffness characteristics are maintained throughout deployment. These types of boom are highly reliable and occupy the least stowage volume per deployed length compared to the other booms studied [5]. Tubular booms also have virtually unlimited length capability; therefore, achieving the required reach capacity is not an issue for this type of boom. Other benefits of tubular booms are their ability to maintain stiffness throughout deployment and to

make length adjustments after deployment. The ability to adjust the length of a boom is important for the inspection scheme outlined later in this document.

Tubular booms obtain their structural properties from their cross-sectional geometry. An important requirement on the geometry is that it must be collapsible, so that it can be rolled onto the motorized reel that is used to deploy the boom. To facilitate the stowage process, the boom should be made from a thin highly elastic material, which could further dictate cross-sectional geometry. These booms operate on the principal that the thickness of structure is sufficiently small that when it is deformed, it remains purely in the elastic range. When the boom is retracted, a large amount of elastic strain energy is stored within the structure.

The simplest geometry is an open cross-section (Figure 1-2a). For this case, the tubular boom is split longitudinally, so it can be opened out flat for stowage. When deployed, the flattened strip reverts to a circular cross-section. This geometry is easy to deploy and requires minimal mass, but has poor torsional stiffness characteristics making it prone to buckling under non-axial loading. To overcome this problem, a closed cross-section geometry can be used to increase the bending and torsional stiffness of the boom without significantly increasing the complexity of the deployment system or reducing system reliability. The open-section geometry can be modified to create a closed-section if the edges of the slit are designed to interlock mechanically (Figure 1-2b) increasing the boom rigidity [5],[6].

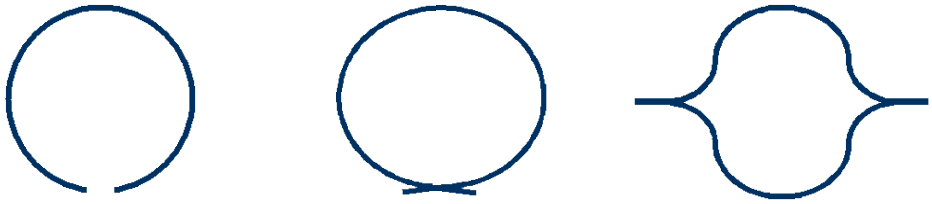

(a) *Open cross-section* *(b)* *Interlocking cross-section* *(c)* *Lenticular cross-section*

Figure 1-2: Tubular extendable boom cross-section geometries

Another option with good structural properties is a lenticular boom cross-section (Figure 1-2c) that consists of two convex shaped tapes that are bonded together. This geometry is collapsible for stowage; yet, large shear stresses may build up along the flange bond lines when the boom is rolled onto the stowage reel. A disadvantage of this geometry is that it is more difficult to manufacture than an open-section made from a single tape because it requires joining two preformed tapes. Traditionally, these types of booms are made from very thin metallic materials [14]; however, recent research [15]-[19] has demonstrated that booms of this geometry can be made from carbon fiber composites. These composite material booms exceed the structural properties of metal booms and allow for a wider variety of geometries with large cross-sections, previously prohibited by material limits.

A lenticular boom cross-section was chosen for the design of the inspection boom system because tubular extendable booms offer compact stowage, unrestricted length capabilities, good structural properties, and high reliability. The remainder of this document assumes a lenticular-shaped extendable boom is used for the boom system extension to the SRMS.

In the next chapter, the inspection system operational requirements are discussed in further detail. This includes the inspection task definition, the boom

system requirements, and deployment and stowage considerations. Following the requirement definitions, chapter three provides an overview of the inspection system design. The mission operations section discusses how the system will be used to carry out the inspection task. Next, the SRMS and boom extension systems are outlined leading to the development of the system kinematics model. Finally, chapter three concludes with a discussion of the risk management issues important to the design of the boom-based inspection system. Chapter four contains the structural analysis of the boom extension system. First, the boom geometry is defined and a prototype boom design is selected. The structural characteristics of the prototype are detailed demonstrating the feasibility of the lenticular boom system. Lastly, fabrication and assembly techniques are presented for creating the boom prototype developed earlier in the chapter. The final chapter draws some conclusions about the proposed boom inspection system design and makes some recommendations for future work.

Chapter 2: Inspection System Operational Requirements

To better understand the operational requirements imposed on the deployable boom-based inspection system, this section defines the inspection task and the constraints essential to the different aspects of the system. A basic schematic of the boom-based inspection system is shown in Figure 2-1.

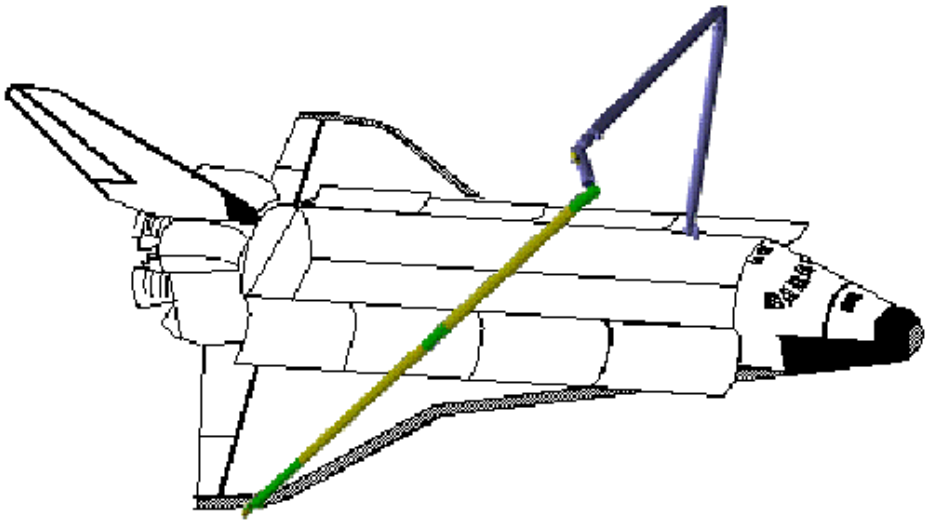

Figure 2-1: Proposed boom-based orbiter inspection system

2.1 Inspection Task Definition

The inspection task is based on surveying the orbiter thermal protection system (TPS). The TPS is composed of various materials fixed to the external surface of the orbiter that protect its structure from the extreme temperatures experienced during atmospheric re-entry. As evidenced by the *Columbia* accident, a breech of the TPS can lead to the catastrophic loss of the vehicle and crew. Damage to the TPS resulting from debris impacts must be identified and addressed before the orbiter can safely re-enter the atmosphere. The on-orbit inspection system must have the

capability to inspect the orbiter TPS over the widest possible range of damage scenarios.

NASA divided the orbiter TPS into zones and assigned preliminary inspection resolution criteria to each zone to form the basis of the TPS inspection system requirements. Eventually, NASA will define damage thresholds below which no repair is required before atmospheric re-entry based on experimental testing and analyses [3]. Inspection criteria for a particular site on the orbiter TPS is a function of the damage surface dimensions, depth, and atmospheric re-entry heating at that location [3]. In order of increasingly stricter resolution requirements, the TPS zones of interest are [3] (Figure 2-2):

- lower surface tiles and vertical tail areas;
- landing gear doors and upper wing leading edge (WLE) reinforced carbon-carbon (RCC) panels;
- nose cap RCC components;
- lower WLE RCC panels.

An orbiter inspection system must be able to meet these resolution requirements for all of the critical orbiter TPS zones.

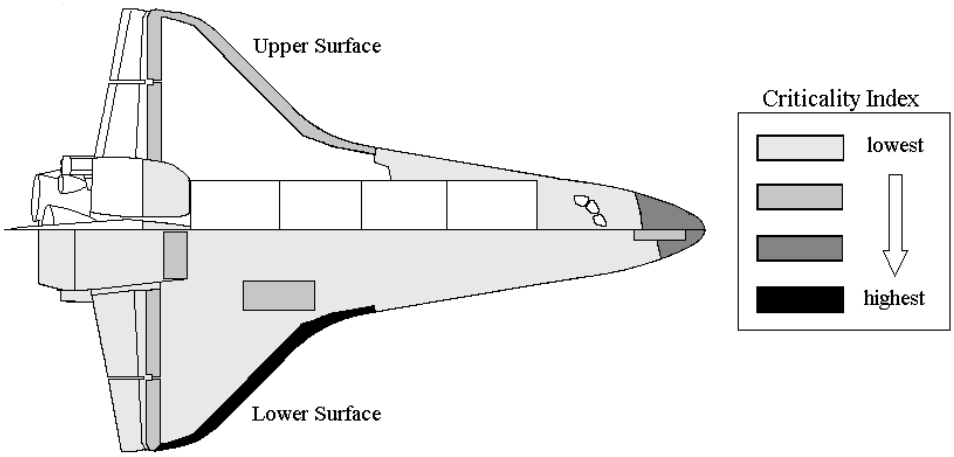

Figure 2-2: Orbiter TPS inspection criteria

2.2 Boom System Requirements

Increasing the reach capability of the SRMS is the primary purpose of the boom extension system. To demonstrate that the boom extension will provide the necessary coverage of the critical orbiter TPS regions, a model of the space shuttle orbiter was made of cardboard and a SRMS with a boom extension was fashioned from drinking straws in the same scale. As seen from the images in Figure 2-3, the proposed inspection system can view the nose cap and starboard regions of the orbiter TPS inaccessible by the SRMS alone. It should also be noted that the deployable boom concept allows the boom length to exceed the length of the orbiter payload bay unlike the fixed boom design, which is limited to approximately 50ft (1520m).

(a) *Top of nose cap* *(b)* *Starboard lower WLE* *(c)* *Starboard aft underbelly*

Figure 2-3: Cardboard-straw model demonstrating reach capabilities of the proposed SRMS-boom inspection system

The top-level requirements on the boom system are that it should not compromise or interfere with the operation of other orbiter systems, payloads, or experiments. In addition, the interaction of the boom system with the space environment and the orbiter must be taken into consideration in the design process. Aspects that drive the boom system design from a feasibility demonstration standpoint are discussed throughout this document as it applies to the system design. For more information regarding the boom system requirements and its integration as an orbiter payload, please see references [4],[20]-[35].

2.3 Deployment Considerations

Several functional requirements placed on the deployment device constrain its design. The purpose of the deployment mechanism is to assure that there is an orderly transition from the flattened tape to the final tubular structure. The deployment device must reliably extend and retract the boom a prescribed number of times within allowable limits. The deployment device must be designed to withstand the launch and landing environments in addition to protecting the boom from structural damage.

The deployment device consists primarily of a stowage reel, a drive motor, velocity regulating electronics, a series of rollers, and a transition region support section (Figure 2-4). The transition section should guide the boom assuring a smooth transition from the flattened strip on the stowage reel to the fully formed boom. To store the boom, the boom is flattened in the transition support section and is rolled onto the reel through a series of guidance rollers that apply the necessary force to maintain the collapsed state of the boom while counteracting the urge of the boom to uncoil due to the stored strain energy. Likewise, to deploy the boom, the boom is extended by the motorized reel and the rollers guide it to the transition section where the tubular shape is formed from the flattened tape.

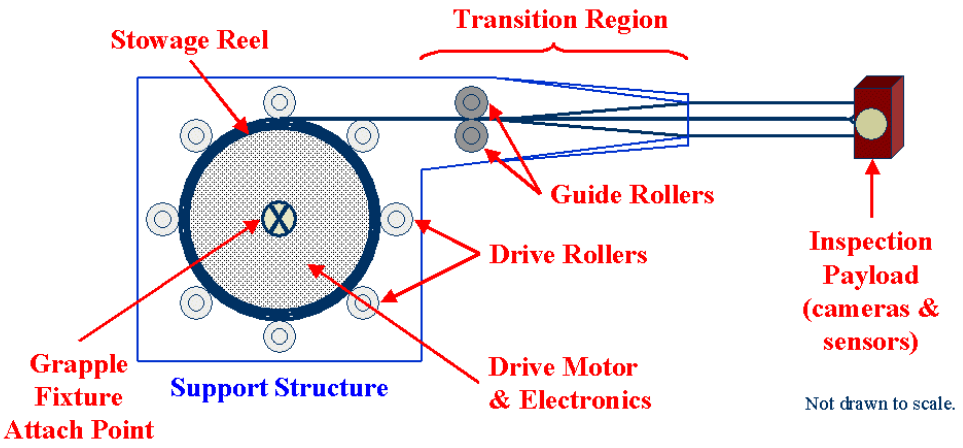

Figure 2-4: Proposed extendable boom deployment device

Monitoring of in-flight boom performance during operation is important in understanding the current state of the boom and diagnosing the cause of any malfunctions. It is recommended that performance characteristics such as length, deployment time, and motor usage be frequently monitored.

Another factor that drives deployment device design is extension and retraction speed. Because the boom will be used as an inspection tool, the deployment

speed must be carefully selected to avoid degrading the system performance especially with regard to sensor requirements. In the case that the boom fails to stop quickly, a slower speed may prevent the boom from potentially colliding with the orbiter. To build confidence in the deployment device, sufficient tests should be performed to protect against an irregular extension velocity and to verify that the safety features built into the system logistics prevent a runaway boom from striking the orbiter. A slow velocity is desirable for the purposes of performing a thorough scan. Other advantages of a slow deployment velocity include:

- reducing the danger of buckling the boom due to small starting and stopping inertial loads;
- reducing the power required by the motor to drive the deployment at the desired speed;
- reducing the stresses on the boom during the transitional portion of deployment;
- avoiding excitation of dynamic vibration of the boom;
- increasing the precision of boom length adjustments.

However, some disadvantages to using a slow deployment velocity are that the motor is required to run for longer periods of time and the boom could temporarily "hang up" due to friction from rubbing or contamination in the mechanism under smaller deployment forces relative to fast deployment velocities.

2.4 Stowage Constraints

To provide an inspection capability on every shuttle mission, the boom extension for the SRMS must be stowed in the orbiter payload bay on each mission.

Payload storing is the process of placing the deployment device containing the stowed boom in a restrained position in the orbiter payload bay for ascent and return from orbit. For launch and landing, the boom system must be stored in a compact and secure form in the orbiter payload bay.

The dimensions and carrying capacity of the orbiter payload bay imposes restrictions on the boom system attributes. The orbiter payload bay is approximately 60ft (18m) long and 15ft (4.5m) in diameter; however, the length of the payload bay is reduced to 48ft (15m) when the orbiter docking system is installed. The approximate volume of the payload bay is 10,600ft^3 (300m^3) where cargo can be stored; however, the storage capacity of the payload bay is often limited by mass. The maximum allowable launch cargo mass is 56,000lb_m (25,000kg); however, this limit varies depending on ascent performance and landing weight limitations of the shuttle. The values given assume that there are no other payloads, but this is not the case. The remaining shuttle missions have carefully planned payloads that must be brought to the ISS, so the inspection system must not interfere with the mission payloads. Space and mass has already been allotted to fly the SRMS on all of the remaining shuttle missions; therefore, the size and mass of the boom system must be minimized to take advantage of the remaining capacity of the orbiter payload bay.

Stowage considerations for the NASA orbiter boom sensor system (OBSS) fixed boom concept are quite different from those of the proposed deployable boom-based inspection system. The fixed boom imposes less volume restrictions, because the boom is stowed on the payload bay sill outside the cargo volume, allowing all planned cargo to be stowed; however, the mass of the OBSS may impose significant

limitations to the available cargo capacity. The deployable boom design will likely be less massive (depending on the deployment device design); therefore, will impose fewer mass restrictions on the orbiter payload, but the deployment device containing the boom must be stored inside the orbiter payload bay, which could limit the placement of other cargo items. Figure 2-5 shows a conservative estimate of the relative boom system size, based on the boom prototype designed in Chapter 4, in the orbiter payload bay; however, the boom system will likely be smaller than illustrated. It may be possible to store the system closer towards the front of the orbiter between the side wall and the docking mechanism, which leaves the main part of the payload bay available for planned cargo. A 2ft (0.6m) clearance envelope must be maintained around the boom system to avoid contact with other payloads or the orbiter structure when the boom is retrieved and returned by the SRMS.

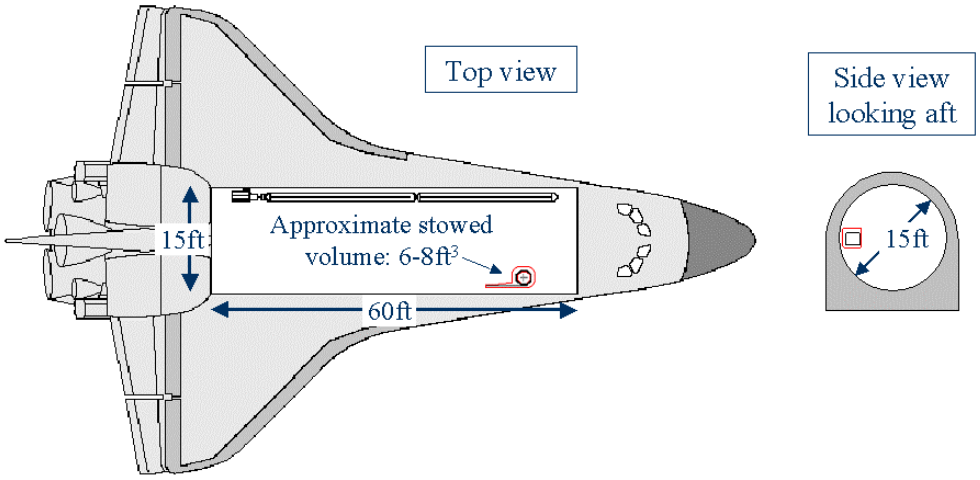

Figure 2-5: Possible stowage configuration for the boom system in the orbiter payload bay

The SRMS will grasp the deployment mechanism via a grapple fixture (GF) located perpendicular to the direction of deployment. To facilitate handling by the

SRMS, the deployment device should be placed on its side so that the GF is pointing upwards in a portion of the payload bay that is accessible by the SRMS. Figure 2-5 shows the boom system orientation relative to the orbiter payload bay.

The deployment device is compact by design and can take advantage of current orbiter payload attachment and storage facilities. Payloads stored in the orbiter payload bay must meet specific requirements set by NASA [4],[28]-[30]. In some cases, waivers can be granted if a requirement cannot be met by the system; however, this boom system is designed to be compatible with the current NASA systems without affecting the planned shuttle mission. Payload retention systems are used to secure the boom system to the payload bay structure for launch and landing. In the case of the boom system, the retention latches used must be for deployable payloads and are provided through the NASA shuttle program office. The lightweight and middleweight longeron latches feature an extra-vehicular activity (EVA) disconnect mechanism that provides manual open and close capability in the event of a jammed gear mechanism or motor failure. Although these latches are designed to be lighter limiting their load capabilities, they may be ideal for the boom system, because in the event that the boom could not be retrieved as scheduled, it could be delayed until an EVA could release the system. For more information concerning the orbiter payload attachment fittings please see references [4],[28]-[30].

Another storage issue of the boom system is how the inspection payload located at the tip of the deployable boom is configured. The payload could be detachable, so the SRMS could grab the stowed boom and then maneuver the tip of the boom to grasp the payload. This method requires a grasping capability at the

boom tip, which could be useful if interchangeable payloads were available such as one for repair in addition to one for inspection. However, this would add potentially complex and unnecessary complications to the boom design. Another solution is to make the payload capable of fitting within the tubular shape of the boom. When the boom is being used for inspection, the payload could deploy from the tip to achieve acceptable view angles. The payload then can be retracted inside the boom structure for protection when the system is stored. Again, this configuration would limit the retraction of the boom at the end; however, it would provide the payload with added protection. One drawback to this method of attachment is that a mechanism is required to move the payload in and out, which introduces reliability concerns due to the additional moving parts. The simplest approach is to permanently attach the payload to the end of the boom with provisions for storage in the payload bay in such a way that the payload is protected. In this case, the boom would be unable to fully retract and this must be taken into consideration when storing the boom to account for the added extrusion. This also leaves the inspection payload susceptible to damage when retrieving and replacing the boom extension. The selection of the best inspection payload attachment solution will depend on the final shape and size of the inspection payload.

Chapter 3: Inspection System Design Overview

The boom-based inspection system developed in this study provides a comprehensive orbiter inspection system independent of the ISS. The system is composed of two main components: the shuttle remote manipulator system (SRMS) located on the port sill of the orbiter payload bay and a boom system, which is composed of a deployment device, a lenticular extendable boom, and an inspection payload (Figure 3-1). This inspection system design uses a deployable boom for increased inspection capabilities as discussed earlier in this document.

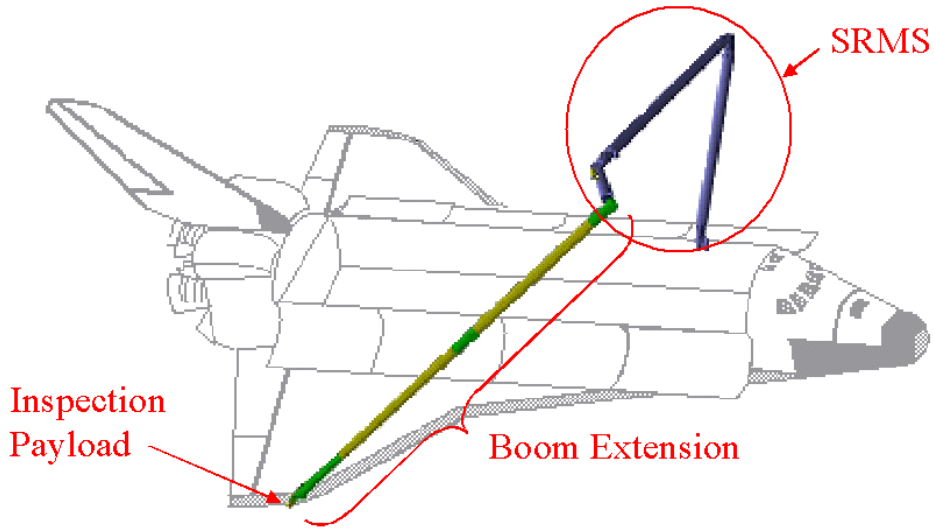

Figure 3-1: Proposed boom-based inspection system highlighting the primary system components

In the following sections, the mission operations planned to conduct an on-orbit inspection of the orbiter thermal protection system (TPS) using the proposed deployable boom extension to the SRMS is discussed. Followed by, an overview of the inspection system components. Bringing the system together, the model of the

system kinematics is presented. Lastly, this chapter looks at the risk management considerations that should be made concerning the design of this system.

3.1 Mission Operations

Prior to reaching ISS, after the orbiter payload bay doors are opened, the SRMS will retrieve the stowed boom system from the payload bay, and use it to conduct a scan of the orbiter TPS, then replace the boom in the payload bay after the inspection is complete. This section discusses the mission operations of the extendable boom-based inspection system.

Two methods of providing the necessary extension to the SRMS are a fixed boom or a deployable boom. Both types of booms serve the same purpose, but have substantially different operational implications. The inspection scheme for the fixed-boom requires that the SRMS be constantly repositioned to bring the tip of the rigid boom in view of various regions of the TPS (Figure 1-1). Although this type of boom extension allows for increased reach, alternatively, a deployable boom extension alleviates many of the logistical concerns associated with a fixed boom system.

A deployable-boom extension to the SRMS allows for increased reach capability while lessening some of the logistical concerns that arise when maneuvering a fixed-boom near the delicate orbiter. As discussed earlier, the extendable boom allows for length adjustment without loss of strength or rigidity permitting the boom to be used throughout all deployment phases. The ideal inspection strategy relies on multiple boom deployments to inspect the orbiter TPS, while minimizing the movement of the SRMS (Figure 3-2). The deployment device is attached to the SRMS with a 90° offset between the grapple fixture and the direction

of the boom deployment, so that the last joint of the SRMS (wrist roll) produces this planar scanning motion prescribed. The SRMS is moved into a predetermined parking position and locked, then the boom scans as it is deployed back and forth in a fan-like pattern surveying the orbiter TPS. After all areas accessible from that particular SRMS parking position are scanned, the boom is retracted and the SRMS is moved to another parking position and the boom continues the inspection. Moving the SRMS only when the boom is fully retracted eliminates many of the concerns due to large accelerations imposed by the SRMS that may cause significant vibration in the fully deployed boom. Another benefit of this inspection scheme is that there may be some overlap in the inspection areas, particularly near the wing leading edges, which are among the most critical inspection regions. As a contingency plan, the fixed-boom inspection scheme (Figure 1-1) can be used if the deployment device becomes stuck and boom length can no longer be adjusted.

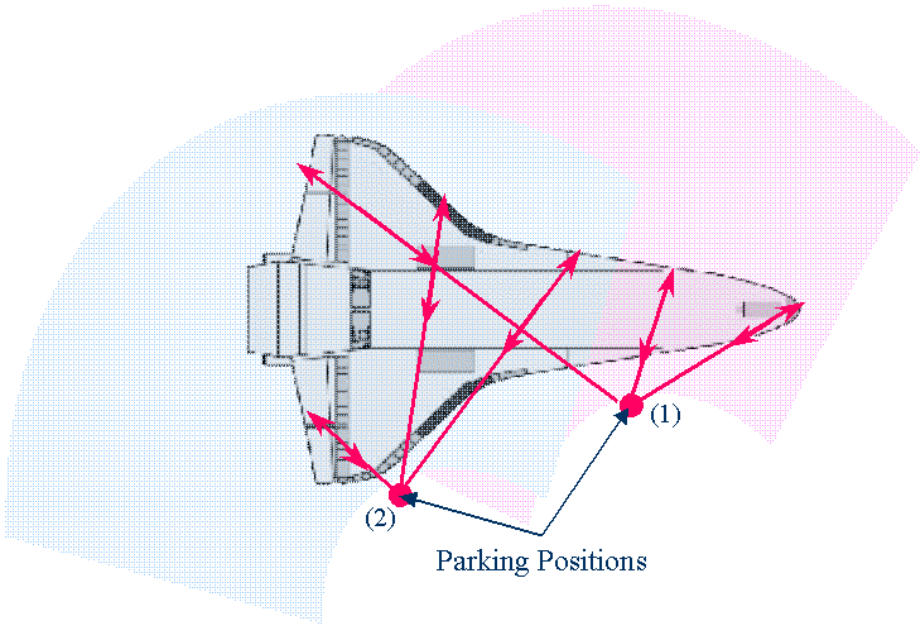

Figure 3-2: Deployment-based inspection scheme

The inspection scheme selected for the deployment-based survey can be implemented using currently available SRMS automatic operating modes. Using information about the geometry of the orbiter and the kinematics of the inspection system, the parking positions can be found and saved for use in a preplanned sequence. Preplanned sequences allow for coordinated six-joint arm movements that can be controlled automatically along a specified trajectory that is comprised of a series of points selected before flight [4]. The SRMS software continuously calculates a straight line from the current position to the next point; however, arm dynamics prevents exact straight-line motion. The points in an auto sequence may be either fly-by or pause points. For fly-by points, as soon as the point-of-reference is within the fly-by sphere, the arm will move towards the next point. For pause points, once the boom tip reaches the washout sphere, the arm will decelerate and stop, holding its position until commanded to move to the next point. Each shuttle flight can accommodate up to 20 preplanned sequences where the total number of points in all of the sequences for any flight cannot exceed 200. Ideally, a preplanned sequence will be stored before flight for the inspection task, a complete scan of the entire orbiter TPS.

To start an auto sequence, the boom tip must be within a specified distance of the first point. For the first point, the SRMS-boom system may start above the boom system storage location in the payload bay, (1), rise up above for a fly-by point, (2), and then over the port payload bay door to the first parking position, (3) (Figure 3-3). The auto sequence will end at this point and the position will be maintained, while the boom deploys and the SRMS wrist roll joint rotates to scan that region of the TPS.

After the inspection of that region is finished, the boom is retracted and the next auto sequence program can pick up from the parking position to move to the next one. A stipulation of using auto sequences is that the auto trajectories designed for the orbiter TPS scan must keep the SRMS and deployable boom at least 5ft (1.5m) from any part of the orbiter structure including payloads fixed in the payload bay at all times [4]. In addition, the auto sequences must be designed such that the SRMS and boom are not maneuvered or parked in positions where the system cannot be safely jettisoned away from the orbiter in the event of an emergency [4].

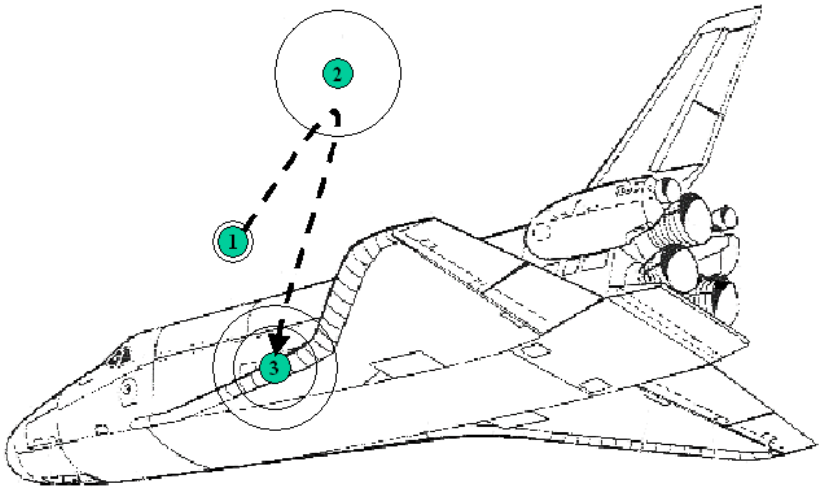

Figure 3-3: Example SRMS trajectory to inspection parking position

After the SRMS reaches a parking position, the SRMS will be held in position and switched into single joint drive mode. This operational mode allows a single joint to be controlled, while the rest of the joints are maintained in their current positions. The joint of interest is the wrist roll joint, which is the last joint of the SRMS. Rotation of the SRMS wrist roll joint coupled with the deployable boom creates the fan-like pattern of the inspection scheme (Figure 3-2).

In addition to preplanned auto sequences, the operator command mode allows the operator to enter the desired position and attitude of the boom tip and after checking to determine whether a set of joint angles exists that can produce the desired point, the SRMS software calculates a straight line from the current position to the desired point. The position and attitude cannot be entered until the operator has verified that there is no obstacle in the path of the sequence. This mode of operation would be most useful if damage was found and the boom needed to return to a position for further investigation.

Operation of the inspection system will be scheduled shortly after launch, but not within the first three hours to guarantee that the orbiter payload bay doors are open. It is important to conduct the orbiter TPS scan early in the mission to provide the maximum amount of time to mitigate the consequences if damage is found. Nominally, the scan will be scheduled during the daylight portion of the orbit. A complete scan of the orbiter TPS will likely take several hours, so depending on inspection payload sensor requirements, the scan may work through both night and day cycles. Depending on the type of inspection cameras and sensors onboard, the orbiter may need to change its attitude to ensure the proper lighting to get an accurate TPS scan. Also, operationally the SRMS cannot be driven unless the crew can observe the arm and boom via the orbiter windows or auxiliary cameras.

To account for arm singularities, the boom is mounted on the SRMS at a right angle. Operationally, singularities occur when one or more controlled degrees of freedom of the arm are lost, usually due to the alignment of several joints. When some degrees of freedom are lost, loads induced in the arm by external forces are not

transferred to the orbiter as expected and may lead to structural failures of the arm. In general, singularities of the arm are managed within the SRMS software; however, the addition of the deployable boom increases the number of degrees of freedom. Every effort should be made to avoid singularities when developing the inspection procedure trajectory points and parking positions.

3.2 Shuttle Remote Manipulator System

Utilized on many past shuttle missions, the serial revolute SRMS is scheduled to fly on all future shuttle missions due to its capability to view portions of the orbiter TPS. The SRMS is composed of six independently controlled revolute joints that allow it to achieve movement similar to that of a human arm. The SRMS is mounted along the port sill of the orbiter payload bay outside the payload envelope reserved for cargo. The approximate overall dimensions of the SRMS are 50ft (15m) with an average diameter of 15in (38cm). The total system mass of the SRMS is 966lb_m (438kg). The SRMS is capable of deploying and retrieving payloads up to 32,000lb_m (14,500kg). The maximum loaded tip-speed of the SRMS is 2.4in/s (6.1cm/s) [36].

The SRMS consists of five main components: the mechanical arm assembly, the end effector (EE), the special purpose EE connector (SPEE), the thermal protection system, and the shoulder brace. The mechanical arm assembly consists of six revolute joints that drive the arm. Two joints at the shoulder drive the upper arm link in azimuth and elevation, the elbow joint controls the angle of flexion between the upper and lower links. The wrist of the robotic manipulator consists of three joints that provide primarily attitude control of the payload. The last joint of the wrist is the roll joint, which is important to the inspection procedure chosen for the deployable

boom-based inspection system. The motion of the arm is coordinated by an onboard computer from either operator inputs or preflight-generated points for auto trajectories [4].

The EE connects the SRMS to the payload grapple fixture (GF). A GF is a structural fitting on a payload that allows it to mate with the SRMS EE. The EE is a hollow cylinder that is 21.5in (54.6cm) long and 13.6in (34.5cm) in diameter. There are two major functions provided by the EE drive system: capture and release of payloads and rigidization and derigidization of payloads. To capture a payload, a rotating ring located at the end of the EE closes three snare cables around the payload-mounted GF. Releasing a payload is accomplished by opening the snare cables. This capture or release process takes approximately one second [4]. In automatic operation mode, when the EE is commanded to capture a payload via its GF, the EE will continue operating until the payload is fully rigidized after capture. In the manual mode of operation, the EE waits for a separate rigidization command to be issued before rigidizing the payload. There are back-up release capabilities for contingencies; however, there is no back-up capture capability. If the primary release capability fails, a back-up clutch can be disengaged to release the payload via a spring mechanism in the EE. In addition, the GF is designed with flight critical release bolts, releasable by a crewmember EVA if necessary.

An electrical connector is available for all SRMS EEs. This special purpose end effector (SPEE) provides +28Vdc electrical power and sixteen command, data, or heater power lines to the payload. To utilize this feature, the payload must be equipped with an electrical GF. This special GF is supplied by NASA through the

space shuttle program office and has an approximate mass of $45lb_m$ (20kg). The standard GF mass is about 30lb (14kg). The customer is also responsible for the interfaces including displays and controls of the SPEE.

The remaining systems, the SRMS TPS and shoulder brace are discussed here for completeness. The SRMS TPS is designed to provide a stable thermal environment for SRMS operations. The shoulder brace is installed between the upper arm boom and the SRMS shoulder pedestal to help carry launch loads. This brace must be released on orbit before using the SRMS and once it is removed, it cannot be reattached in space.

The SRMS motion is controlled by onboard computer software that contains algorithms that converts operator commands into output rates for each joint of the arm. The software serves three main functions: it translates operator commands into SRMS-payload motion, it monitors and displays the SRMS operational status, and it generates caution and warning annunciations and places the system into a safe-mode if certain failures are detected. The software also prevents the joints from driving beyond their mechanical hard-stops. The upper limits on the SRMS joint movement rates are calculated before launch based on the mass characteristics of the payload to guarantee that the EE can stop within 2ft (0.6m) in the event that there is a runaway joint failure. As expected, the heavier the payload, the lower the rates resulting in longer maneuvering times. In the case of the deployable inspection system, a low mass is desired in order to limit the amount of maneuvering time required of the SRMS.

NASA calculated the reach capability of the SRMS and found that the achievable inspection resolution for the orbiter TPS was inadequate, particularly for the lower aft surface tiles and most of the RCC components of the TPS [2],[3]. An extension of the SRMS is needed to inspect regions of the TPS inaccessible with the SRMS alone.

3.3 Boom Extension System

The boom extension system is composed of a deployable boom, deployment device, and inspection payload located at the tip of the boom. The following sections discuss the chosen extendable boom technology, requirements for the deployment device, and possible system payloads.

3.3.1 Extendable Boom

An extendable boom was chosen to achieve the increased reach capacity required to inspect the orbiter TPS. This discussion of the boom refers to the boom extension element, not including the deployment device or inspection payload, which will be discussed in the next sections. An extendable boom, sometimes referred to as a tubular boom, design was chosen for its simplicity and high reliability compared to the other booms studied. In addition, extendable booms have the ability to achieve great lengths with minimal stowage volume and mass. This type of boom is elastically flattened and rolled on a reel for stowage; it is deployed by unrolling the reel and reacquires its original curved or tubular shape when deployed, like a carpenter's tape measure. The geometry of the boom is dictated by application;

typically, a closed or interlocking cross-section results in good stiffness properties for both bending and torsion loads.

A lenticular cross-section was selected for the extendable boom design due to its structural characteristics and ability to flatten for stowage in a relatively small volume. This particular geometry has good structural properties that allow for strength and rigidity throughout deployment. Lenticular booms have a cross-sectional geometry that is obtained by joining two curved sections together to form a tubular shape (Figure 3-4). The development of large shear stresses along the flange joint between the two halves limits the stowage diameter and must be taken into account when selecting the boom materials. Fiber-reinforced composite materials offer greater flexibility over traditional metallic materials allowing for higher specific strength and stiffness. The selection of a flexible adhesive for the joints allows for more compact stowage compared to welds used with metallic materials.

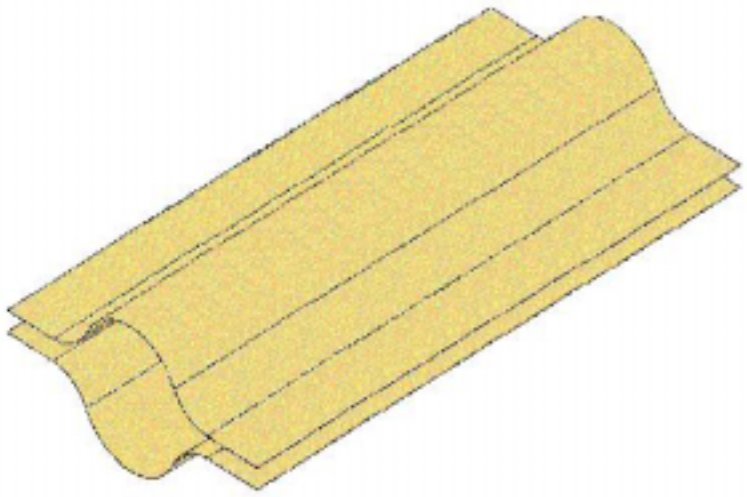

Figure 3-4: Extendable boom concept with a lenticular cross-section

The extendable boom design for the orbiter inspection system utilizes composite material technology to meet the structural requirements presented in this

document. The German Aerospace Center (DLR) has demonstrated manufacturing and deployment techniques for a lenticular boom design using carbon fiber reinforced plastics (CFRP) [15]-[18],[37]. The collapsible tube mast (CTM) project through the European Space Agency (ESA) also fabricated similar booms using carbon-fiber composites [19]. Although designing composite extendable booms is still an innovative process, a knowledge base can be established through modeling and experimental testing. The research at DLR has shown comparable results between analytical, linear finite element modeling (FEM), and non-linear FEM for a composite lenticular boom. The CTM project also studied the performance characteristics of booms made from different resin systems under environmental loading including repeated deployment and extended stowage effects on the cross-sectional geometry [19]. Drawing on these results, the boom designed in this document uses composite technology to achieve its structural performance requirements.

3.3.2 Deployment Device

The requirements for the boom deployment device are dictated by how the boom will be used. The inspection scheme (Figure 3-2) presented in this document relies on an intermittently operated deployment device that will be used only while inspecting the orbiter in space. Deployment implies that the boom is either extended or retracted by the deployment device. The deployment device must be capable of operating under the following three modes: deploying at a constant rate, locking and clamping the boom at any partially deployed position, and readjusting the boom length from any position. In the event of a mechanism failure, the boom will be

clamped at its current position through a fail-safe mode or manual clamping to avoid possible damage to the orbiter while the failure is assessed. If the boom cannot be retracted, either the boom or the entire SRMS with boom attached can be jettisoned, so the orbiter can return safely to Earth.

The deployment device containing the boom and inspection payload must be designed to withstand the various environmental loading conditions throughout its use. The boom extension system may be subjected to stresses caused by the manufacturing and assembly process as well as stresses applied during acceptance testing. Shipping the boom system to the launch site may impart loads on the system as well. The boom system may be stowed for extended periods of time leading up to launch or between launches. If stowed for long periods, the boom may be affected by material creep degradation particularly along the flanges of the lenticular-shaped boom. Spacecraft integration and checkout will verify that the system is ready for launch, but also must be considered when designing the system. The boom extension system will be subjected to a variety of conditions on-orbit in addition to its intended operational conditions. All of these environmental situations must be taken into account throughout the design process.

The proposed boom deployment device consists of several basic components: the stowage drum, drive rollers and motor, electronic circuitry, guide rollers, the transition section, and the support structure including the electrical grapple fixture (EGF) (Figure 2-4). The lenticular boom cross-section can be flattened into a single tape; therefore, only one stowage reel is required. Design of the device must ensure that the stored strain energy of the coiled boom is released in a controlled fashion.

Another area of major concern is the transition region where the boom is formed from a flattened tape into a circular cross-section. In this zone, the boom undergoes significant geometrical changes resulting in the temporary loss of boom stiffness in this region. This can be overcome in several ways. First, the deployment device should provide added support to the boom in the transition region. This support comes from a specially designed structure that can control extension and retraction of the boom. Secondly, whenever practical, the plane of maximum boom stiffness should be placed in the direction of the maximum anticipated bending load. Thirdly, the stiffness issue can be overcome using doublers or varied wall thicknesses. Doublers allow for locally increased stiffness. A tapered effect would likely be most effective as the boom length increases; the reaction forces at the cantilevered point become greater. Using doublers is preferable over increasing the wall-thickness along entire length of boom due to increased mass concerns. The deployment device is attached to the SRMS EE through an EGF that provides the necessary electrical power to operate the motor and drive rollers.

An underlying design principle is that the deployment mechanism should only apply tensile loads to the boom. This is important because the boom element is made from fiber-reinforced composites that obtain their stiffness and strength characteristics under tensile loading. To apply tensile loads during extension, the drive rollers operating on the flanges pull the boom off the passive stowage drum. For tensile loading during retraction, the stowage drum is powered to pull the boom into the flattened and rolled configuration, while the rollers remain inactive. Typical deployment speeds vary from 0.47in/s to 18in/s (1.2cm/s to 46 cm/s) [14]; however,

as discussed earlier a slower speed should be selected depending on payload requirements and operational comfort. The deployment mechanism electronics should regulate the extension and retraction velocity through the motor speed of the roller or stowage reel torques. To maintain a constant deployment velocity, the motor speed of the rollers or stowage reel torques should be tapered as more of the boom extends off the reel.

3.3.3 Inspection Payload

An inspection imagery and sensor payload will be located at the tip of the extendable boom. The inspection imagery and sensor package will consist of cameras and sensors capable of performing non-destructive inspection of the orbiter TPS surfaces. Possible non-destructive inspection techniques for identifying damage in addition to visual imaging are eddy current and thermography. NASA is studying potential payloads that include a laser-based imaging system to provide damage depth measurements [3]. A conservative payload mass estimate of $33lb_m$ (15kg) was used for the preliminary design of this boom-based inspection system.

Recommendations imposed on the payload are that the extended object should be as light and compact as possible and should be nearly symmetrical to minimize undesirable inertial loads acting on the boom during extension and retraction movements. Operationally, the payload sensors should be capable of scanning the orbiter TPS surface from a distance of greater than 5ft (1.5m), if not, a wavier is needed to violate SRMS mission rule requiring that the boom system maintain at least a 5ft (1.5m) distance of separation from the orbiter and any other payload elements [4]. In addition, the payload sensors must tolerate some vibration forces as the boom

is deploying during the inspection process. The SRMS and the thermal environment also impart some additional vibration to the system payload. If the inspection payload is sensitive to vibration, the boom can deploy partially, scan and then deploy some more and scan again. A method relying on more SRMS movement would be to scan the orbiter TPS in arcs at various boom lengths, however this strategy may impart unacceptable vibration. Lastly, the boom can be used as a fixed boom primarily for contingency operations, but the boom flexibility would likely create unacceptable vibrations in the system.

Communication between the payload and the orbiter is a major concern. Due to the nature of the deployment, running wires along the boom would be more complicated than using a wireless design. In the wireless design, the payload will operate using battery power and will transmit data back to the orbiter or ground computers using wireless communication technology. The data storage system of the payload must store the data from the inspection region until the inspection of that region is completed, then the SRMS will move into view of a wireless receiver to off-load the inspection data. If the payload must be wired to the deployment mechanism, the wires can be attached along the flanges of the boom, but the addition of the wires adds complexity and risk to the system.

The payload will be attached to the end of the boom using an end cap or plug that fits inside the boom. Depending on the size of the payload, it can be placed inside the end of the boom to offer protection when stowed, but it would need to extend out to inspect like an extendable camera lens. If the payload is larger than the diameter of the boom, then an end cap will be fashioned to preserve the boom geometry

(imparting additional rigidity) and the payload will be attached at the tip. In either case, the end portion of the boom cannot be rolled onto the reel unless the payload is detachable. This will affect how the system is stowed in the orbiter payload bay.

3.4 System Kinematics Model

To understand the kinematics of the proposed system, it was modeled as a seven degree-of-freedom (DOF) robotic manipulator [38]-[41]. The SRMS contains six revolute joints and the boom was modeled as a prismatic joint. Link frames were assigned to each joint following the Denavit-Hartenberg (D-H) convention [16] (Figure 3-5). The manipulator joints in sequential order as shown in Figure 3-5 are:

- SRMS shoulder yaw (SY), a revolute joint;
- SRMS shoulder pitch (SP), a revolute joint;
- SRMS elbow pitch (EP), a revolute joint;
- SRMS wrist pitch (WP), a revolute joint;
- SRMS wrist yaw (WY), a revolute joint;
- SRMS wrist roll (WR), a revolute joint;
- boom system extendable deployable boom (DB), a prismatic joint.

The local coordinate system for the inspection system is based on the SRMS shoulder pitch joint, which is located near the attachment point in the orbiter payload bay.

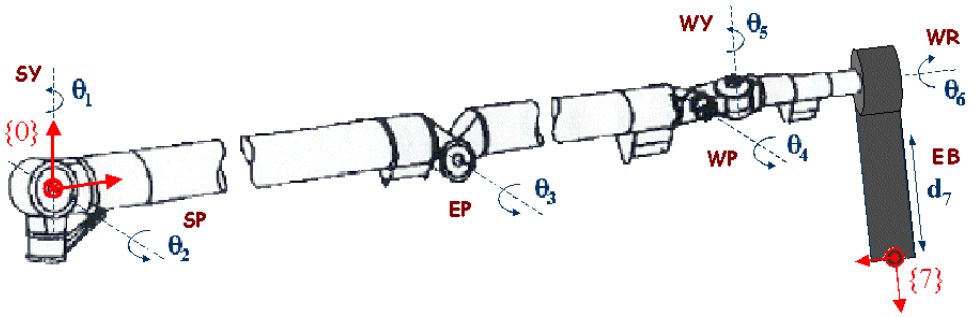

Figure 3-5: SRMS and boom system degrees of freedom based on the D-H convention

From these coordinate frame definitions the forward kinematics were found relating the joint parameters to the position and orientation of the tip payload. First, the D-H parameters describing the different joint offsets and twists were tabulated (Table 3-1). The link length given by a_i is the distance between the z-axes of two adjacent frames measured in the direction of the x-axis of the first frame. Similarly, the link twist, α_i, is the angle between two adjacent z-axes measured about the x-axis of the previous frame. The link offset, d_i, is the distance between the x-axes of two adjacent joint frames measured along the z-axis of the current frame. The joint angle, θ_i, is the angle between the x-axes of two adjacent link frames measured about the z-axis of the current frame. The joint parameters of the deployable boom based system are given by

$$\vec{q} = \{\theta_1 \quad \theta_2 \quad \theta_3 \quad \theta_4 \quad \theta_5 \quad \theta_6 \quad d_7\}. \tag{3-1}$$

These parameters can vary within the limitations of the joints while of the all other parameters remain constant. Table 3-1 gives the limitations for each joint. The limits on the SRMS joints are specified by NASA in reference [4]. For the deployable boom, the limits on the joint parameter, d_7, are assumed based on the boom prototype

developed in the next chapter. The lower bound is approximately equal to the transition region of the deployment device, which is assumed to be 24in (61cm). The upper bound of the boom length parameter, d_7. is equal to the total length, *L*, of the boom when it is fully deployed, 720in (1830cm).

Table 3-1: Inspection System D-H Parameters

i	a_{i-1} (in)	α_{i-1} (deg)	d_i (in)	θ_i (deg)	Lower Joint Limit	Upper Joint Limit
1	0	0	0	θ_1	-180°	+180°
2	0	90	0	θ_2	-3.1°	+143.9°
3	251.1	0	0	θ_3	-158.9°	+4.53°
4	278.0	0	0	θ_4	-122.4°	+120.4°
5	19.6	-90	0	θ_5	-31.3°	+211.3°
6	0	-90	38.9	θ_6	-447°	+447°
7	0	0	d_7	0	24in	720in

From the D-H parameters, the local link transformation matrices were found relating adjacent link frames. By combining these matrices, the position and attitude of the boom tip was expressed in the base frame, located at the center of the SRMS shoulder pitch joint, as a function of the joint parameters.

Payloads intending to use the SRMS for deployment or retrieval must supply all desired positions and attitudes in the orbiter body axis system (OBAS) and the orbiter rotation axis system (ORAS). Both systems have the same origin, which is located 236in (6m) forward of the orbiter nose and 400in (10m) below the centerline of the orbiter [4],[42] (Figure 3-6). SRMS and payload point-of-reference positions

must always be given in the OBAS coordinate system. In this system, the negative *x*-axis points towards the orbiter tail, the positive *y*-axis points towards the starboard wing, and the positive *z*-axis points down to complete the right-hand coordinate system (Figure 3-6a). The ORAS is a rotated version of the OBAS, where the positive *x*-axis points towards the orbiter tail, the positive *y*-axis points towards the port wing, and the positive *z*-axis points down to complete the right-hand coordinate system (Figure 3-6b). Point-of-reference attitudes for the SRMS and payload are given in the ORAS system where a positive roll rotates the port wing up, a positive pitch rotates the nose up, and a positive yaw rotates the nose starboard. The position of the shoulder pitch joint of the SRMS in the OBAS coordinate system is 679.5in (1726cm) in the negative *x*-direction, 108.0in (274.3cm) in the negative *y*-direction, and 444.77in (1130cm) in the negative *z*-direction [4].

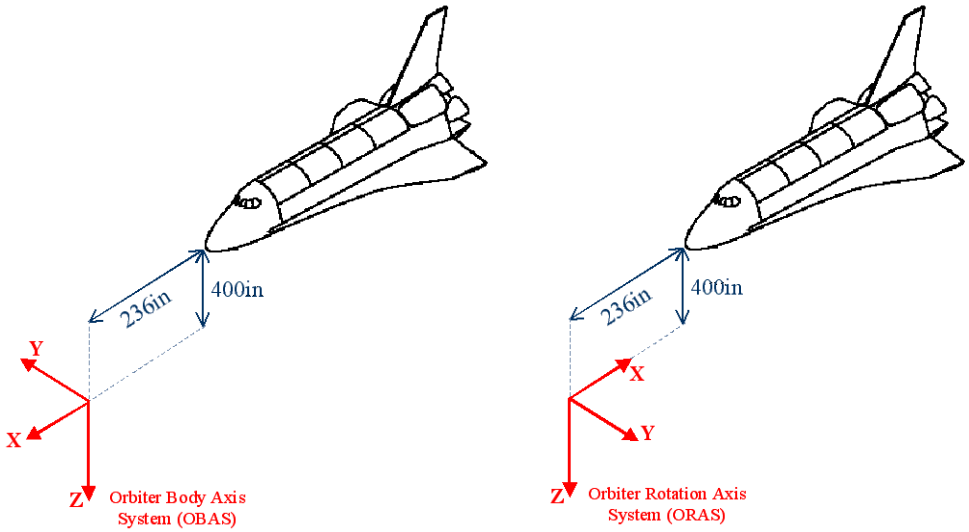

(a)
Orbiter body axis system (OBAS)

(b)
Orbiter rotation axis system (ORAS)

Figure 3-6: Orbiter reference coordinate frames

With the forward kinematics between the boom tip and the inspection system base frame, the location of the boom tip relative to the OBAS can be found. The shoulder pitch joint of the SRMS is the origin of the boom-based inspection system base frame. From the forward kinematics, the location of the boom tip can be found relative to the base frame, which in turn can be related back to OBAS coordinates (Figure 3-7). A Mathematica® program was made to find the forward kinematics of the system (Appendix B). The position of the boom tip relative to the OBAS frame (in inches) is denoted

$$ {}^{\mathrm{OBAS}}\vec{\mathrm{p}}_{\mathrm{tip}} = \left\{ {}^{\mathrm{OBAS}}\mathrm{X}_{\mathrm{tip}} \quad {}^{\mathrm{OBAS}}\mathrm{Y}_{\mathrm{tip}} \quad {}^{\mathrm{OBAS}}\mathrm{Z}_{\mathrm{tip}} \right\}, \tag{3-2} $$

where

$$ \begin{aligned} {}^{OBAS}X_{tip} &= -679.5 + 38.9c_5\,\mathrm{s}_1 - c_1\left(X_1\right) - d_7\left(X_2\right) \\ X_1 &= 251.1c_2 + 278c_{23} + c_{234}\left(19.6 - 38.9s_5\right), \\ X_2 &= \mathrm{s}_1\,s_5s_6 + c_1\left(c_6s_{234} - c_{234}c_5s_6\right) \end{aligned} \tag{3-3} $$

$$ \begin{aligned} {}^{OBAS}Y_{tip} &= -108 + 38.9c_1c_5 + s_1\left(Y_1\right) - d_7\left(Y_2\right) \\ Y_1 &= 251.1c_2 + 278c_{23} + c_{234}\left(19.6 - 38.9s_5\right), \\ Y_2 &= c_1s_5s_6 - s_1\left(c_6s_{234} - c_{234}c_5s_6\right) \end{aligned} \tag{3-4} $$

and

$$ \begin{aligned} {}^{OBAS}Z_{tip} &= -444.77 - 251.1s_2 - 278s_{23} + s_{234}\left(Z_1\right) + d_7\left(Z_2\right) \\ Z_1 &= 38.9s_5 - 19.65 \\ Z_2 &= c_5s_{234}s_6 + c_{234}c_6 \end{aligned} \quad . \tag{3-5} $$

These equations are expressed using a shorthand for the trigonometric functions of sine and cosine, where c_1 is equivalent to $\cos(\theta_1)$, s_1 is equivalent to $\sin(\theta_1)$, c_{23} is equivalent to $\cos(\theta_2+\theta_3)$, s_{23} is equivalent to $\sin(\theta_2+\theta_3)$, etc. Similarly, the attitude of the boom tip expressed in terms of the ORAS is

$$ {}^{ORAS}R_{tip} = \begin{bmatrix} -c_6 s_1 s_5 + c_1\left(c_{234}c_5c_6 + s_{234}s_6\right) & c_5 s_1 + c_1 c_{234} s_5 & s_1 s_5 s_6 + c_1\left(c_6 s_{234} - c_{234}c_5 s_6\right) \\ -c_6\left(c_{234}c_5 s_1 + c_1 s_5\right) - s_1 s_{234} s_6 & c_1 c_5 - c_{234} s_1 s_5 & -c_6 s_1 s_{234} + s_6\left(c_{234}c_5 s_1 + c_1 s_5\right) \\ -c_5 c_6 s_{234} + c_{234} s_6 & -s_{234} s_5 & c_{234} c_6 + c_5 s_{234} s_6 \end{bmatrix}. \quad (3\text{-}6) $$

The previous equations are important because the SRMS software must know the location and attitude of the boom tip in the OBAS and ORAS coordinate frames to maneuver the inspection system.

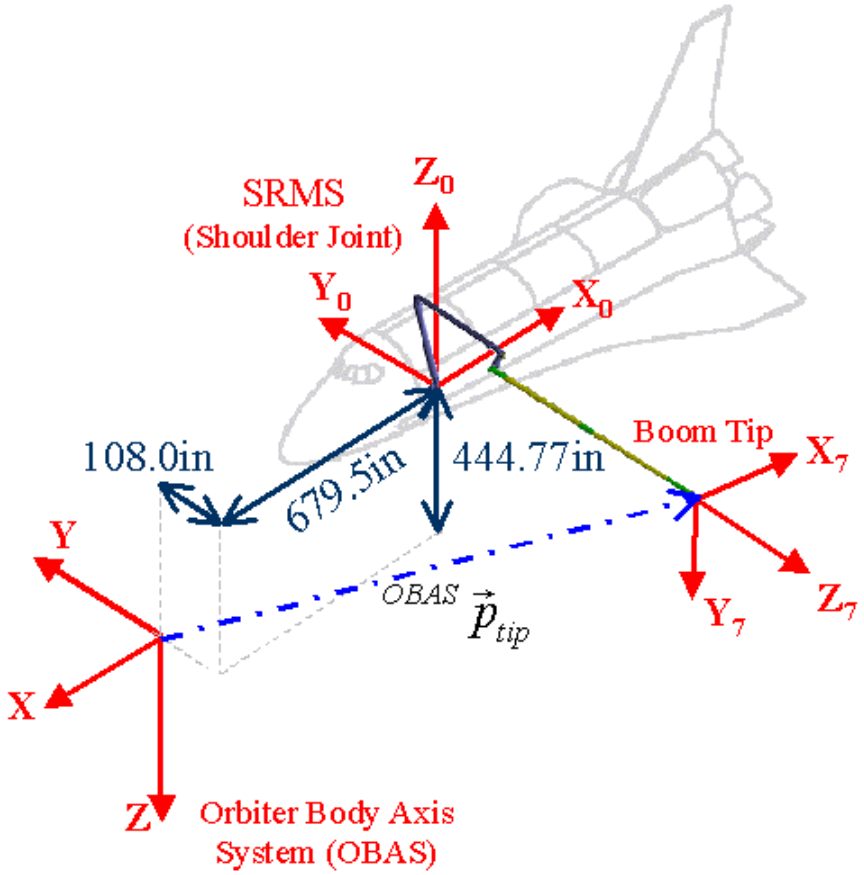

Figure 3-7: Boom tip reference to OBAS

The redundancy in this system due to the addition of the extendable boom allows for extended reach; however, the system does not have a closed-form inverse kinematics solution unless one joint parameter is defined. By defining a deployed boom length, the problem reduces to a six DOF manipulator that has a closed-form inverse kinematics solution. Taking into account the inspection scheme presented for the deployable boom inspection system, the SRMS is positioned and the boom deploys to scan from that position. The positions for the SRMS allowing the best coverage of the orbiter TPS can be determined using the inverse kinematics solution when the boom is fully extended or retracted. However, this is a difficult problem to solve because the system joints must remain within their mechanical limitations, avoid singularities, and avoid interference from the orbiter structure. Once the SRMS parking positions have been determined in OBAS coordinates, then a computer algorithm can be developed that will move the SRMS to these locations. The forward kinematics can be used to verify that the joint parameters obtained from the inverse kinematics solution produces the desired position and orientation of the boom tip. At these parking positions, all of the SRMS joints except the last one, the wrist roll joint, are locked in place while the boom scans from that parking position. This reduces the system to a two DOF manipulator, where the boom is extended and the SRMS wrist roll joint is rotated to create the fan-like scan pattern of the inspection system (Figure 3-2). If a particular location on the orbiter TPS needs further examination, the system is brought to an appropriate parking position, then the boom is rotated and translated using the SRMS wrist roll joint and deployment device, respectively (Figure 3-8).

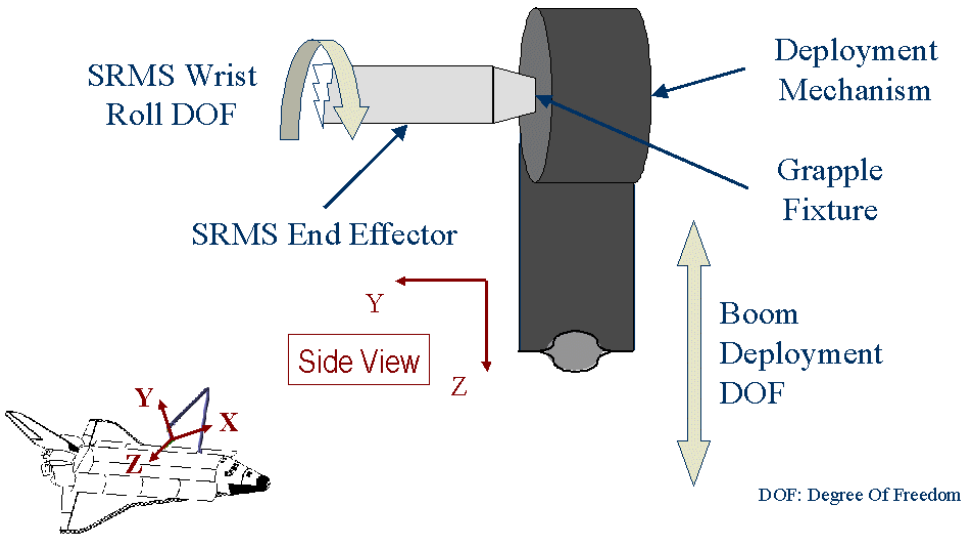

Figure 3-8: SRMS end-effector and boom interface

3.5 Risk Management

As with any design there are numerous risks involved that must be managed to provide the best system for the intended application. The use of a deployment device adds complexity and risk to the mission; however, the capabilities due to the deployment feature far outweigh the drawbacks of this deployment-based boom design compared to the fixed boom concept. To mitigate some of the added risk, potential threats must be identified and recognized from the beginning and good design practices must be adopted. Ways to ensure a safe system are to set high standards for the manufacturing and assembly process and to perform ample testing of the finished hardware before flight and between flights.

The primary aim of determining the system reliability is to prevent failures that may affect the operational capability of the system. Methods to reduce the probability of failure are employing a conservative design, using analysis tools and techniques, building in system redundancy, and performing extensive experimental

testing of the system components to ensure proper performance. The overlying design philosophy with system reliability in mind is to build a redundant system that it is fail-safe such that a single failure will not result in catastrophic consequences.

Concerning risk management, the risks associated with the inspection system design and operation should be identified early in the design process, so that risks that are not acceptable can be mitigated or eliminated through design or operational changes. Risk analysis is a technique for identifying, characterizing, quantifying, and evaluating hazards that may interfere with successful completion of the objectives of the on-orbit inspection system [43]. Managing risk is a means of controlling system risks by reducing them to a comfortable level that is consistent with the uncertainties inherent in the system.

To assess the risks of the inspection system design and operation, four steps should be followed [44]. First, the risk context is the most important objective of the system. In this case, this is the identification of critical damage to the orbiter TPS. In the context of this design, the inspection payload cameras and sensors are assumed to never fail; failures are limited to the boom system. If the system objective is not met, then the system did not perform its intended purpose; therefore, this is called a system failure. Second, risk identification is the process of determining and recording events or conditions that could cause trouble within the risk context. After the risks are identified, each one must be assessed to identify its severity. Risk severity is determined by two factors: impact and likelihood. The impact is a measurement of the effect the risk will have on the system objective if it occurs. Typically, impact is represented by a number on a scale of five, where one is very low impact with short-

term effects and five is very high impact with multiple catastrophic effects. The second factor, likelihood is a measurement of the extent that the risk is likely to occur. Likelihood is often measured on a scale representing intervention difficulty, where the level of difficulty involved in preventing the risk from occurring is assessed. The intervention difficulty is on a scale of five also, where one corresponds to easy intervention such as changing operational procedures and five corresponds to almost impossible intervention where the ability to affect the risk outcome is negligible. The greater the impact and likelihood of a risk, the greater the severity of the risk is. Lastly, the response to a risk is the plan of action if the event occurs. This often translates into contingency planning in the event that a failure of the system does occur. Risk cannot be avoided, so it must be dealt with in a systematic and planned way to prevent catastrophic consequences. To ensure that the system is functioning properly critical components identified in the risk assessment need to be monitored and controlled.

For this particular design, several features minimize risks to the orbiter and its crew. First, the inspection procedure reduces the system to a two DOF system that minimizes the risk of the SRMS joints contacting the orbiter surface, where the only joints of concern when the SRMS is at a parking position are the wrist roll and extendable boom. The SRMS is moved only when the boom is fully retracted, so its movement is similar to moving any other payload of comparable mass. Once the SRMS is positioned, the orbiter TPS is scanned parallel to the orbiter surface using the deployment feature of the boom and the wrist roll joint of the SRMS to rotate the boom about an axis perpendicular to orbiter surface. Ideally, the boom will always be

fully retracted when the SRMS moves, but there may be a situation when the boom cannot be retracted and the SRMS must move with the partially deployed boom attached. The worst-case loading scenario discussed in the boom structural design sections anticipates this situation and defines a reasonable stiffness to limit the maximum deflection of the fully deployed boom. As an extra safe guard, the boom should be oriented such that the larger area moment of the inertia is pointed towards the orbiter surface so that any vibration will be favored in the direction parallel to the orbiter surface, thus minimizing the potential of the system contacting the orbiter surface.

3.5.1 Failure Modes and Mechanisms

To understand how a system may fail, the failure modes and mechanisms should be identified as part of the risk assessment process. A failure mode is the effect by which a failure is observed, whereas a failure mechanism is the physical, chemical, thermodynamic, or other process resulting in a failure. This section seeks to identify some of the major failure modes and mechanisms; however, for each design iteration, a reassessment of the failure modes and mechanisms should be conducted. Each failure mode should be addressed in the context of mission success to determine if system or component redundancy or additional evaluation testing is required to ensure reliable operation of the entire inspection system. For the purposes of this study, the SRMS and inspection payload are assumed to not fail under any circumstance; therefore, the failure of the boom extension system is the primary focus of this failure assessment.

Boom system failures can be broken down into two major categories: failures due to the boom itself and failures due to the deployment device. First, failures of the boom itself will be addressed. A structural failure of the boom due to inadequate material strength, particularly at the root, is considered a non-credible failure mode assuming that sufficiently high factors of safety are demonstrated by analysis or experimental testing. The boom prototype design developed in the next chapter demonstrates the feasibility of the deployable boom concept; however, it does not employ safety factors beyond the conservative load estimations used in the analysis. For the case of this design, experimental testing should be performed to determine the destruct, operating, and design margins of the system, so that the proper specification limits can be determined. The destruct margin is the expected value of permanent failure of the boom structure due to overstressed loading conditions. The operating margins are the expected value for a recoverable failure of the boom structure. The design margin is the value of loading that the boom structure is designed to survive. From these margins, the specification limits can be determined, such that they are lower than the design margins to ensure that the boom will not fail structurally. Other boom failures occur when the boom becomes unstable due to the space environment. Primarily environmental instabilities of the boom occur due to thermal phenomena, but may also occur due to micrometeoroid impacts on the boom itself. These environmental risks may impart vibration on the boom system causing it to become unstable and possibly fail. To avoid this type of failure, measures should be taken to protect the boom from these effects in addition to adding ample damping to the system to dissipate any unwanted vibration. Another problem associated with boom

performance is straightness degradation. Often this occurs due to differential thermal bending or manufacturing defects such as nonhomogenous material properties, uneven material curing or surface treatments, and aging materials.

There are many failure modes that are associated with the deployment device, many of which can be avoided through design and testing. Several failure modes pertaining to the boom element are discussed first. Boom blossoming occurs when the boom uncoils on the stowage reel like a partially unwound clock spring [14]. A blossomed boom buckles and can jam the deployment device when deployment is attempted. Launch vibrations or inadequate deployment device roller restraints usually cause boom blossoming. To ensure against boom blossoming, the deployment should have an adequate roller restraint system that is experimentally tested under launch loading to sufficiently high safety margins. Closely related to boom blossoming is the desire of the boom to explosively unwind due to the all of the pent-up strain energy in the stowed boom. The constraining rollers of the deployment device must ensure that the coiled boom remains rolled tight on the stowage reel to prevent jamming. The rollers must also allow for the controlled release of the stored energy as the boom is deployed. Related to jamming, the boom may have a tendency to pull to one side of the stowage reel when rolled. Boom derailing can also be controlled through properly designed rollers that maintain boom alignment with the stowage drum. Another problem is the development of splinters from the edges of the boom after repeated deployments. These splinters may interfere with the inspection cameras and sensors or may cause problems for other payloads in the orbiter cargo bay, or in a worst-case scenario, the splinters could harm the orbiter itself. To

eliminate these splinters, the boom material must be carefully selected and the edges should be protected against splintering. Some experimentation may be required to eliminate this failure concern.

Failures associated with the deployment device are focused primarily on the extension and retraction of the boom. A preliminary fault tree was developed to illustrate some of the failures that may lead to a boom extension or retraction failure (Figure 3-9). The control system consists of computers and manual controls that are used to initiate and stop the boom extension and retraction processes. The deployment system consists primarily of the deployment motor, rollers, clamping, and braking mechanisms. The power system is controlled via the orbiter power systems; therefore, the reasons for power failure were not developed beyond a simple failure event that causes power loss to the boom system. As more of the boom system is designed, the fault tree in Figure 3-9 should be developed further.

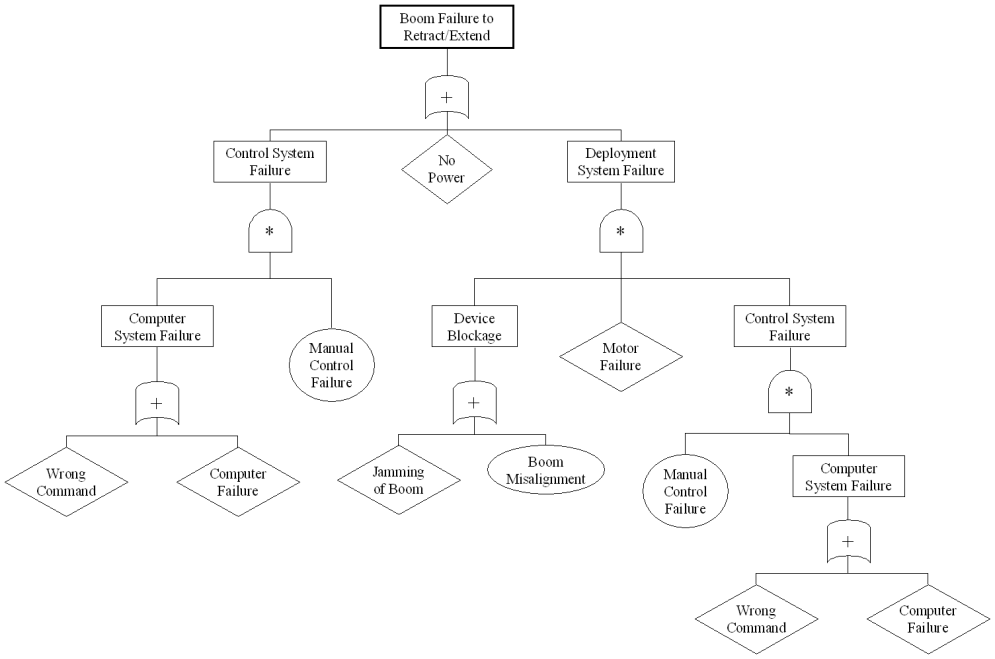

Figure 3-9: Preliminary boom extension or retraction failure fault tree

3.5.2 Contingency Plans

Not all failures can be avoided; therefore, contingency plans should be developed in the event that a failure does occur. In general, all systems designed for use on the space shuttle should be two-fault tolerant. Under this design principle, after the first fault, contingency procedures should be put into action so even if a second fault occurs, the system can be brought to a safe position. All shuttle payloads must always provide two-fault tolerance with respect to preventing payload bay door closure and assuring a safe return configuration of the orbiter [31]-[34]. As a third option, a contingency extra-vehicular activity (EVA) can be performed to affect the safe return of the orbiter and crew if other contingency plans fail. In addition, the boom system should be designed to be fail-safe, where the structure maintains sufficient residual strength or adequate fracture arrest capability to sustain loads experienced during any shuttle flight event in a damaged condition [29]. In the event of a shuttle contingency, the inspection system should be able to perform its intended task if called upon. For example, in the case of an abort-to-orbit scenario, the orbiter cannot reach the International Space Station (ISS), but the orbiter TPS may still need to be inspected before NASA is comfortable allowing the orbiter to re-enter the atmosphere.

NASA has developed several contingency plans for the SRMS in the event of a failure because the SRMS features a single string design with zero-fault tolerance [4],[33]. Because there is no collision detection or avoidance system that prevents an incorrect SRMS command from causing the system to hit the orbiter, precautions must be used to avoid collisions with the orbiter. The safety of each SRMS command

must be verified before it can be used to move the SRMS. To ensure that undesired motion of the SRMS does not exceed 2ft (0.61m), payload-dependent joint rate limits are used. Safing the SRMS entails stopping the arm motion by zeroing the joint rate commands and maximizing the current available to dynamically stop the joint motors [4]. Automatic braking may also be used to stop individual joint runaways. In the event that the SRMS prevents the closure of the payload bay doors, the SRMS assembly can be jettisoned with or without a payload attached. If it is merely the payload that is preventing proper SRMS storage in the payload bay, an unscheduled EVA can be performed to disconnect the payload GF from a failed SRMS EE. Positioning limitations are placed on the SRMS such that the arm and its payload cannot come closer to the orbiter structure than the limits provided by NASA [4]. In addition, the SRMS cannot be positioned where it cannot be safely jettisoned.

Additional contingency plans pertain to the boom system in the event of a deployment device-related failure. In the worst-case scenario, a deployment device failure prevents the closure of the orbiter payload bay doors. The boom deployment device design must feature two-fault tolerance as required for all shuttle payloads. If the deployment mechanism fails while deploying the boom, this could threaten the orbiter due to the unrestrained nature of the partially deployed structure. To deal with this type of failure, the deployment mechanism will have the capability to clamp the boom at any length either automatically or manually. If the deployment device failure cannot be fixed and the boom remains extended, then the boom may need to be jettisoned so that the orbiter can close the payload bay doors before re-entry. Efforts to fix the deployment device will be attempted before abandoning the boom. After

assessing the failure, the inspection procedure may continue using the fixed-boom approach. Before attempting to close the payload bay doors, the deployment device and partially deployed boom must be either stored in the orbiter payload bay or safely jettisoned away from the orbiter, if there is insufficient space in the cargo bay for the additional protruding boom. There may also be a provision that allows the boom to be jettisoned, while the deployment device is replaced in the cargo bay and brought back to earth for reuse after the cause of failure is identified and fixed. The booms are designed to last for a single mission; therefore, jettisoning the boom has a small impact on the boom-based inspection program because the booms are replaced after every mission; however, creating excess space debris should be avoided. Inspection and testing of the deployment device prior to flight will minimize the risk of failures while on-orbit. As a back-up plan, a spare boom could be stored in the payload bay due to its compact size depending on available cargo space. This system redundancy may be unnecessary depending on the results of the risk assessment of the deployable boom-based inspection system.

3.5.3 Testing and Verification

Testing and verification of the boom system is essential before it can be flown on the shuttle as an on-orbit inspection device. Some of the operational and test considerations for this system are the verification of failure modes through testing. The failure modes that should be investigated are shock, vibration, and dynamic loads resulting from operational conditions that affect the boom system. Tests should be designed to demonstrate that the boom system will not fail under any operating conditions including pre-launch, ascent flight, boom extension and retraction on orbit,

and landing. Under launch and landing environment conditions, the deployment device should be tested to verify that it adequately constrains the boom preventing blossoming or misalignment that could lead to jamming of the boom in the deployment device. In addition to physical testing, the boom should be subjected to an intense inspection program during manufacturing, assembly, and before flight to assure confidence in the boom structure.

To understand the limits of the boom system, at least one boom system should undergo qualification testing. If significant design changes are made to the system, then the qualification testing must be repeated to verify the new design. The types of testing often included in qualification testing are system vibration and shock, combined thermal and vacuum, electromagnetic interference, unbalanced magnetic moment, storage capability, and humidity resistance exposure testing.

Testing is also needed to determine the useful life of the boom. A boom element should be subjected to accelerated testing to find the structural limits under repeated extension and retraction. Typically, a boom should be tested to at least four times the expected operational life to ensure the reliability of the deployment system. From the results of this testing, the overstress limits of the boom structure can be avoided through limitation of the boom operational life. Miner's rule can be used to determine the number of extensions and retractions that can be performed before flight to adequately verify the without compromising the operational life of the boom. Assuming that each boom will be used for only one mission, the boom is subjected to n acceptance test deployments and has an operational life of N deployments as determined from the qualification deployment testing; then, the remaining life of the

boom is *1-n/N* or roughly *N-n* deployments. The inspection scheme must ensure that the boom will not be used beyond its operational deployment limit. The number of deployments per mission should be well below the total life of the boom to minimize the risk of failure due to over-deployment of the boom.

Acceptance testing should be performed to ensure proper functioning of the boom system. Functional testing of the system ensures the mechanical and thermal properties of the boom and qualifies specific booms before flight after eliminating early boom failures. Acceptable limits for compression, bending, and torsion loadings on the boom must be ensured so that the required boom stiffness and support in the transition region is provided. Acceptance testing should be performed on each deliverable boom prior to flight.

Chapter 4: Boom System Structural Analysis

The design of the extendable boom should be consistent with imposed requirements and as simple, direct, and foolproof as practical. This study focused on a preliminary boom design, where estimates of required structural parameters were made to determine the feasibility of the concept. The numbers calculated for the prototype boom are provided to illustrate the capability of this design and are not optimized to maximize its properties. Structural design is an iterative process and as more is known about specific boom requirements, the design should be updated to reflect those changes. The preliminary design presented in this document should be used as starting point towards a sophisticated flight-worthy design. Calculations presented in this section are analytical and should be validated through a series of analytical studies, component tests, system tests, and reliability assessments.

This chapter examines the boom system design process first by studying the boom geometry and selecting a reasonable prototype geometry for further analysis. A boom prototype was developed for illustration of the feasibility of this concept throughout this chapter. The anticipated worst-case loading conditions on the boom structure are discussed in relation to the material selection for the boom. The bending and torsional stiffness, boom dynamics, and buckling characteristics of the extendable boom are presented for the prototype boom design. This section concludes by discussing some other properties related to the extendable boom design such as thermal protective measures. After the boom is designed structurally, calculations pertaining to the stowage characteristics of the boom are presented. The final section

of this chapter discusses several fabrication and assembly processes to manufacture a boom such as the prototype boom designed throughout this chapter.

4.1 Boom Geometry

A preliminary design for the extendable boom was chosen based on the requirements for the boom to achieve the desired closed-section geometry selected for torsion stiffness and buckling prevention. A symmetric cross-section was chosen to prevent flexural-torsional buckling of the boom. A simple circle could not be used because the boom would be difficult to fabricate and nearly impossible to stow in a rolled configuration. A modification to the circle design added flanges to the cross-section allowing it to be flattened (Figure 4-1a). However, high stress concentrations at the flange-to-curve transition point would result upon collapse leading to premature structural failure of the boom structure. Thus, the sharp turns between the semi-circular halves and the flanges were replaced with fillets to produce the design shown in Figure 4-1b. Formed by two identical complementary parts joined along the flange portions, this nearly circular lenticular boom closed cross-section design can be flattened (Figure 4-2) and rolled onto a reel for deployment (Figure 4-3). This type of boom flattens as the flange portions move apart from each other collapsing the profile geometry. A different method to flatten the boom as it rolls onto the stowage reel is required compared to open cross-section designs commonly used.

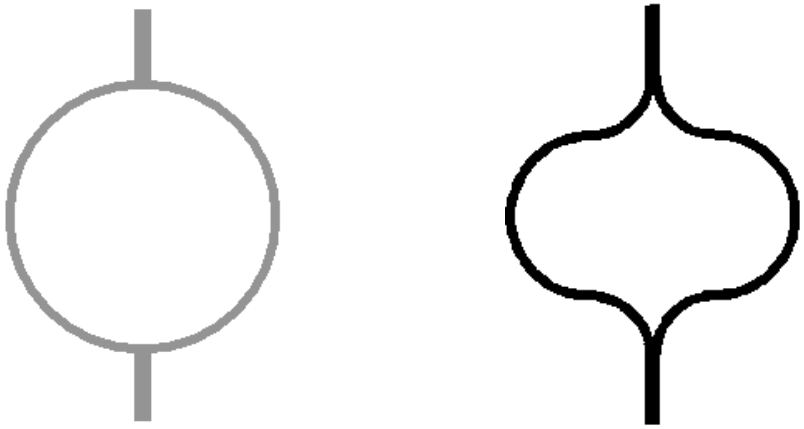

(a) *(b)*
Preliminary circular cross-section design *Final lenticular cross-section design*

Figure 4-1: Extendable boom cross-section geometry designs

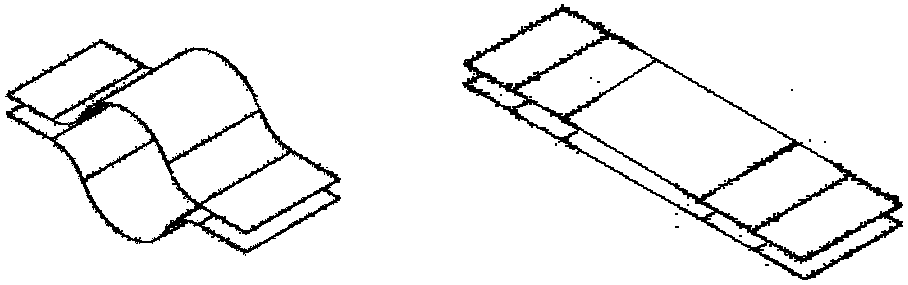

(a) *(b)*
Deployed shape *Collapsed shape*

Figure 4-2: Extendable boom geometry

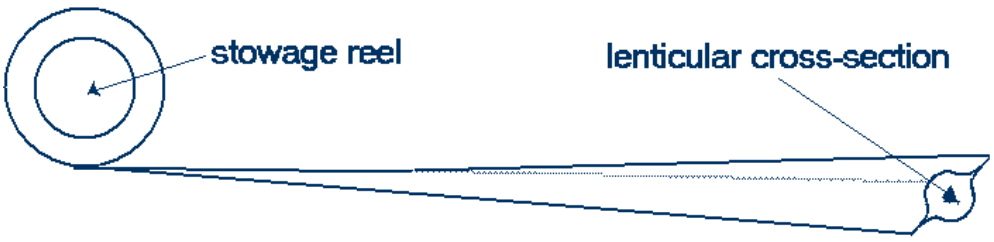

Figure 4-3: Boom stowage concept

4.1.1 Boom Profile Parameter Definitions

To understand geometrical properties of a boom with a lenticular cross-section, a parameterized model was developed. The symmetric cross-section features a curve with tangential fillet curves and flanges. A coordinate system for the boom was established, the *x*- and *y*-axes are shown in Figure 4-4 and the *z*-axis runs along the length of the boom to complete the right-handed coordinate system. The parameters used to define the boom cross-section were: the shape radius, *R*, the fillet radius, *r*, the center offset, *a*, the flange width, *b*, the profile thickness, *t*, the flange bond width, b_a, and the flange bond thickness, t_a (Figure 4-4). The model assumes a uniform thickness throughout the upper and lower profiles and allows for additional thickness due to the adhesive bonds along the flanges.

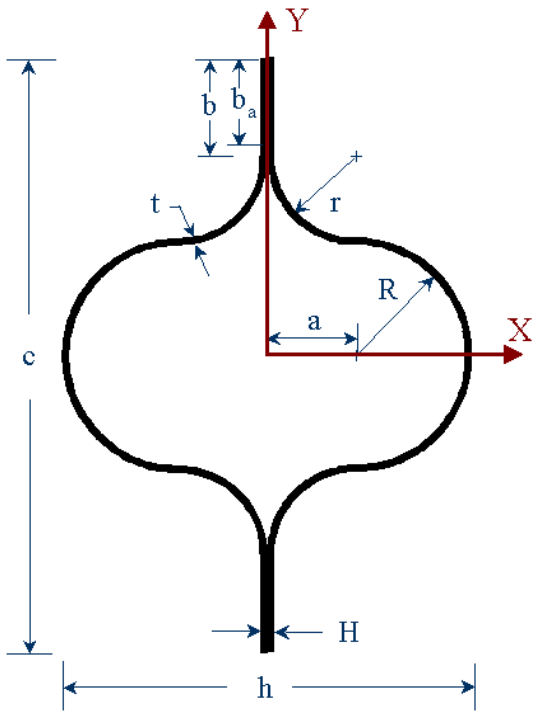

Figure 4-4: Extendable boom cross-section geometry

To further characterize the extendable boom geometry, quantities representing the overall boom dimensions in the expanded and collapsed configurations were defined based on the boom profile parameters (Figure 4-4 and Figure 4-5).

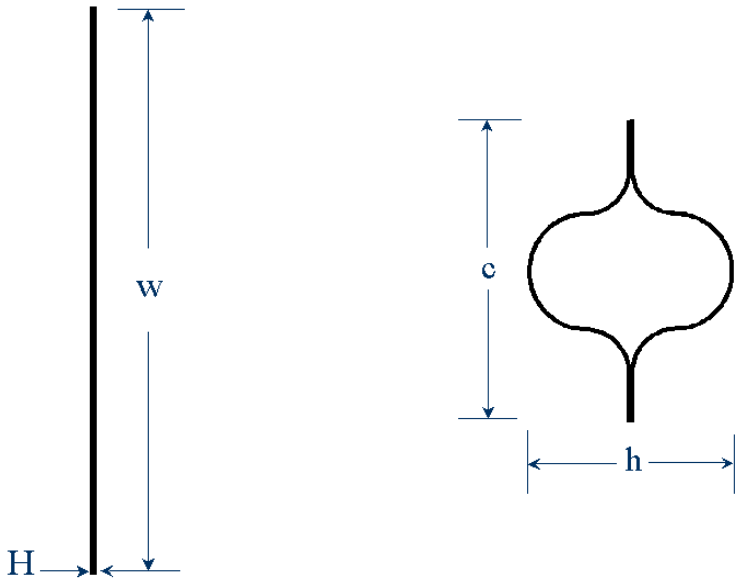

(a)
Collapsed configuration

(b)
Expanded configuration

Figure 4-5: Overall dimensions of the boom cross-section

In the collapsed configuration, the cross-section is defined by a flattened width, w, and thickness, H (Figure 4-5a). The equation for the flattened width,

$$w = 2b + 2\left(r - \frac{t}{2}\right)\phi_r + 2\left(R + \frac{t}{2}\right)\phi_R, \tag{4-1}$$

is a function of the cross-sectional geometrical parameters plus the fillet angle, ϕ_r, and the shape angle, ϕ_R. Because the geometry of the boom cross-section is more complex than quarter-circular fillets and semi-circular curves, the angles that define the arc-length of the fillet and curve segments were calculated to find the flattened width (Figure 4-6). These angles are given by,

$$\phi_r = \cos^{-1}\left(\frac{\frac{1}{2}(d_{in} + d_{out})}{R + \frac{t}{2}}\right) \tag{4-2}$$

and

$$\phi_R = \cos^{-1}\left(\frac{r - a - \frac{1}{2}(d_{in} + d_{out})}{r - \frac{t}{2}}\right), \tag{4-3}$$

where the inner fillet transition point, d_{in}, and the outer fillet transition point, d_{out}, are defined in the next section. The width of material used to create the boom cross-section based on the model parameters is given by w. The flattened thickness of the boom cross-section, H, is important in determining the boom stowage diameter as discussed later in this chapter. The equation of the flattened thickness,

$$H = 2t + t_a, \tag{4-4}$$

is equivalent to the thickness of the flange portion of the boom cross-section.

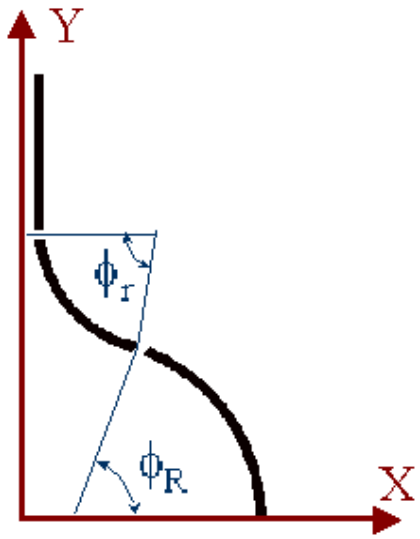

Figure 4-6: Boom cross-section fillet and curve angles

For the expanded cross-section, the overall dimensions are given by c and h (Figure 4-5b). The expanded width of the boom is

$$c = 2\left(b + \sqrt{(R+r)^2 - (r-a)^2}\right), \tag{4-5}$$

which is derived from the geometry, where c is twice the distance between the cross-section center and the outer edge of the flange. Similarly, the expanded thickness,

$$h = 2(R + a + t) + t_a, \tag{4-6}$$

is derived from the distance from the center of the cross-section to the outer edge of the curve segment.

4.1.2 Boom Profile Model and Cross-Section Properties

A program developed using MATLAB® technical computing software calculates the integral area moments of inertia of the boom cross-section for a given set of boom shape parameters. Due to symmetry about the x- and y-axis, only a quarter section of the boom geometry is required for analysis to obtain the geometrical properties. First, the boom section was divided into three segments: flange, fillet, and curve represented by the functions A(x,y), B(x,y), and C(x,y) respectively (Figure 4-7). The equation for the flange portion is a constant function parallel to the y-axis, therefore its equation is defined only by x and y limits to be discussed later. The fillet and curve equations are defined as portions of circles that share tangential points defined by d_{in} and d_{out} to be discussed later. The equations for the inner and outer fillet arcs as functions of both x- and y-coordinates are

$$B_{in}(x,y)=\left(x-\left(r+\frac{t_a}{2}\right)\right)^2+\left(y-\sqrt{(R+t)^2-(r-a)^2}\right)^2-r^2 \tag{4-7}$$

and

$$B_{out}(x,y)=\left(x-\left(r+\frac{t_a}{2}\right)\right)^2+\left(y-\sqrt{(R+t)^2-(r-a)^2}\right)^2-(r-t)^2, \tag{4-8}$$

where the boom model parameter definitions are given in Figure 4-4. Similarly, the equations for the inner and outer curve segments as functions of both *x*- and *y*-coordinates are

$$C_{in}(x,y)=\left(x-\left(a+\frac{t_a}{2}\right)\right)^2+y^2-R^2 \tag{4-9}$$

and

$$C_{out}(x,y)=\left(x-\left(a+\frac{t_a}{2}\right)\right)^2+y^2-(R+t)^2. \tag{4-10}$$

These functions are limited in the *x*- and *y*-directions to obtain the desired lenticular geometry. Functions representing the other quadrants of the boom cross-section are obtained through symmetry properties.

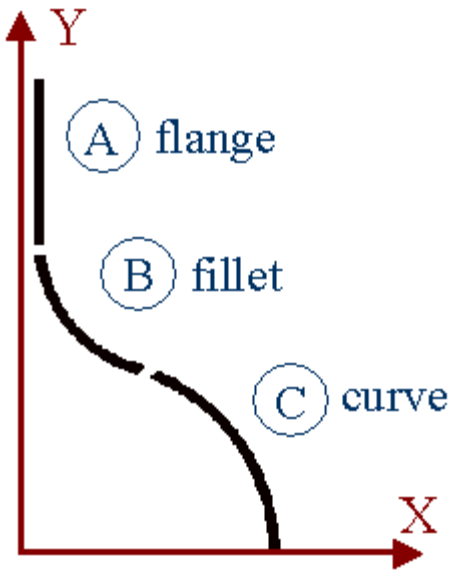

Figure 4-7: Boom cross-section geometry breakdown

The points of tangential intersection between the fillet and the curve segments were found using similar triangles (Figure 4-8). Representing the tangential point of intersection for the inner profile,

$$d_{in} = R\left(\frac{r-a}{R+r}\right), \tag{4-11}$$

and for the outer profile,

$$d_{out} = (R+t)\left(\frac{r-t-a}{R+r}\right). \tag{4-12}$$

With this definition for the tangential intersection points, the limits in the *x*- and *y*-directions of the cross-section were found with some additional geometry (Table 4-1). From these limits, the intersection points between each segment of the boom profile were determined. These limits were used to determine the area moments of inertia for the boom cross-section.

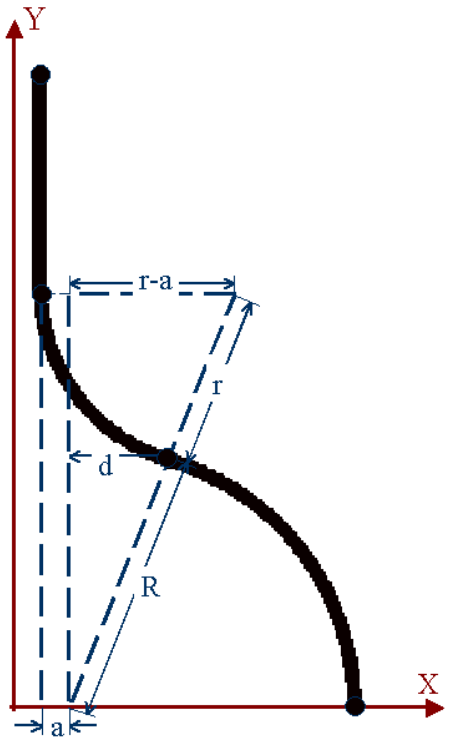

Figure 4-8: Curve tangential point derivation

Table 4-1: *X* and *Y* Limits for Lenticular Geometry

	***X* Limits**	***Y* Limits**
Adhesive Bond	$\left[0, \frac{t_a}{2}\right]$	$[-b_a, 0]+\left(b+\sqrt{(R+r)^2-(r-a)^2}\right)$
Flange	$[0,t]+\frac{t_a}{2}$	$[0,b]+\sqrt{(R+r)^2-(r-a)^2}$
Inner Fillet	$[0, d_{in}+a]+\frac{t_a}{2}$	$\left[\sqrt{R^2-d_{in}^2}, \sqrt{(R+r)^2-(r-a)^2}\right]$
Outer Fillet	$[t, d_{out}+a]+\frac{t_a}{2}$	$\left[\sqrt{(R+t)^2-d_{out}^2}, \sqrt{(R+r)^2-(r-a)^2}\right]$
Inner Curve	$[d_{in}+a, R+a]+\frac{t_a}{2}$	$\left[-\sqrt{R^2-d_{in}^2}, \sqrt{R^2-d_{in}^2}\right]$
Outer Curve	$[d_{out}+a, R+t+a]+\frac{t_a}{2}$	$\left[-\sqrt{(R+t)^2-d_{out}^2}, \sqrt{(R+t)^2-d_{out}^2}\right]$

Equations for the integral form of the boom cross-sectional area moments of inertia about the *x*- and *y*-axes were programmed into MATLAB® to determine the inertias for specific boom designs based on the boom profile parameters (Appendix A). The equations for each part of the boom cross-section, A(*x*,*y*), B(*x*,*y*), and C(*x*,*y*), were solved in terms of one variable, then integrated with respect to the other variable to obtain the desired area property. The inertias were calculated for the outer and inner profiles and the difference was taken to obtain the final inertia value. Simplified forms of the integral equations used to solve for the area moment of inertia about the *x*- and *y*-axis are

$$I_X = 2\left\{2\left(\int_{\text{flange}} y^2 A(y)dy\right) + 2\left(\int_{\text{fillet}} y^2 B(y)dy\right) + 2\left(\int_{\text{curve}} y^2 C(y)dy\right)\right\} \qquad (4\text{-}13)$$

and

$$I_Y = 2\left\{2\left(\int_{\text{flange}} x^2 A(x)dx\right) + 2\left(\int_{\text{fillet}} x^2 B(x)dx\right) + 2\left(\int_{\text{curve}} x^2 C(x)dx\right)\right\}, \qquad (4\text{-}14)$$

where the limits of integration used were the geometrical limits defined in Table 4-1. Similarly, the boom cross-sectional area,

$$A = 2\left\{2\left(\int_{\text{flange}} A(y)dy\right) + 2\left(\int_{\text{fillet}} B(y)dy\right) + 2\left(\int_{\text{curve}} C(y)dy\right)\right\}, \qquad (4\text{-}15)$$

was determined using the same curve definitions. These formulas utilize symmetry to reduce the calculations. In addition, it should be noted that these equations can be used to obtain the cross-sectional area and inertias for any reasonable values of the

boom profile parameters. For the complete integral formulations, please consult the MATLAB® programs in Appendix A.

Symbolic solutions of the integral equations (4-13), (4-14), and (4-15) were attempted, but were too cumbersome to obtain useful information for geometry optimization purposes using this boom profile definition. Other geometrical definitions have been developed for similar lenticular cross-sections [15]-[19]; however, in-depth details of these geometries were not disclosed. Future work could look at using trigonometric functions to reduce the number of parameters that define the boom cross-section geometry and to avoid issues with imaginary numbers that arise because of the square-root functions inherent in Cartesian circle functions.

To further simplify the boom cross-sectional geometry, the center offset was set equal to the fillet radius, which reduced the cross-section to a series of rectangular, quarter-pipe, and half-pipe segments (Figure 4-9). Symbolic formulas* for the area moments of inertia for the simplified cross-sectional geometry are given by

$$I_X = \frac{1}{3}tb^3 + 4tb\left(R + r + \frac{w}{2}\right)^2 + \pi tR^3 + 4tr^3\left(\frac{\pi\left(2R^2 + 3r^2 + 4rR\right)}{4r^2} - \frac{2(r+R)}{r}\right) \qquad (4\text{-}16)$$

and

$$I_Y = 4tR^3\left[\frac{\pi}{2}\left(\frac{r}{R}\right)^2 + \frac{\pi}{4} + \frac{2r}{R} + \left(\frac{3\pi}{4} - 2\right)\left(\frac{r}{R}\right)^3\right]. \qquad (4\text{-}17)$$

The cross-sectional area of the simplified geometry is

$$A = 2t\left(2b + \pi\left(r + R\right)\right). \qquad (4\text{-}18)$$

* Farley, R., "Lenticular Boom," MS PowerPoint presentation, personal communication, 9 June 2003.

It is important to note that equations (4-16), (4-17), and (4-18) only hold when the center offset, *a*, is equal to the filet radius, *r*. To illustrate this, a plot was generated showing the variation in the actual value of the boom inertia determined from the integral equations (4-13) and (4-14) versus the center offset parameter, *a*, for values from zero to the fillet radius (Figure 4-10). For this plot, all other parameters were held constant. As seen from the results, there is a significant difference in the boom stiffness based on cross-sectional orientation. By introducing an offset, making the center offset parameter, *a*, nonzero leads to more balanced inertias. It is assumed that there is no bond-line thickness in this analysis.

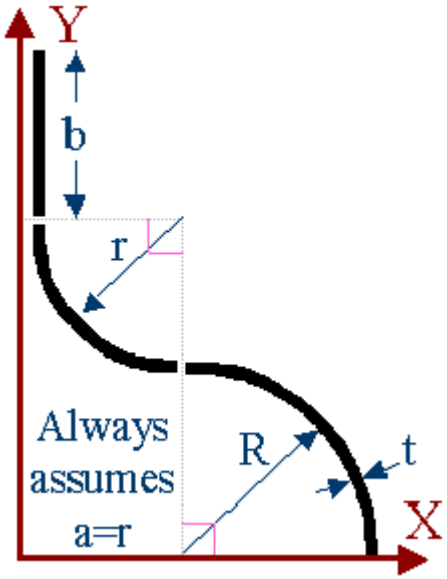

Figure 4-9: Simplified boom cross-sectional geometry

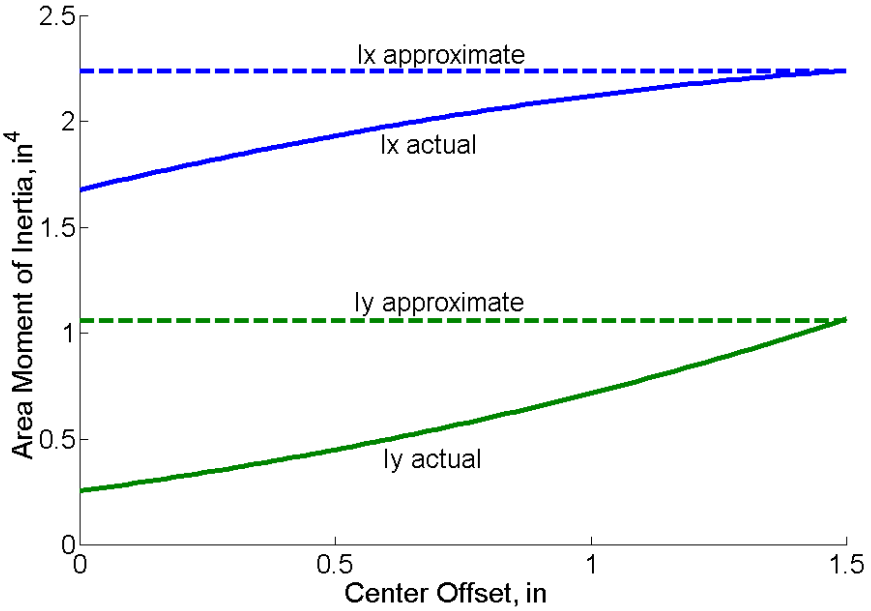

Figure 4-10: Comparison of actual and approximate area moments of inertia versus value of the center offset parameter

4.1.3 Geometry Optimization

To determine the best geometrical parameters for the extendable boom, several trade-off analyses were performed to select the best initial boom prototype design. First, the prototype was chosen to have a center offset, *a*, equal to the fillet radius, allowing for the use of the simplified equations (4-16), (4-17), and (4-18) for the cross-sectional inertias and area.

Selection of the cross-sectional geometrical parameters was based on similar prototype designs[†] [15]-[19], where the flange width, *b*, and fillet radius, *r*, parameters are related to the shape radius, *R*. To determine the best ratios of these parameters to the shape radius, trade-off plots of area moment of inertia versus shape radius were created to compare various ratios of flange width and fillet radius to

[†] Farley, R., "Lenticular Boom," MS PowerPoint presentation, personal communication, 9 June 2003.

shape radius. In the first case, the fillet radius-to-shape radius ratio (*r/R*) was assumed to be constant at 0.75 and the flange width-to-shape radius ratio (*b/R*) was varied from 0.1 to 0.9 to obtain the boom inertia values for shape radii between 0.5in and 4in (1cm and 10cm) (Figure 4-11). The curves on this plot, show that as the shape radius increases, the area moments of inertia also increase as expected. Also, the area moment of inertia about the *y*-axis, I_Y, remains constant since its simplified equation (4–17) does not depend on the flange width, *b*. For small *b/R* ratios (*b/R=0.1-0.3*), the boom inertias are nearly equal about both axes; however, dependent on the value of the shape radius, these ratios may represent flange width values having inadequate flange bond area. A flange width must be chosen to provide the necessary bond area to ensure proper adhesion and shear strength between the two complementary boom half-profiles. For larger *b/R* ratios (*b/R>0.3*), the boom inertia about the *x*-axis begins to rapidly increase. At large shape radii (*R>2in (5cm)*), the inertia about the *x*-axis dominates. The limiting factor of the boom becomes the inertia about the *y*-axis for stiffness and dynamics considerations. It is desirable to minimize the width of the flanges to reduce the overall stowage volume, yet the flanges must be wide enough to engage the deployment mechanism drive rollers, to provide adequate bonding surface area between the boom half-profiles, and to contain the strain energy stored within the boom [19].

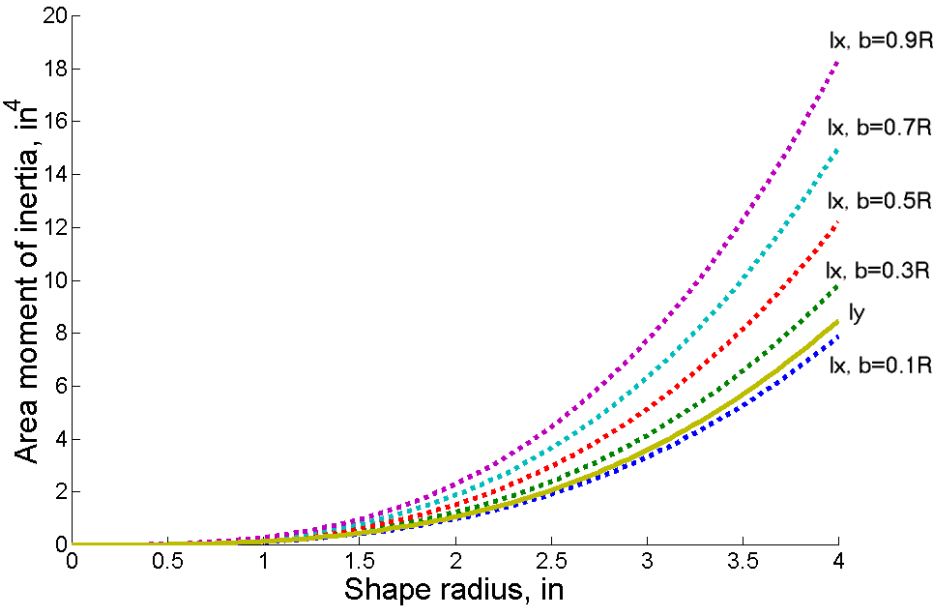

Figure 4-11: Trade-off plot of boom inertia versus shape radius, where the flange width varies with the shape radius and the fillet radius-to-shape radius ratio is 0.75

Similarly, another trade-off plot was generated where *b/R* was set to 0.5 and *r/R* was varied from 0.5 to 1 to obtain the boom inertia values for shape radii between 0.5in and 4in (1cm to 10cm) (Figure 4-12). This plot shows that as the *r/R* ratio is increased, the area moments of inertia increase at a faster rate. Because the *b/R* ratio was held constant, the relative difference between the inertias about the *x*- and *y*-axis remained approximately the same as the *r/R* ratio was increased. Another interesting feature of the geometry shown in this plot is that for adjacent values of the *r/R* ratio, the inertia curves almost overlap. For example, the curves representing I_X when *r/R=0.5* and I_Y when *r/R=0.75* nearly overlap; however, as the shape radius increases, the curves begin to diverge more from one another.

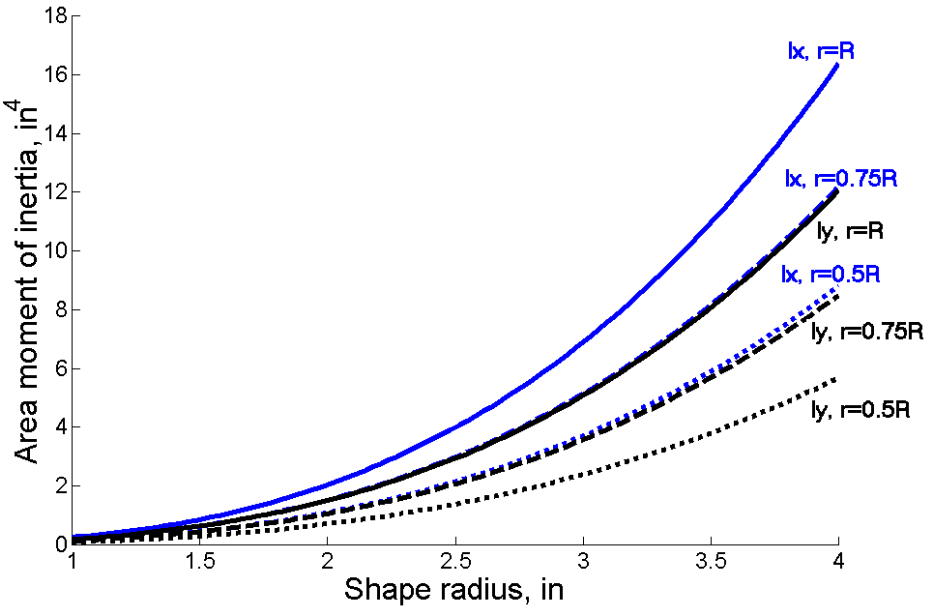

Figure 4-12: Trade-off plot of boom inertia versus shape radius, where the fillet radius varies with the shape radius and the flange width-to-shape radius ratio is 0.5

Further examination of the boom inertia properties for a specific shape radius, *R*, was conducted to obtain additional information about the *b/R* and *r/R* proportions. A shape radius of 2in (5cm) was assumed and the *b/R* and *r/R* ratios were varied to determine the best boom inertia combinations (Figure 4-13). In this plot, a gird was created to show the relationships between the different flange width and fillet radius proportions in relation to the boom inertia about the *x*- and *y*-axes. Because the formula for I_Y, equation (4-17), does not depend on the flange width, *b*, the boom inertia about the *y*-axis remains constant for all values of the flange width. In the case of varying flange width, *b*, the inertia about the *x*-axis increases quicker than the inertia about the *y*-axis. Nearly equal stiffness about both of the principal axes (*x* and *y*) is desired; therefore, nearly equal inertias are preferred. Stiffness of the boom can be tailored through material selection and fiber orientation; thus, equal inertias are not

required, but if equal inertias are achievable, they allow for the use of materials whose properties are equal in the principal axes directions such as composite weave materials. From the plot, the parameter ratios of 0.5 and 0.75 were chosen for *b/R* and *r/R* respectively. These values correspond to similar inertias about the *x*- and *y*-axes.

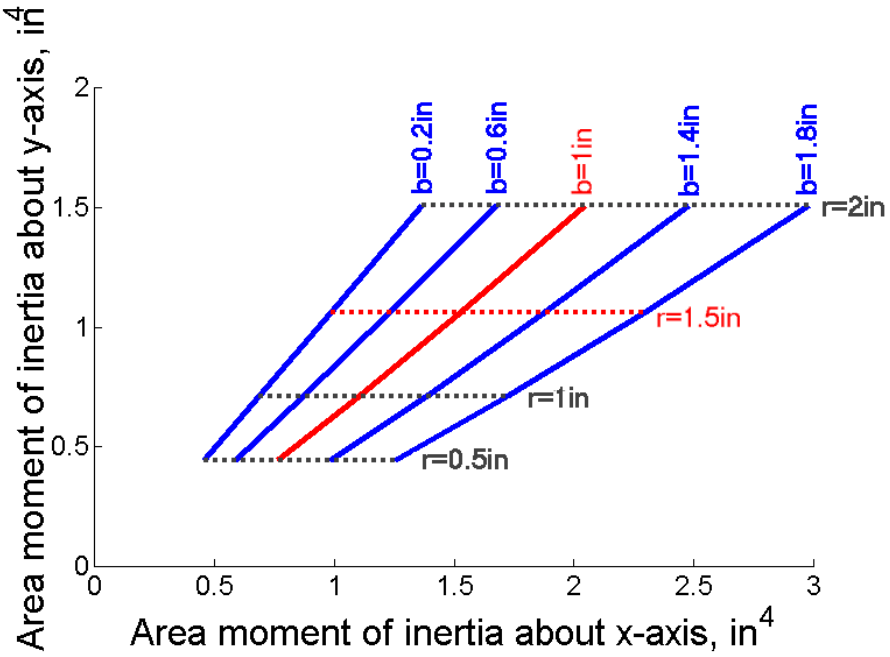

Figure 4-13: Trade-off plot of boom inertia about *y*-axis versus boom inertia about *x*-axis, where flange width and fillet radius are proportional to the shape radius

As a result of this trade-off analysis, a prototype geometry was selected to illustrate the feasibility of this extendable boom design. This prototype boom design was not fully optimized, yet it meets the system requirements making it a reasonable design option. The geometrical parameters for the boom prototype model are given in Table 4-2. The shape radius, *R*, was selected to be 2in (5cm). Based on the trade-off analysis, the fillet radius, *r*, was set equal to three-quarters of the shape radius, *R*. The

center offset, a, is equal to the fillet radius validating the use of the simplified inertia and area equations. The wall thickness, t, is the total thickness of each half profile of the boom prototype, so if multiple layers are used to make each half-profile, t is the sum of each ply-layer thickness. It was assumed that there is no bond-line thickness, t_a, from the adhesive used to bond the two parts to create the cross-section. The flange length, b, is equal to one-half of the shape radius, R, based on the trade-off analysis. It was assumed that to provide adequate bond area, the flange width, b, must be at least 1in (2.5cm); therefore, smaller b/R ratios were not selected although they may have provided a better balance of the boom inertias. The bond width, b_a, was assumed to be three-quarters of the flange width, b, to avoid adhesive interference with the fillets of the boom. The length of the prototype, L, is assumed to be 720in (1830cm) to provide adequate reach capability to the SRMS. This boom length exceeds the length of the orbiter payload bay, which is an added benefit of the deployable boom concept. To refine the boom length, further examination of the system kinematics is required to ensure that all areas of the orbiter thermal protection system (TPS) are accessible via the boom extension. The remaining geometrical parameters were determined using the equations developed in section 4.1.1. In comparison to another lenticular boom design, the expanded dimensions of the German DLR booms are approximately 5.9in by 4.3in (15cm by 11cm) [15]. Despite having larger expanded dimensions than the DLR boom design, the boom prototype design developed in this section has approximately the same ratio, 1.3, between the expanded width and thickness, c/h, of the boom as the DLR boom design.

Table 4-2: Prototype Geometrical Parameters

Parameter	Symbol	Value
Shape radius	R	2in (5.1cm)
Fillet radius	$r=0.75R$	1.5in (3.8cm)
Center offset	$a=r$	1.5in (3.8cm)
Profile thickness	t	0.01in (0.025cm)
Flange bond thickness	t_a	0in (0cm)
Flange bond width	$b=0.5R$	1.0in (2.5cm)
Bond width	$b_a=0.75b$	0.75in (1.9cm)
Total boom length	L	720in (1830cm)
Shape angle	ϕ_R	90° (1.57rad)
Fillet angle	ϕ_r	90° (1.57rad)
Flattened width	w	13in (33cm)
Flattened thickness	H	0.02in (0.051cm)
Expanded width	c	9.0in (23cm)
Expanded thickness	h	7.02in (18cm)

From the established prototype geometry, the cross-sectional area and moments of inertia were calculated and tabulated (Table 4-3). This table shows a direct comparison between the actual and estimated cross-section properties. The actual properties were calculated using a MATLAB® program (Appendix A) created to solve the integral forms of the inertia and area equations. The estimated values were determined using the simplified geometry assumption, because the center offset is equal to the fillet radius, thus creating quarter-circular sections that have known symbolic inertia equations. The direct comparison between the two methods for the case of the prototype geometry results in small errors. The most error occurs between the actual and estimated values of the inertia about the *y*-axis, I_Y. This may be because the equation for I_Y, (4-17), does not include any contribution from the flanges of the boom profile.

Table 4-3: Prototype Area Property Comparison

	Actual	Estimate	Error
Inertia about *x*-axis, I_X	1.5264in^4	1.5252in^4	0.08%
Inertia about *y*-axis, I_Y	1.0672in^4	1.0622in^4	0.5%
Cross-sectional area, *A*	0.2599in^2	0.2599in^2	~ 0

4.2 Boom Design Structural Characteristics

Now that the boom geometry has been defined, the structural characteristics of the boom can be calculated. This section examines the process of material selection for the boom prototype and the anticipated worst-case loading conditions, which determine the required structural characteristics of the boom. Next, the structural characteristics related to the boom design such as bending and torsional stiffness, boom dynamics, and buckling concerns are addressed. Lastly, other design considerations related to the structure are mentioned along with some possible solutions.

4.2.1 Material Selection

The material selection for the boom is not only based on mass and stiffness requirements, but also on the flexibility characteristics required to ensure proper deployment. The material must also pass spaceflight qualification tests to ensure that the material will not interfere with instruments or degrade significantly in the space environment.

The boom must be lightweight and stiff, yet flexible enough to flatten and roll onto a stowage reel. The boom is fabricated such that the expanded or deployed configuration of the boom is stress-free. The stresses induced due to flattening and

rolling of the boom structure for stowage in addition to longitudinal stiffness requirements of the deployed boom dictate that an ideal material has orthotropic properties [19]. Fiber-reinforced composite materials have orthotropic properties and offer increased stiffness and flexibility characteristics, often with significant mass savings, compared to metallic materials. In addition, composite materials provide considerable flexibility in selecting material properties through the selection of an optimized sequence of fiber orientations depending on the application; therefore, it is possible to meet the extendable boom structural requirements through material lay-up. Another requirement on the boom material is that it must resist visco-elastic relaxation while stowed to ensure proper structural characteristics when the boom is deployed.

For illustration purposes, a common aerospace carbon-fiber plain weave composite material was chosen for the boom prototype. The material chosen for the prototype design was the T300 (1K)/RS-3 plain weave fabric laminate manufactured by YLA [45]. The properties of this material are given in Table 4-4, where *1* and *2* represent the principal fiber directions. All of the properties provided in Table 4-4 are normalized to 60% fiber volume except for Poisson's ratio. These values are used merely as guidelines for the boom prototype design; the boom prototype should be experimentally tested to verify material and structural properties before spaceflight. This composite material is composed of plain-woven T300 carbon fibers in a polycyanate resin system (RS-3). The RS-3 has extensive spaceflight history and is fully spaceflight qualified [46].

Table 4-4: YLA T300 (1K)/RS-3 Plain Weave Fabric Laminate Properties

Property	Symbol	Value
Tensile moduli	E_{11}, E_{22}	9.7×10^6psi (6.7×10^{10}Pa)
In-plane shear modulus	G_{12}	0.70×10^6psi (4.8×10^9Pa)
Major Poisson's ratio	ν_{12}	0.30

The adhesive used to join the two boom half-profiles together to form the lenticular geometry must be flexible to minimize shear stresses that will occur in the stowed configuration particularly for a tight stowage diameter. For the purposes of this study, the bond-line thickness was assumed to be zero allowing the properties of the bonding adhesive to be neglected to simplify calculations in the demonstration of the design feasibility.

The prototype boom is made from tow profile halves that are bonded together along the flange segments. Each half profile consists of two composite weave plied aligned along the *y*- and *z*-axes of the boom (Figure 4-14). The principal fiber direction *1*- and *2*-coordinates coincides with the *z*- and *y*-coordinates of boom. Each ply of composite weave was assumed to have a thickness of 0.005in (0.013cm). This lay-up was chosen to create high bending and torsional stiffness and approximate thermal neutrality [15]. Adding plies or changing the ply-orientation of the lay-up can be used to gain added structural characteristics such as increased off-axis stiffness of the extendable boom. The lay-up of the boom prototype was chosen for its simplicity and ease of fabrication. A schematic of the lay-up of the flange portion of the boom prototype is shown in Figure 4-15, where layer 3 corresponds to the adhesive bond and the other layers correspond to the composite boom material. In the case of the prototype boom example, the third layer has a thickness of zero, therefore does not

contribute to the structural properties of the boom. Further iterations of the boom design should include an adhesive material that complements the boom material. The adhesive bonds may add stiffness and damping properties to the extendable boom structure.

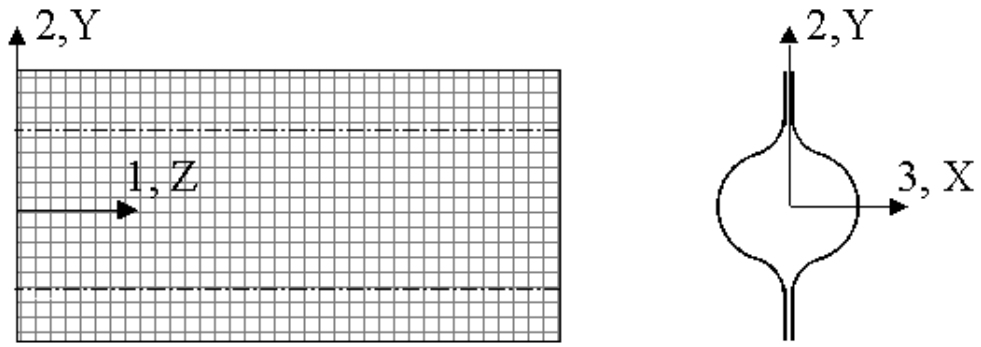

Figure 4-14: Principal fiber coordinates and material orientation

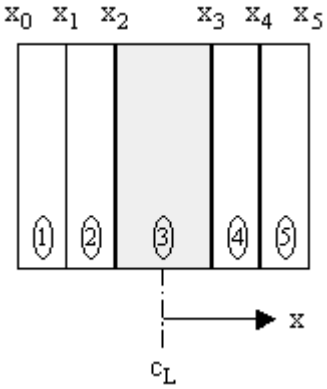

Figure 4-15: Boom prototype lay-up of a flange segment

The initial design of the boom prototype is based on data for material properties provided by the material manufacturer [45],[46]. Samples of the proposed laminate construction should be produced and tested to verify the material properties. Following testing, the design is re-evaluated with the revised property values and the

laminate modified if necessary. Finally, a full-size boom prototype is built and tested under representative load cycles for the operational lifetime of the boom system.

All materials used for the extendable boom must undergo and pass spaceflight qualification testing to ensure its compatibility with the space environment. Spaceflight qualification testing focuses on material outgassing characteristics to establish the effect of the vacuum environment of space on the material to protect susceptible instruments or surfaces. When non-metallic materials are exposed to the vacuum of the space environment, these materials vent gases such as silicones and organics in a process called outgassing. The standard outgassing requirement is that a material "must not lose more than 1% of its mass nor transfer more than 0.1% of its mass to an adjacent cooler surface under standard space-simulating conditions" [21]. This requirement is measured by two indices: total mass loss (TML) and volatile condensable material (VCM). These indices are measured using standardized tests and equipment to get robust results. To pass spaceflight qualification testing, the boom structural materials must have a TML index less than 1% and a VCM index less than 0.1% [21].

4.2.2 Worst Case Boom Loading Conditions

The preliminary structural requirements for the deployable boom were determined assuming that the shuttle remote manipulator system (SRMS) is rigid which allows the boom to be modeled as a cantilevered beam. Although the SRMS is flexible, it was assumed rigid for this analysis to develop preliminary structural requirements and as the design is refined, the flexibility of the SRMS should be taken into account. The cantilever beam assumption is valid because, as stated previously,

the boom will be clamped by the deployment mechanism at its root. The preliminary model assumes that the boom follows cantilevered bending under tip and distributed loads (Figure 4-16).

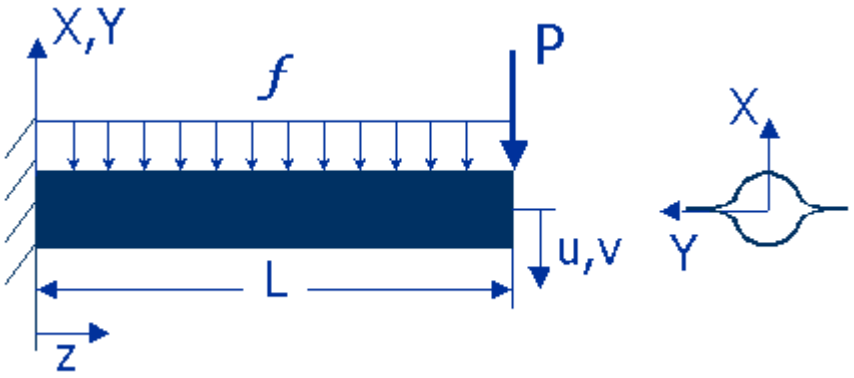

Figure 4-16: Load diagram of the extendable boom

The analysis presented in this chapter is based on basic engineering (Euler-Bernoulli) beam theory with clamped-free boundary conditions. Euler-Bernoulli beam theory accounts for inertia forces due to the transverse translation and neglects the effect of shear deflection and rotary inertia [47]. The important assumptions of this theory are:

- beam cross-sections remain planar and orthogonal to the neutral axis;
- longitudinal fibers along the beam do not compress each other;
- rotational inertia within the beam is neglected.

The boundary conditions for the cantilevered beam at the clamped end are that there is no displacement or beam slope at the attachment point. The free end is not constrained.

Analyses of the load diagram (Figure 4-16) for the worst-case loading scenario results in the determination of the reaction shear force and moment at the clamped root of the beam. The worst-case loading scenario occurs when the boom is

oriented such that bending occurs about the *y*-axis due to its lower area moment of inertia. The equation for the shear force in the beam as a function of the deployed length, *z*, is

$$V(z) = P_x + f_x(L - z), \tag{4-19}$$

where P_x is the tip load due to the tip mass, f_x is the distributed load due to the boom mass, and L is the fully deployed-length of the boom. The moment equation for the boom under the loading shown in Figure 4-16 is given by

$$M_Y(z) = P_x(L - z) + \frac{1}{2} f_x(L - z)^2, \tag{4-20}$$

where the moment varies with the deployed boom-length, *z*. The derivative of the moment equation gives the equation for shear force. The moment equation is used to determine the boom stiffness.

To find the minimum stiffness requirements, the boom model was subjected to the worst-case loading scenario (Table 4-5). For this case, the boom is fully deployed to its maximum length of 720in (1830cm). Under the worst-case loading, the boom is decelerated from the maximum loaded SRMS velocity to a stand still over a one second time period. This corresponds to a deceleration, a_{SRMS}, of 2.4in/s^2 (6.1cm/s^2) applied to the boom. The mass at the tip of the boom, M_{tip}, was assumed to be 1.0slug (15kg), which leads to a 0.2lb (0.9N) tip force, P_x. The boom mass per length, *m*, was chosen as 4.5x10^{-4}slug/in (2.5x10^{-6}kg/cm) based on the density and flattened dimensions of the boom prototype. This corresponds to a constant distributed load of 8.9x10^{-5}lb/in (1.6x10^{-4}N/cm) along the length of the boom. The maximum deflection, u_{max}, allowed at the tip of the boom was 4in (10cm). The worst-case loading scenario

is when the boom is oriented in such a way that the deceleration causes the forces to create bending moments about the *y*-axis, which has the lower area moment of inertia.

Table 4-5: Summary of Worst Case Loading Parameter Values

Parameter	Symbol	Value
SRMS maximum velocity	v_{SRMS}	2.4in/s (6.1cm/s)
SRMS stopping time	t_{SRMS}	1s
Acceleration	$a_{SRMS} = v_{SRMS} / t_{SRMS}$	2.4in/s^2 (6.1cm/s^2)
Tip mass	M_{tip}	1.0slug (15kg)
Tip load	P_x	0.2lb (0.9N)
Distributed mass	m	4.5x10^{-4}slug/in (2.5x10^{-6}kg/cm)
Distributed load	f_x	8.9x10^{-5}lb/in (1.6x10^{-4}N/cm)
Maximum deflection	u_{max}	4in (10cm)
Boom length	L	720in (1830cm)

4.2.3 Bending Stiffness Design

The necessary bending stiffness of the boom can be derived from cantilever bending equations and elementary beam theory. Using the moment-curvature relationship, the differential equation for the cantilevered boom under distributed and tip loading assuming pure bending about the *y*-axis is

$$\frac{d^2u}{dx^2} = \frac{M_Y(z)}{EI_Y} = \frac{P_x(L-z) + \frac{1}{2} f_x (L-z)^2}{EI_Y}, \qquad (4\text{-}21)$$

where u is the deflection of the boom tip in the *x*-direction, E is the boom material elastic modulus, and I_Y is the area moment of inertia about the *y*-axis. Solving equation (4-21) for the displacement in the *x*-direction, u, as a function of the boom deployed-length, x, yields

$$u(z) = \frac{1}{24EI_Y}\left(f_x z^4 - 4\left(P_x + f_x L\right) z^3 + 6\left(2P_x L + f_x L^2\right) z^2 \right), \qquad (4\text{-}22)$$

assuming the boundary conditions of a cantilevers boom, where the displacement, u, and its derivative, du/dx, are zero at the root (x=0). To find the required stiffness, EI_Y, for a given maximum deflection in the x-direction, u_{max}, equation (4-22) was evaluated at $x=L$ and solved in terms of the stiffness,

$$EI_Y = \frac{1}{24u_{\max}}\left(3 f_x L^4 + 8P_x L^3\right). \qquad (4\text{-}23)$$

The bending stiffness required of the boom under the worst-case loading scenario was calculated to be $7.1\text{x}10^6$lb-in^2 ($2.0\text{x}10^8$N-cm^2) assuming a maximum vertical deflection of 4in (10cm). This value determines the required area moment of inertia, I_Y, for the chosen material to achieve the desired stiffness.

In addition, the orientation of the boom must be taken into account. The stiffness requirement was based off the worst-case loading scenario, which assumes bending about the weaker y-axis; however, if the boom is positioned relative to the orbiter in such a way that the deflections about this axis pose little threat of damage, the overall stiffness requirement may be reduced for that orientation. From the cross-sectional geometry (Figure 4-4), the boom is stiffer about the x-axis. If the boom were oriented such that the x-axis of the cross-section is parallel to the surface of the orbiter, then the maximum deflection in the y-direction (towards the orbiter) would be less than maximum deflection in the x-direction, u_{max}. Therefore, the desired boom orientation is with its stiffer x-axis parallel to the orbiter surface.

To determine the desired boom inertia for the prototype design, the boom stiffness calculated was used for comparison to the inertias calculated for the boom

prototype (Table 4-2). The desired minimum area inertia is 0.73in^4 (30cm^4) calculated from the boom stiffness requirement, EI=7.1x10^{6}psi (4.9x10^{10}Pa) divided by the carbon weave composite material elastic modulus, E=9.7x10^{6}psi (6.7x10^{10}Pa). The boom inertias about the *x*- and *y*-axes for the prototype were 1.5in^4 (58cm^4) and 1.1in^4 (46cm^4) respectively. These inertia values are well above the stiffness requirement. In fact, the expected deflection in the *x*-direction is 1.9in (4.8cm) and in the *y*-direction is 2.6in (6.6cm) for the boom prototype. As expected, the deflection in the *y*-direction is greater than the *x*-direction due to the smaller area moment of inertia about the *y*-axis.

4.2.4 Torsion Stiffness Design

The torsional stiffness requirements for the extendable boom are dependent on many variables pertaining to the inspection equipment and technique. For example, the sensor and camera payload package located at the tip of the boom may induce torsion forces on the boom that must be counteracted. Also, dependent on the type of inspection being carried out, the orbiter may be required to maintain a particular attitude, which may include additional loading on the boom due to thruster firings from the orbiter control systems. For the case of a laser-based inspection system, the surface of the orbiter under inspection may need to be directed away from the earth's surface to avoid light inference. For a visual-based inspection system, the sun angle incident on the inspection region may be critical to the analysis of the inspection data. To maintain the orbiter position, attitude adjustments must be made using small control thrusters located in various locations on the orbiter. When a thruster is fired, the boom extension may start to oscillate and could possibly see torsional reaction

forces. Therefore, the torsional stiffness of the boom extension is important to characterize to define the thresholds of tolerable torsion forces on the boom.

The torsional stiffness for the boom prototype can be calculated knowing the material and geometrical properties of the boom cross-section. The torsional stiffness, *GJ*, is the product of the in-plane shear modulus of the boom material, *G*, and the polar moment of inertia about the *z*-axis, J_Z, which is the sum of the area moments of inertia about the *x*- and *y*-axes. The in-plane shear modulus, *G*, for the carbon weave material selected for the boom prototype design, whose properties are given in Table 4-4, is 0.70×10^6psi (4.8×10^9Pa). For the prototype, with the cross-sectional parameters defined in Table 4-2, the polar moment of inertia about the *z*-axis, J_Z, is 2.6in^4 (110cm^4). From these values, the torsional stiffness of the boom prototype was calculated as $1.8 \times 10^6\text{lb-in}^2$ ($5.2 \times 10^7\text{N-cm}^2$).

To further examine the effect of torsion forces acting on the boom, the internal torque relative to the twist angle of the boom was calculated for the boom prototype. The twist angle, ϕ, of the boom is the angle of twist of the tip of the boom with respect to the clamped end expressed in radians. The equation for internal torque relative to twist angle is

$$\frac{T}{\phi} = \frac{GJ_z}{z} \tag{4-24}$$

where, *G* is the in-plane shear modulus of the boom material, J_z is the polar moment of inertia about the *z*-axis, and *z* is the deployed length of the boom. To illustrate that the boom is able to withstand less internal torque as the boom is deployed, while maintaining a constant twist angle, a plot of the internal torque relative to the twist

angle versus the deployed boom length was created (Figure 4-17). As expected, when the boom is fully deployed (*L=720in (1830cm)*), the torsional stiffness of the boom is the smallest. To further demonstrate this, the internal torque resulting from an angle of twist, ϕ, of one degree over the fully deployed boom length, 2.4×10^{-5}rad/in (9.5×10^{-6}rad/cm), is 44lb-in (500N-cm).

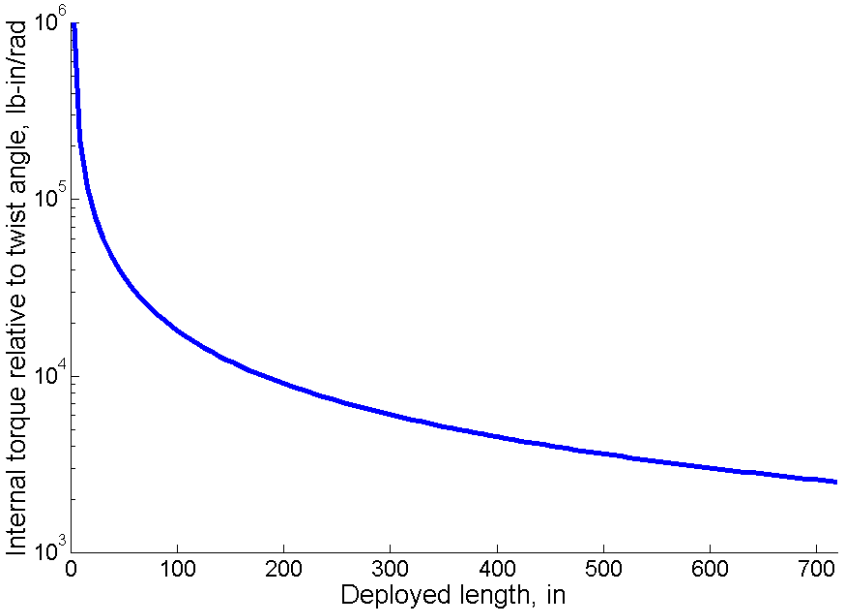

Figure 4-17: Boom internal torque relative to twist angle versus the deployed boom length

From these calculations, the torsion ability of the extendable boom is characterized. Further work could look at adjusting the material lay-up to accommodate larger torsion loads that may result from the inspection payload structural requirements.

4.2.5 Dynamics Considerations

The boom structure is subject to dynamic loads that vary throughout different operational modes of the normal inspection procedure. To understand the dynamics

for the boom extension to the SRMS, the natural frequency of the boom was calculated. The equation used to determine the approximate natural frequency, λ, as the boom is deployed is given by [48]

$$\lambda = \frac{1.732}{2\pi}\sqrt{\frac{EIa_{SRMS}}{Pz^3 + 0.236\,fz^4}}, \tag{4-25}$$

where E is the elastic modulus of the boom material, I is the area moment of inertia, a_{SRMS} is the applied acceleration, P is the boom tip load, f is the constant distributed load along the boom, and z is the deployed-length of the boom. A plot was created showing the frequency versus the deployed length of the boom for vibration about the x- and y-axes (Figure 4-18). As seen from the plot, the natural frequency decreases rapidly as the boom is deployed. When the boom is fully deployed, the natural frequency of the boom is approximately 0.5Hz about the x-axis and 0.4Hz about the y-axis. According to NASA flight rules for use of the SRMS, the major structural vibration frequencies of a payload and its grapple fixture interface, when cantilevered from the GF, must be greater than or equal to 0.2Hz for payloads under 1000lb_m (450kg) [4]. The boom prototype meets this requirement; however, experimental testing of the structure must be performed to verify these frequency values. The natural frequency may also limit the speed of deployment, so that the resonant frequencies of the boom are avoided. Methods to minimize the structural vibration may include adding damping materials to the boom possibly along the adhesive bonds between the two half-profiles to help dissipate structural vibrations. Additional stiffness could be added locally to the boom through doublers that may help limit the amplitude of vibration especially when the boom is fully deployed to prevent the

potential of the boom buckling under vibration loading. Also, by selecting a boom geometry with equal area moments of inertia, the vibration of the boom may be evenly distributed.

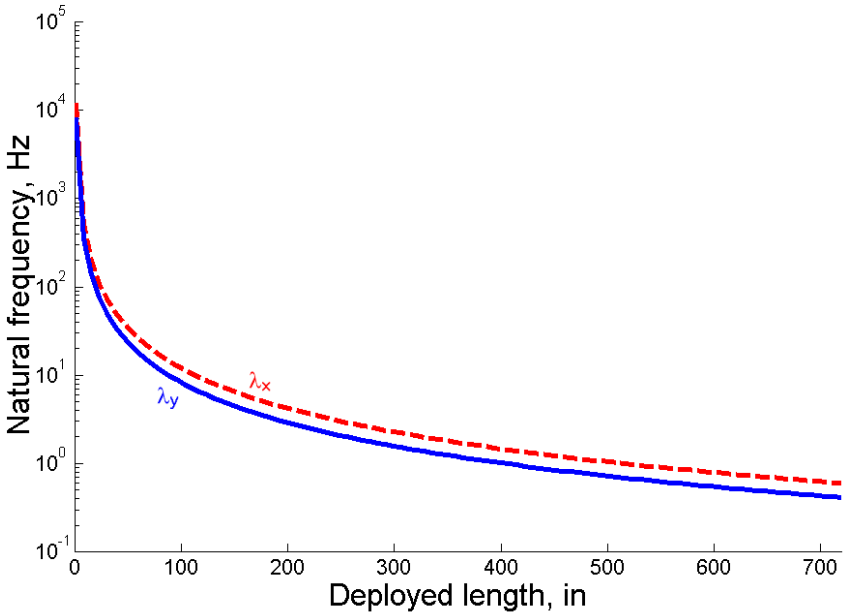

Figure 4-18: Boom natural frequency throughout deployment

Other precautions may be taken to minimize risk associated with the boom due to vibration such as operating the system at a safe distance from the orbiter structure and specifying a particular boom orientation relative to the orbiter surface to eliminate possible contact with the surface. To reduce the risk of contact with the orbiter structure, the boom will operate at a distance greater than 5ft (1.5m) from the surface as dictated by SRMS mission rules [4]. In addition to this, the boom should be oriented in such a way that the vibration behavior of the structure is well defined and can be accounted for in the inspection imagery data processing. The first boom orientation concept is to position the boom cross-section such that the *x*-axis is parallel to the orbiter surface (Figure 4-19a), the larger frequency of vibration would

occur about the *y*-axis due to the smaller area moment of inertia, therefore sustaining little danger of contact with the orbiter surface. The largest deflections will occur about the *y*-axis, further emphasizing this orientation; however, this orientation favors vibrations that would cause the camera and sensor payload to sway side-to-side while scanning an inspection region. The second boom orientation concept is to have the boom oriented such that the *y*-axis is parallel to the orbiter surface (Figure 4-19b). The orientation favors oscillation towards the orbiter, which would not endanger the orbiter given the mission rule of operating at least 5ft (1.5m) from the surface. The expected amplitude of vibration towards the orbiter would be approximately 2.6in (6.6cm) for the boom prototype design. This number should be experimentally verified to determine the minimum operating distance from the orbiter surface for the inspection payload cameras and sensors. A benefit of this boom orientation is that the motion of the cameras and sensors will be toward and away from the orbiter surface, which may be easier to accommodate in the data correction software. The system kinematics and inspection procedure were selected assuming the first orientation and if the second orientation is selected instead of the first, then the inspection task operations of the boom must be modified to ensure proper orientation of the boom relative to the orbiter surface.

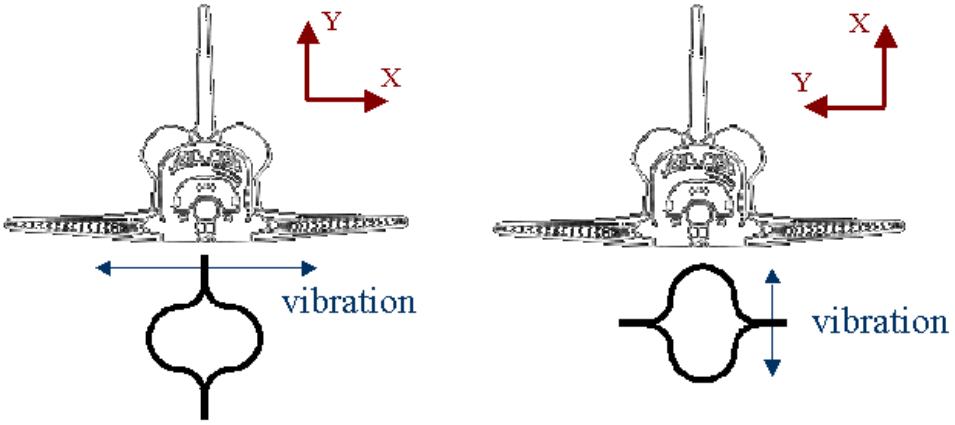

(a)
Boom orientation favoring vibration
parallel *to the orbiter surface*

(b)
Boom orientation favoring vibration
perpendicular *to the orbiter surface*

Figure 4-19: Boom orientation options for the inspection task

Additional concerns for the dynamics of the boom are effects due to partial deployment and the space environment. Due to the length of the boom, the loads during deployment are not negligible. These loads include inertia de-spin forces as the boom is extended, Coriolis effects, and internally induced tension and compression loads if the boom is stopped partially extended and then extended further. Other loads that must be considered are loads due to the task, gravity-gradient torques, thermal loads, and solar pressure. Many of these loads will limit how the boom inspection system is used so that the dynamics of the boom do not compromise the safety of the orbiter and its crew.

4.2.6 Global and Local Boom Buckling

This section examines the global and local buckling risks associated with the extendable boom design and methods to minimize their threat to the orbiter. Global buckling occurs when axial loading along the boom bifurcates from pure compression to bending. With a boom as long as the prototype, 720in (1830cm), buckling when

the boom is fully deployed could result in catastrophic damage to the orbiter; therefore, special precautions must be made to ensure the likelihood of global buckling is nearly eliminated. The primary sources of buckling include

- compressive loads induced by extension and retraction of the boom;
- inertial forces causing compressive loads due to the acceleration of the tip mass and of the boom itself when extension is initiated and when retraction is terminated;
- compressive rebound forces due to moving parts when extension is terminated;
- inertial forces due to orbiter attitude changes.

No matter how stiff the boom is the strength of the tubular boom is generally limited by buckling at the root. Because the boom will be used at multiple lengths, the root is constantly changing. However, in the fully deployed configuration, the root will be under the largest stresses. To counteract these stresses, the strength and stiffness of the boom can be increased at the root through doublers that increase the local area moment of inertia. Due to the stiffness requirements on the boom and its proposed length, the thickness of the cross-section could be varied along the length of the boom increasing stiffness as it is deployed to minimize deflections near the orbiter. Methods to prevent buckling are

- to increase the boom stiffness to resist compressive loads;
- to limit the compression loads due to dynamics;
- to employ a slow deployment velocity;
- to taper the deployment velocity through slow deceleration;

- to minimize the inspection payload mass extended by the boom.

To gain an idea of the amount of compressive loading that may occur due to boom extension, a deployment velocity and stopping time were assumed to obtain an axial load on the boom prototype, which was compared to the critical buckling load for a cantilevered beam. This analysis considered the boom prototype developed in this chapter at its fully deployed length. The axial force acting on the free-end (payload tip) of the boom was assumed to be equal to the product of the payload mass and the stopping or starting acceleration. The acceleration was assumed to be the ratio of the maximum deployment velocity of similar reel-stored booms, 180in/s^2 (460cm/s^2) [14], over a 0.1s stopping or starting time. The payload mass, 1.0slug (15kg), was selected earlier in the development of the worst-case loading on the boom prototype. This results in an axial force on the boom of 15lb (69N). The critical buckling load, P_{cr}, of the boom assuming clamped-free boundary conditions is given by

$$P_{cr} = \frac{\pi^2 E I_y}{4L^2}, \tag{4-26}$$

where E is the elastic modulus of the boom material, I_y is the area moment of inertia about the y-axis, and L is the fully deployed boom length. The area moment of inertia about the y-axis was chosen for this calculation because it is smaller than the inertia about the x-axis for the boom prototype geometry. The smallest inertia will lead to the limiting critical load, because the boom has the tendency to bend about its weaker axis, therefore, it will favor bending about the y-axis. The smallest value of the critical load occurs when the boom is fully deployed; therefore, the critical load was

calculated for a fully deployed boom under axial loading. From equation (4-26), the critical load for the boom prototype is 50lb (220N), where the elastic modulus is $9.7x10^6$psi ($6.7x10^{10}$Pa), the area inertia about the *y*-axis is $1.1in^4$ ($46cm^4$), and the fully deployed boom length is 720in (1830cm). The value of the expected axial load due to starting and stopping at an elevated deployment speed is much less than the critical buckling load; therefore, the boom prototype should not suffer from global buckling. As mentioned previously, experimental testing of the boom prototype should be performed to verify these calculations.

Another buckling issue pertaining to the boom mainly during stowage is local buckling or crippling. When long booms are wound onto stowage reels, flat spots are developed on the outside nominally cylindrical surface in addition to a ripple-like effect seen along the flanges of the rolled boom due to the difference in curvature of the two half-profiles of the boom (Figure 4-20). These effects will always be present when stowing the boom, but are not harmful to the boom structure as long as stresses on the boom due to stowage are maintained within acceptable elastic material behavior. The selection of rubber-like bonding adhesive for joining the boom half-profiles may alleviate some of the rippling effect, but will not eliminate it entirely. These effects may cause some irregularity of the deployment velocity that must be accounted for in the mission operations and procedures.

Figure 4-20: Example of local buckling of stowed boom

To account for these buckling features of the stowage boom, a stacking factor is given to estimate how the boom will stack when rolled onto the stowage reel. Typical the staking factor for similar reel-stored booms is 1.1 [14]. This implies that there will be approximately one-tenth of the flattened boom thickness between each layer when it is rolled onto the stowage reel.

4.2.7 Other Structural Concerns

Beyond the structural characteristics discussed so far in this chapter, several others to consider are thermal effects and material fatigue, impact, and creep resistance. The boom system must be designed to be compatible with structural loading as the result of a shuttle abort during any mission phase.

Due to the combination of a very low mass boom prototype with a relatively large black surface, thermal problems must generally be taken into account in the structural design. Thermal concerns on the boom structure are thermally induced

oscillations, thermal bending, and thermal shock. Vibration and bending due to the thermal environment of space occurs as the result of uneven temperature distributions along the boom. Similarly, thermal shock occurs as the result of abrupt changes in temperature resulting every time the orbiting spacecraft passes the boundary between sunlight and shadow. These thermal conditions cause an impulsive excitation of the boom system that must be controlled to avoid damage to the boom structure. Surface coatings should be used to minimize the effects from these thermal phenomena. Highly reflective surface finishes, such as silver and aluminum, offer good thermal protection. Gold surface finishes should be avoided because it can cause localized cold-welding between adjacent layers of the stowed boom [14]. Special precautions should be taken to prevent tarnishing a surface coating, such as silver, from exposure to air, gases, and humidity.

In a similar carbon composite lenticular boom design, the German Aerospace Center (DLR) used a thermal coating to minimize thermal degradation effects due to the space environment for a solar sail application [15]-[18]. An aluminized coating was applied to the boom surface to avoid thermal shocks to the structure. The coating was designed to achieve thermal neutrality along the length of the boom, meaning that the solar absorptivity of the coated boom is approximately zero. Research done at DLR shows that using a thermally protective coating on the boom minimizes thermal deformations due to the space environment [15]-[18].

An issue associated with thermal coatings is that they may flake off after multiple deployments. Because the proposed boom prototype design relies on an inspection scheme requiring many deployments to complete the inspection tasks, the

boom should be replaced after each mission to ensure proper thermal protection. This system requirement emphasizes the design of a cost-effective boom that can be mass-produced. Replacement after each mission is also beneficial in regards to structural fatigue damage due to the multiple-deployment inspection strategy.

The boom design must minimize the risk of structural failure due to material fatigue, impact, or creep. Several sources of these types of failures are repeated deployment, micrometeoroid impact, and prolonged storage of the stowed boom. In the case of structural fatigue, composite materials usually develop matrix micro-cracks or fiber-matrix debonding, which tends to grow under cyclic loading. For the case of this boom design, if fatigue cracking occurs during the inspection procedure and the boom continues its deployment routine, the cracks may grow to the point where they pose a threat to the structure. Matrix-only damage in composite structures is difficult to identify through ground testing, so inspection between flights may not be the best method to prevent fatigue failure of the boom structure. This risk provides further reasoning towards the boom replacement strategy of using a new boom on each shuttle mission. Extensive experience in the aerospace industry and elsewhere has shown that in carbon fiber laminates, fatigue damage accumulation can be avoided by ensuring that the component is not subjected to strains above approximately 0.4% (4000μstrain) [49]. Other means of fatigue protection are creating redundancy in the structure and structural constructions that are tolerant of fatigue damage. As far as impacts go, the threat of a micrometeoroid impacting the boom is small, due to its slender profile and natural shield of the orbiter, which is protected against minor impacts. If the boom were to suffer damage as the result of a

micrometeoroid, the boom may be rendered useless, yet should pose minimal threat to the safe return of the orbiter and its crew. There is a small possibility that the boom could contact the orbiter structure; however, this is unlikely because the boom will follow SRMS mission rules, which dictate safe trajectories, velocities, and contingency plans to keep the boom or SRMS from striking the vehicle.

Lastly, the boom is likely to remain flattened and rolled for periods of time between fabrication and launch, that may last several months or even years, yet must still successfully deploy and retract while in orbit. A critical factor for the design of the extendable boom is the ability of the boom to survive repeated flattening, and rolling operations without deterioration of structural properties. When the boom is stored for extended periods of time, the boom material is subject to creep. The boom concept relies on the elastic behavior of the boom materials, which may exhibit visco-elastic relaxation in the matrix materials causing the expanded cross-section to flatten by decreasing in height. In visco-elastic tests of a similar carbon composite lenticular boom, the changes in height of the boom profile after stowage in the flattened condition at a constant temperature for a predetermined period of time were monitored and it was found to change up to 15% under 176°F (80°C) stowage temperature conditions [19]. Similar booms that were developed in a NASA exploratory research project[‡] showed little cross-sectional geometry degradation after stowage for several years (Figure 4-21).

[‡] Farley, R. and Wienhold, P., Re: NASA GSFC lenticular boom project, personal communication, 2003-2004.

Figure 4-21: Boom cross-section profile after prolonged stowage

4.3 Boom Stowage Calculations

Following the discussion of the deployed boom structural characteristics, the properties of the boom in its stowage configuration are presented. The extendable boom relies on a rolled deployment concept that must accommodate the boom in such a way that excessive stresses to the structure are avoided. The boom stowage calculations entail the strains encountered during flattening and rolling.

The bridge between the deployed boom and its stowage is the transition region. In the transition region, the boom is in mid-deployment between the flattened and expanded states (Figure 4-22). The structural characteristics of the boom in this region are substantially different from those in the stowed or deployed configurations; therefore, the deployment device contains an apparatus to maintain structural properties throughout this region. The previous section focused on the deployed structure, now the properties of the stowed boom are discussed.

Figure 4-22: Boom transition region

The stowage of the boom can be broken into two steps: flattening of the boom cross-section and rolling of the boom onto the stowage reel. During these processes, the strain on the boom must not exceed the acceptable limit of 0.4% established in the last section concerning structural fatigue avoidance.

To flatten the boom, forces are applied on the boom as it enters the transition zone of the deployment device causing the cross-section to gradually collapse. In the fully deployed state, the cross-section is strain-free, but as it collapses strains are imposed on the collapsed curves. The strains developed across the boom profile are equal to the ratio of half of the section thickness to the radius of the section curvature. The curve segment has a half-thickness of 0.005in (0.01cm) and a radius of 2.005in (5.1cm) resulting in a flattening strain of 0.25% across this section. However, the fillet curves experience larger strains due to its smaller radius of curvature. The fillet has the same thickness as the curve segment, but its radius of curvature is 1.495in (3.8cm) resulting in a flattening strain of 0.33% across the fillet.

The last step in the stowage process is to apply a bending moment on the flattened boom to roll it onto the stowage drum. This process induces further strain on the boom as a curvature is induced as it is rolled up. The diameter of the stowage reel should be large enough to prevent permanent deformation of the stowed boom due to excessive bending stresses at the innermost windings. The minimum stowage radius, ρ_{min}, was found using

$$\rho_{\min} = \frac{H/2}{\varepsilon_{\max}}, \tag{4-27}$$

where H is the flattened thickness of the boom and ε_{max} is the maximum allowable strain due to rolling. To maintain low stress levels in the stowed boom, ε_{max} was selected to be 0.2% to ensure that the overall boom strains remain below the 0.4% strain-limit. The flattened thickness of the boom prototype is 0.02in (0.05cm) leading to a minimum stowage radius of 5in (13cm). Therefore, the diameter of the stowage reel must be at least 10in (25cm) to maintain the boom within acceptable strain levels.

As mentioned earlier, the acceptable limit of strain in the boom structure is 0.4%, which accounts for both flattening the rolling strains. To obtain a conservative estimate of the total strain on the boom due to stowage the root-sum of the largest flattening strain, 0.33%, and the rolling strain, 0.2%, gives a total strain of 0.38%, which is below the acceptable limit. Experimental measurements of the strains on the boom structure due to stowage should be used to verify that they are within acceptable limits.

given the stowage diameter, preliminary dimensions were assigned to the deployment device to obtain a storage volume estimate (Figure 4-23). Based on these

dimensions, the estimated storage volume required in the orbiter payload bay is approximately $8ft^3$ ($0.23m^3$).

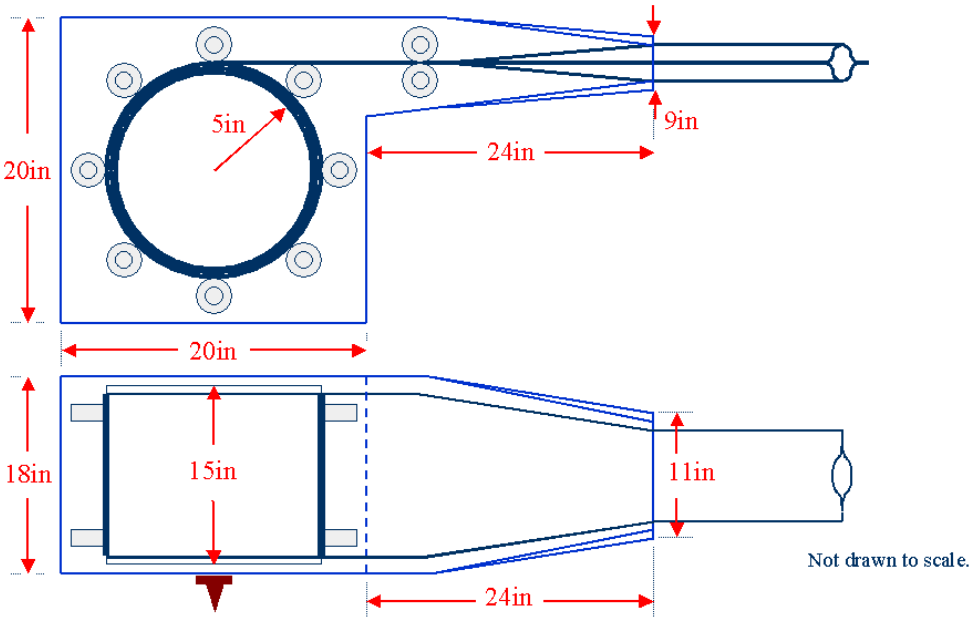

Figure 4-23: Approximate deployment device dimensions based on boom stowage calculations

4.4 Fabrication and Assembly Methods

Now that the extendable boom has been designed, a fabrication and assembly process must be selected. It is important to consider how the component will be manufactured during the design process to avoid processing problems that may result from a difficult to fabricate design. The key ingredient to the successful production of a component is a cost-effective and reliable manufacturing method [50]. This section examines two methods of manufacturing the boom prototype designed throughout this chapter to aid in selection of the best process. The two manufacturing processes considered were a classical lay-up and autoclave curing process and an automated continuous fabrication process similar to pultrusion.

The need to fabricate an extendable boom of considerable length suggested that a plain weave fabric composite would be best suited from a manufacturing standpoint. As discussed earlier, a carbon fiber plain weave laminate was selected as the boom prototype material. Weave fabrics are ideal for manufacturing because are easy to handle and can be used in automated processing.

The flattened cross-sectional parameters are the most useful in determining the amount of material that is required to create the desired boom profile geometry. For the boom prototype, the most basic dimensions for the required material are 13in by 720in (33cm by 1830cm), which was determined from the flattened width and boom length (Table 4-2). Due to the deployment device, additional length must be added to laminate to ensure that the boom has a deployable length of 720in (1830cm) as specified by the prototype design. Because the deployment mechanism has not been designed, the additional length required must be estimated. Knowing that the stowage diameter is approximately 10in (25cm), tripling this number should provide enough length to clear the transition zone. Also, the width should be increased so the edges of the flanges can be trimmed to the specification leaving them uniform and smooth to minimize interfere due to friction in the deployment device. An increase of 1in (2.5cm) to the width should be satisfactory. The new material dimensions are 14in by 810in (36cm by 2060cm). The profile thickness is 0.01in (0.025cm), which assumes a lay-up of two layers of the carbon weave material with the principal axes aligned with the longitudinal (z) and transverse (y) directions of the boom (Figure 4-14); therefore, each layer has a thickness of 0.005in (0.013cm).

4.4.1 Classical Autoclave Process

The classical autoclave processing technique entails tool design, part lay-up and bagging, and autoclave curing. This technique is widely used in the aerospace industry and is easy to implement. Relying only on a forming tool for a boom half-profile, this process can be performed at virtually any composite manufacturing facility, where the tool size is only limited by the autoclave size. A benefit of the hand lay-up process is that it produces highly reliable components, yet tends to be very slow and labor intensive.

A tool or mold is necessary for the fabrication of the prototype part and must resemble the part geometry. Several ideas considered for the tool included modifying an existing tool for a similar boom design, making one out of several aluminum pieces, or having one made from aluminum sheet metal. Aluminum was chosen because it is easy to machine, inexpensive, lightweight, non-corrosive, and thermally stable at typical composite material cure temperatures. Temporary modifications to existing tools would likely be more difficult and dependent on available resources than alternative ideas, so other options were pursued. The least expensive alternative is to make a tool from several pieces of aluminum with adhesive fillets. Problems relating to this method are that tolerances on the boom geometry may be compromised and the adhesive-aluminum thermal expansion mismatch could lead to cracking of the adhesive fillets. Machining a tool from aluminum sheet metal is recommended as the best choice, because tolerances can be adequately controlled and the tool would be less likely to crack during cure requiring fewer repairs between each part cure.

Next, the style of tool was selected. Two styles of tool designs are a male or female tool, which will affect the lay-up process. A male tool design, meaning that the boom part will rest on the top of the tool, was chosen. In the female tool design, the boom part would lay inside the tool, which is more prone to causing wrinkles in the materials that will lead to defects in the cured boom. In similar boom tool designs, both male and female tools have been used[§] [15]-[18].

The tool shape is dictated by the part geometry and the dimensions of the autoclave used to cure the part. An example tool cross-section is shown in Figure 4-24. To reduce the weight of the tool, some of the aluminum material can be removed from beneath the profile curve.

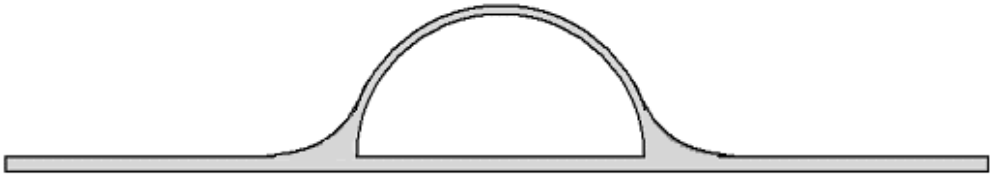

Figure 4-24: Aluminum tool cross-section

To ensure an even distribution of pressure over the test part during the curing process, a caul plate was fabricated. To make the caul plate, several layers of the prototype material or another similar material should be cut larger than the prototype material dimensions and stacked together to provide a symmetric lay-up. Teflon sheeting should be ironed onto both sides of the caul plate lay-up to ensure a smooth and even surface. The caul plate should be cured using the same autoclave process as the prototype. The resulting caul plate should be smooth towards the side cured against the tool. The caul plate is used to evenly distribute the pressure forces exerted

[§] Wienhold, P., Re: NASA GSFC lenticular boom tool design, personal communication, Fall 2003.

by the bagging material during cure to produce a boom profile that is smooth on both the top and bottom surfaces.

Given the boom prototype material and lay-up, the half-profile is fabricated, first by laying-up the part, preparing it for cure, and then curing it. The preimpregnated carbon/polycyanate weave for two parts should be cut to the designed measurements. Because it is unlikely that an autoclave capable of curing an 810in (2060cm) boom will be used for the cure, the boom must be made in sections and later assembled to achieve the desired length. The pre-cut parts are placed onto the tool, bagged, and cured in the autoclave. The finished half-profiles are bonded together using an adhesive to create the prototype.

Each boom half-profile is composed of two layers of plain weave preimpregnated fabric stacked such that the fiber directions coincide with the boom length and width. In the hand lay-up process, the material is cut to the predetermined dimensions based on the tool and autoclave limitations. Because the boom cannot be made from a single continuous piece due to autoclave dimension restrictions, the lay-up is tapered at the ends of the boom profile to create a shear lap joint (Figure 4-25). After the material is cut and stacked, strips of peel-ply should be placed where adhesive will later be applied for assembly. The peel-ply strips create a rough surface to aid in the bonding process. The peel-ply fabric should be placed along the length of the flanges of the boom profile and on the lap-joint ends, where the other boom section will be later attached. After applying the peel-ply fabric, Teflon film should be ironed onto each side of the laminate to ensure a smooth release after cure.

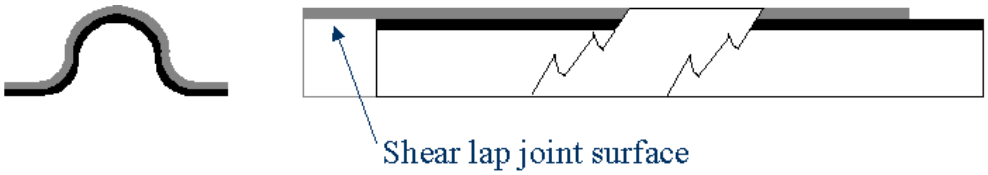

Figure 4-25: Spliced boom lap joint

The bagging process entails a careful stacking sequence on the tool to cure the boom part. First, the tool is prepared for cure by cleaning the upper surface using an abrasive pad, acetone, and alcohol. After the surface dries, several layers of a releasing agent should be applied to the tool surface to ensure that the cured part will not stick to the tool. The releasing agent should not be applied along a 1in (2.5cm) border around the edges of the tool to allow for a good seal between the tool, tacky tape, and bag material. Next, a piece of Teflon sheeting should be placed on the clean tool and secured at the ends to keep it from moving and potentially causing wrinkles in the part. Then the Teflon-sided part should be carefully centered and placed onto the tool leaving extra space at one end of the tool for a vacuum port. A heat gun may be used to warm the partially cured resin in the preimpregnated material to gently bend the part to the tool shape. Another piece of Teflon sheeting should be placed on top of the laminate followed by the caul plate, fabricated beforehand from the same tool, followed by another piece of Teflon sheeting. Breather material is added on top of the last layer of Teflon sheeting. An extra piece of breather material should be placed under the vacuum port. A piece of vacuum bag is placed on top of the tool and secured using tacky tape placed along the edges of the tool. A schematic of the bagging process is shown in Figure 4-26. After bagging, the part is brought under

vacuum to consolidate the entire assembly ensuring a good fit to the tool before curing.

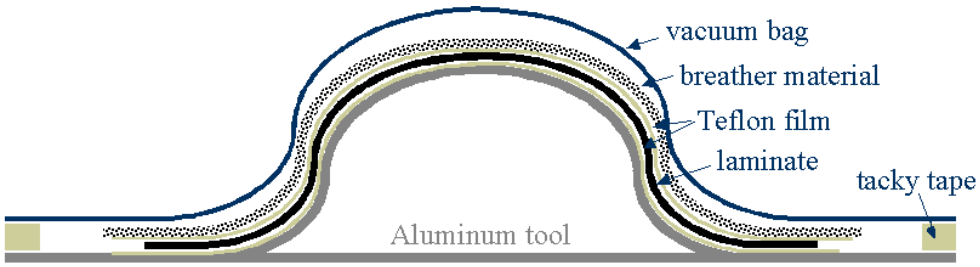

Figure 4-26: Boom half-profile bagging diagram

After bagging the boom part, the entire assembly should be placed in the autoclave for curing. The cure cycle used to cure the part is dependent on the material as specified by the manufacturer. For the boom prototype material, the manufacturer recommends a cure cycle of 350°F (177°C) for two hours under vacuum and 45psi to 100psi (3.1×10^5Pa to 6.9×10^5Pa) pressure [46].

After curing, the part is allowed to cool and is removed from the autoclave. The tool is repaired (if needed), cleaned, and prepared for the next part cure. The fabrication process is repeated until enough parts are made to complete the boom structure.

To complete the lenticular boom prototype, two parts are bonded together using an adhesive. The adhesive should be applied along the flanges of one part and the second part should be aligned with the first part, clamped in the flattened configuration, and allowed to dry until the adhesive is fully cured. This completes the fabrication of the prototype segments that still must be joined together to form the final boom.

The spliced boom assembly technique was developed[**] to overcome the boom length limitation imposed by the autoclave dimensions. A major benefit of this process is that the original tool can be used to create numerous boom sections that can be joined together to form a boom of considerable length. The step-scarf joints created during the lay-up are used to attach the boom sections together. The boom sections are adhesively joined together end-to-end in a male-female attachment process (Figure 4-27).

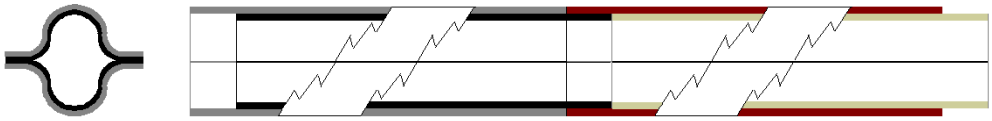

Figure 4-27: Spliced boom assembly concept

The classical autoclave manufacturing process requires simple set-ups, yet is labor and time intensive. To expedite the manufacturing process, multiple tools can be made, so that several parts can be made in a single autoclave cure cycle. A drawback to the splicing technique is that these joints may be structurally weaker. The boom prototype was designed assuming that the properties of the boom were uniform throughout. These affects may be mitigated through selection an adhesive for the splicing that has similar properties to the laminate, therefore eliminating the risk of thermal mismatch or other deformations due to heterogeneous materials. To avoid this issue all together, a continuous fabrication method could be used instead of this process.

[**] Farley, R., Re: splicing technique, personal communication, 8 June 2004.

4.4.2 Continuous Fabrication Method

Continuous fabrication methods are capable of producing long, straight structural members with constant cross-sectional areas. The process explained in this section is similar to the pultursion process, but has been modified to avoid damaging or distorting the very thin fabrics required to make the boom profile.

Pultrusion is one of the least expensive manufacturing processes for making high performance constant cross-section structural composite parts [51]. This fabrication technique begins with raw materials progressing through an uninterrupted stream resulting in fully cured parts. Once the process is set-up, it is less labor intensive and may be quicker than the splicing method resulting in a homogenous boom prototype.

To make the boom using a continuous process, the boom must be produced in two stages. First, the half-profiles are fabricated to the proper dimensions, then the second stage joins the profiles together to form the finished boom. The method presented here is similar to the sequential molding process developed for the European Space Agency for their collapsible tube mast design [19].

The first phase of the continuous fabrication process focuses on creating the boom half-profile. The preimpregnated fabric selected for the boom prototype is fed through a press and die assembly to create the boom half-profile geometry. The final shaping, compaction, and curing of the boom profile takes place inside the die. The die temperature, length, and feed speed are controlled to allow the resin to cure completely before the part exits the die. Due to the thin material used for the boom prototype, the part may only require one side of the die to be heated to fully cure the

part. After the part leaves the die it is allowed to cool in air, then the excess material is trimmed from the flanges leaving a clean edge. After trimming, the half-profile is flattened and rolled onto a storage drum where it will be bonded to another half-profile to complete the boom.

The second stage assembles the half-profiles to get the final boom prototype. Two identical half-profiles made during the first phase of the fabrication process are bonded together using a film adhesive. The half-profiles are unrolled and the adhesive is applied to the lower profile, while the other is inverted and brought coincident to create the lenticular geometry. Carrier templates are clamped to the top and bottom of the boom to ensure that two half-profiles are properly aligned before entering the press for cure. Pressure is applied along the flanges to bond the two profiles together completing the curing process. The completed boom is then flattened and rolled onto a storage drum, where it can be later inserted into to the deployment device in preparation for flight. A schematic of the entire fabrication process is shown in Figure 4-28.

The continuous molding process offers many advantages over classical autoclave fabrication; however, it is not without its own disadvantages. Major advantages are the time and cost savings associated with the assembly line characteristic of this process. A major drawback is that substantial set-up is required; however, after the process is set-up it can be used multiple times to create many booms. If booms are replaced after each mission, the demand for booms may justify the added complexity of the continuous fabrication method.

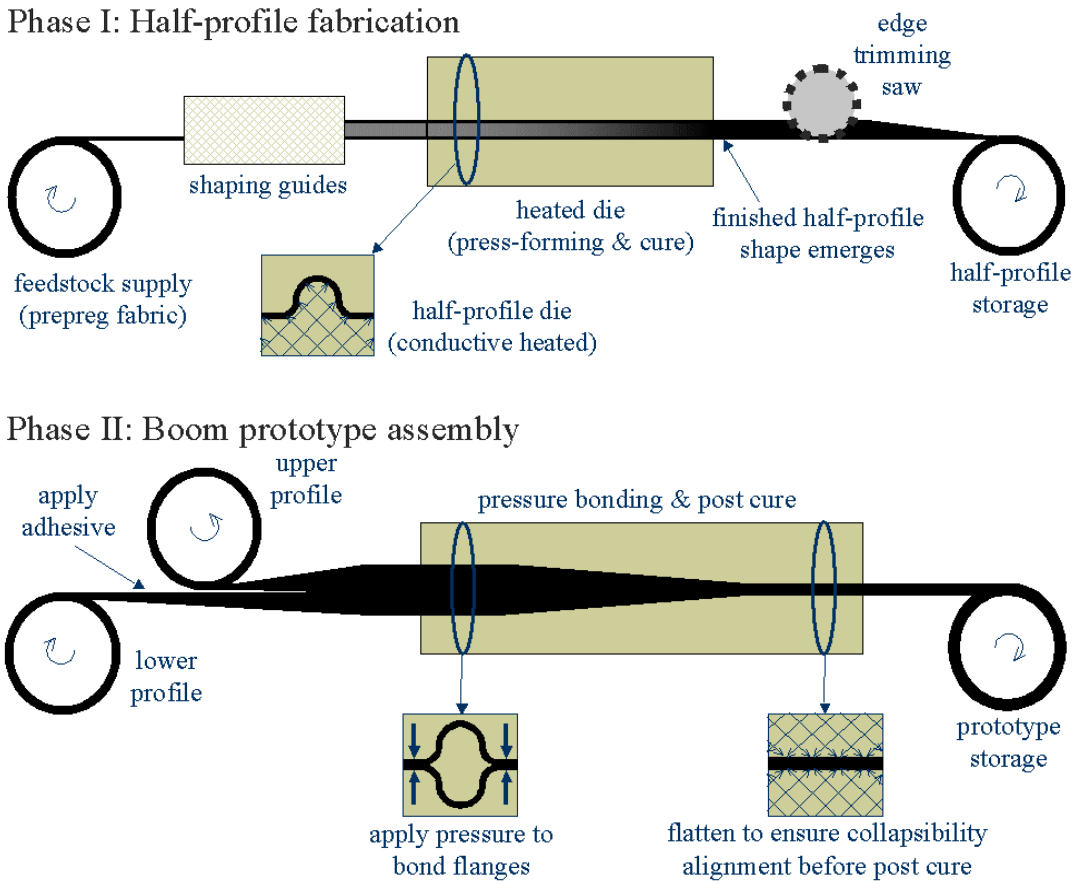

Figure 4-28: Continuous extendable boom molding processes

Based on the information discussed in this chapter, a fabrication method must be selected based on the available resources and demands. A trade-off analysis should be completed before selecting a process to ensure that the boom will be fabricated to the specified standards of its design. After fabrication, the booms should be tested for comparison to the analytical properties and the fabrication process can be modified if needed.

Chapter 5: Conclusions and Recommendations

The goal of this project was to develop an on-orbit inspection system utilizing an extendable boom. Although this design is not currently under development at NASA, it is hoped that this feasibility demonstration of a deployment-based system may lead to its future consideration in the return to flight (RTF) efforts. In the following sections, the conclusions of this research are restated along with recommendations for future work. The recommendations are discussed in hopes that this project will continue where this research ended. The chapter concludes with a few final thoughts about this project.

5.1 Conclusions

The preliminary design analysis for a deployable boom extension to the shuttle remote manipulator system (SRMS) resulted in a feasible orbiter inspection system. The extendable boom provides the necessary extension to SRMS to adequately inspect all regions of the orbiter thermal protection system (TPS). Compared to the planned fixed-boom design, the extendable boom design more than meets the inspection system requirements with orbiter system compatibility.

An extendable boom was selected for this orbiter inspection system design because it offers an unrestricted length capability, compact stowage, good structural properties, and high reliability. The ability of the boom to extend allows for increased reach over a fixed boom extension to the SRMS. Unlike the fixed boom concept, the length of the orbiter payload bay does not limit the length of the extendable boom.

The boom stows onto a reel that is encased in a deployment device that can be stored in the orbiter payload bay.

The structural properties of the boom depend on the cross-sectional geometry and the boom material. A parameterized model of the boom profile was developed. A modification made to this model, requiring that the center offset of the cross-section must be equal to the fillet radius simplified the cross-sectional area and inertia equations. To ensure accuracy of these simplified equations, the results from the simplified equations were compared with the integral solutions and the largest error between the values was found to be 0.5%. Further simplification was made through a trade-off analysis, where the fillet radius and flange width were assumed proportional to the shape radius. From the results of the trade-off analysis, a prototype geometry was selected for the structural analysis. The orthotropic composite weave material that was selected for the boom prototype met all of the preliminary boom structural requirements.

The inspection scheme for the deployable boom-based system relies on minimal movement of the SRMS to scan the orbiter TPS. The deployment feature of the boom extension and the SRMS wrist roll joint are primarily used for the orbiter TPS inspection reducing the system degrees of freedom and overall wear on the SRMS. When the SRMS must move to another scanning location, the boom is fully retracted, minimizing risk to the orbiter and reducing the system motion to six degrees of freedom. The boom design must account for the multiple boom deployments required for this inspection procedure. Additionally, the boom is oriented such that vibration in the system is favored about an axis perpendicular to the

orbiter surface. A slow deployment velocity is desirable to reduce system vibrations and to thoroughly scan the orbiter TPS.

This inspection procedure can be automated using existing SRMS software. Before flight, the SRMS parking positions must be selected and saved as auto trajectories for use on orbit. The auto sequences will move the SRMS to a parking position, so that the deployable boom can inspect that particular region of the TPS using the SRMS wrist roll joint for planar motion. Another benefit of this inspection scheme is that there may be some overlap in the inspection areas, particularly near the wing leading edges, which are among the most critical inspection regions.

Finally, the deployable boom system provides mission assurance, because the system can adequately inspect the orbiter TPS without the aid of the International Space Station (ISS). This system can be used in the event that the ISS cannot be relied upon to carry out a thorough orbiter TPS inspection. In addition to inspection duties, the boom-based system can also be used as an auxiliary camera system for other shuttle activities.

5.2 Recommendations For Future Work

Future efforts should focus on the further development of the deployable boom inspection system. The recommendations presented here can be separated into two categories: the optimization of boom properties and the optimization of system characteristics. Engineering design is an iterative process; so, as more knowledge is gained about the system requirements, the design will change accordingly and must be analyzed with the same rigor after each design iteration to ensure that the new system design meets the current requirements.

The first category of recommendations focuses primarily on the boom system properties. An alternative definition of the boom profile geometry should be determined. The current definition relies on Cartesian equations that may result in imaginary solutions for some parameter values. By defining a trigonometric function to represent the boom profile, the number of parameters required to describe the lenticular shape may be reduced. Fewer design parameters make optimization of the boom geometry simpler. The resulting model can be optimized for a particular area moment of inertia.

Related directly to the boom structural characteristics, final selections of the boom and adhesive bonding materials should be made. If a fiber-reinforced composite material is selected for the boom design, the lay-up sequence should be optimized to create the desired structural properties of the boom. Adhesive selection was not addressed in this research, but it plays a vital role in the boom assembly. The adhesive should be selected based on shear stresses that are likely to occur due stowage and also ideally, the adhesive will have damping properties that may help dissipate vibration loads on the boom structure. Additional materials could be selected for use as damping aids or stiffness doublers.

Along with material selection, a fabrication process should be selected to manufacture the boom elements. The fabrication methods presented in this document serve as a starting point for selecting a boom manufacturing process. The fabrication process may directly affect the quality and structural characteristics of the boom; therefore, a careful trade-off analysis should be performed to determine the most cost-

effect method before committing to a fabrication process that does not meet all of the fabrication requirements of the boom.

The adhesive bonds should be included in future structural calculations of the boom. The equations developed for the boom geometry include provisions for flange bonds in the area moment of inertia and cross-sectional area calculations. This research assumed there was zero bond-line thickness due to the adhesive to simplify the equations for the purpose of demonstrating the deployable boom concept. Another simplification made in the structural analysis of this prototype was that the SRMS remains rigid, which allowed the boom system to be modeled as a cantilevered beam; however, the SRMS is flexible and will cause additional dynamics to the system that must be accounted for in the final boom design.

As with any good design, the boom prototype should be subjected to ample testing. Particular boom features of interest are

- verification of material properties;
- measuring bending and torsional stiffness properties;
- measuring and characterizing boom natural frequencies;
- testing thermal coating effectiveness;
- measuring the boom transition length;
- determining the force required to flatten the boom cross-section for stowage;
- measuring the strains and shear forces on the boom in the stowage configuration;
- examining the effects of prolonged boom stowage;

- determining the operational life of the boom;
- investigating fatigue effects due to multiple deployments.

The items listed here are not all-inclusive, but contain the major properties of the boom that need to be determined before the system design can be finalized. After addressing this list of suggested boom characterization items, a great deal of knowledge will be added to the development of lenticular extendable booms. Through these tests, structural confidence in the boom structure will be gained, making it more likely that this type of boom may be included in future system designs such as the orbiter inspection system proposed in this document.

To deal with the issue of the large amount of stored strain energy in the stowed boom, bi-stable structures could be investigated [52]-[54]. These types of structures feature an anti-symmetric composite construction that is stable in two configurations. Open-section extendable booms have been developed using this technology with great success [52]-[54]; however, it has not been applied towards lenticular cross-section extendable booms. For the open-section booms, they are stable in the deployed and stowed configurations eliminating some of the concern due to the large amount of strain energy stored in rolled lenticular booms.

The second category of recommendations focuses on the optimization of the boom system characteristics. The primary focus of these recommendations rests on the development of the deployment device. This document developed a general design for the device, but stopped short of selecting hardware and designing the mechanism. The majority of the deployment device design is straightforward. The issues that may cause the most trouble in the hardware design is providing the proper

support to the boom in the transition section so that the boom maintains its structural integrity throughout all phases of the deployment process. Another issue is the design of an adequate clamping mechanism. The structural calculations presented in this document assumed cantilevered beam boundary conditions imparted by a clamping device at the boom root. The clamping device must maintain the expanded cross-section for structural stiffness at the root and extended boom uniformity. After the deployment device is designed, it should be subjected to rigorous testing to ensure that it can reliably extend and retract the boom and in the case of a failure, it does not compromise the safety of the orbiter or its crew.

After the deployment device is designed and the prototype has been tested, the boom system can be put through qualification testing and verification. Design changes should be made if needed. After successful completion of qualification testing of the boom system, it can be put into production. Each boom must undergo acceptance testing before flight.

Additionally, the boom system design should continue to be monitored in regards to risk management. The design should be modified to eliminate failure modes if possible to increase the system reliability. For failures that cannot be mitigated through design, contingency plans should be developed to ensure that all critical systems are at least two-fault tolerant.

As far as the inspection procedure goes, the kinematics of the entire system should be thoroughly examined to determine the best positions to park the SRMS to scan different regions of the orbiter TPS. These positions need to be verified to make sure that the system does not threaten the orbiter structure at any time and that the

inspection task can be adequately accomplished. Once the points have been verified, they can be stored as auto trajectories for the SRMS. Ideally, the deployable boom-based inspection system can survey the orbiter TPS automatically without placing demands on the crewmembers unless damage is detected.

Lastly, the inspection payload needs to be further designed. This project did not address the inspection payload beyond stating a few assumptions. This design was not intended for a specific payload, so the ability to adapt the system for repair tasks may also be investigated.

5.3 Final Thoughts

It is hoped that NASA will consider examining the proposed extendable boom-based inspection system presented in this document. It is not expected that this system will be fully designed to meet mission and safety requirements for the first RTF shuttle mission; however, if efforts are put forth now, the shuttle can use this system in addition to other inspection methodologies on future shuttle missions. With the addition of the deployment-based system to the shuttle repertoire of inspection capabilities, the fixed-boom developed for the early RTF missions can be left at the ISS for repair task assistance.

The ultimate goal of this research was to propose a solution to the on-orbit inspection problem that has temporarily halted shuttle launches. Whether the proposed deployable boom system is selected to solve this problem or not, it is hoped that efforts will continue towards improving the safety of the space shuttle and that astronauts will continue the fly the shuttle until a replacement vehicle is developed.

Appendix A: MATLAB Computer Code

This appendix contains the code developed using MATLAB® software. The first program was created to plot the lenticular boom geometry. The second program determines the area and inertia properties of the boom given a particular lenticular cross-sectional geometry. The third program develops a set of trade-off plots examining the effect of different cross-sectional parameters. The last program looks at some of the boom design parameters including both geometrical and structural characteristics.

A.1. boomplot.m

```
%Plots the boom geometry for a given set of boom profile parameters
%
% (c) Copyright 2004, Sadie K. Michael. All Rights Reserved.
%
% Last Modified: 07/31/2004

fig = 0; %figure count

%Parameters
%all dimensions are defined in inches
R=2;          % R: shape radius
r=0.75*R;     % r: fillet radius
a=r;          % a: center offset
b=0.5*R;      % b: flange width
t=0.01;       % t: profile thickness
ba=0.75*b;    % ba: flange bond width
ta=0;         % ta: flange adhesive thickness
L=720;        % L: boom length

% d=tanget point between curve and fillet
din = R*(r-a)/(R+r);
dout = (R+t)*(r-t-a)/(R+r);

%coordinate axes
syms x y
```

```
%Part Curves
curve_in = (x-(a+ta/2))^2 + y^2 - R^2;
curve_in_xlimit = [din+a, R+a]+ta/2;
curve_in_ylimit = [-sqrt(R^2-din^2), sqrt(R^2-din^2)];

curve_out = (x-(a+ta/2))^2 + y^2 - (R+t)^2;
curve_out_xlimit = [dout+a, R+t+a]+ta/2;
curve_out_ylimit = [-sqrt((R+t)^2-dout^2), sqrt((R+t)^2-dout^2)];

fillet_in = (x-(r+ta/2))^2 + (y-sqrt((R+r)^2-(r-a)^2))^2 - r^2;
fillet_in_xlimit = [0, din+a]+ta/2;
fillet_in_ylimit = [sqrt(R^2-din^2), sqrt((R+r)^2-(r-a)^2)];

fillet_out = (x-(r+ta/2))^2 + (y-sqrt((R+r)^2-(r-a)^2))^2 - (r-t)^2;
fillet_out_xlimit = [t, dout+a]+ta/2;
fillet_out_ylimit = [sqrt((R+t)^2-dout^2), sqrt((R+r)^2-(r-a)^2)];

flange_xlimit = [0, t]+ta/2;
flange_ylimit = [sqrt((R+r)^2-(r-a)^2), sqrt((R+r)^2-(r-a)^2)+b];

adhesive_xlimit = [0 ta/2];
adhesive_ylimit = [(sqrt((R+r)^2-(r-a)^2)+b)-ba, sqrt((R+r)^2-(r-a)^2)+b];

% Boom Geometry Plot (x(y))
hold off; fig = fig+1; figure(fig); hold on;

xlimits = [-curve_out_xlimit(2), curve_out_xlimit(2)];
ylimits = [-flange_ylimit(2), flange_ylimit(2)];

curve_out_x = solve(curve_out,x); curve_out_x = curve_out_x(1);
fillet_out_x = solve(fillet_out,x); fillet_out_x = fillet_out_x(2);
curve_in_x = solve(curve_in,x); curve_in_x = curve_in_x(1);
fillet_in_x = solve(fillet_in,x); fillet_in_x = fillet_in_x(2);

%plot y-sections
ysec5 = linspace(flange_ylimit(1),flange_ylimit(2)); %right flange
ysec4o = linspace(fillet_out_ylimit(1),fillet_out_ylimit(2)); %right outer fillet
ysec4i = linspace(fillet_in_ylimit(1),fillet_in_ylimit(2)); %right inner fillet
ysec3o = linspace(curve_out_ylimit(1),curve_out_ylimit(2)); %outer curve
ysec3i = linspace(curve_in_ylimit(1),curve_in_ylimit(2)); %inner curve
ysec2o = sort(-ysec4o); %left outer fillet
ysec2i = sort(-ysec4i); %left inner fillet
ysec1 = sort(-ysec5); %left flange
```

```
%outer top curve
outery=[ysec1 ysec2o ysec3o ysec4o ysec5];
curve=subs(curve_out_x,y,ysec3o);
fillet1=subs(subs(fillet_out_x,y,-y),y,ysec2o);
fillet2=subs(fillet_out_x,y,ysec4o);
flange=flange_xlimit(2)*ones(size(ysec1));
topouterx = [flange fillet1 curve fillet2 flange];

%outer bottom curve
curve=subs(-curve_out_x,y,ysec3o);
fillet1=subs(-subs(fillet_out_x,y,-y),y,ysec2o);
fillet2=subs(-fillet_out_x,y,ysec4o);
flange=-flange_xlimit(2)*ones(size(ysec1));
botouterx = [flange fillet1 curve fillet2 flange];

outerx = [topouterx; botouterx];

%inner top curve
innery=[ysec1 ysec2i ysec3i ysec4i ysec5];
curve=subs(curve_in_x,y,ysec3i);
fillet1=subs(subs(fillet_in_x,y,-y),y,ysec2i);
fillet2=subs(fillet_in_x,y,ysec4i);
flange=flange_xlimit(1)*ones(size(ysec1));
topinnerx = [flange fillet1 curve fillet2 flange];

%inner bottom curve
curve=subs(-curve_in_x,y,ysec3i);
fillet1=subs(-subs(fillet_in_x,y,-y),y,ysec2i);
fillet2=subs(-fillet_in_x,y,ysec4i);
flange=-flange_xlimit(1)*ones(size(ysec1));
botinnerx = [flange fillet1 curve fillet2 flange];

innerx = [topinnerx; botinnerx];

plot(outerx,outery,'r');
plot(innerx,innery,'b');

axis tight; axis equal;
title('Boom Cross-Section Geometry');
xlabel('X'); ylabel('Y');

% Boom Geometry Plot (y(x))
hold off; fig = fig+1; figure(fig); hold on;

curve_out_y = solve(curve_out,y); curve_out_y = curve_out_y(1);
fillet_out_y = solve(fillet_out,y); fillet_out_y = fillet_out_y(2);
```

```
curve_in_y = solve(curve_in,y); curve_in_y = curve_in_y(1);
fillet_in_y = solve(fillet_in,y); fillet_in_y = fillet_in_y(2);

xsec1o = linspace(curve_out_xlimit(2),curve_out_xlimit(1)); %upper curve
xsec1i = linspace(curve_in_xlimit(2),curve_in_xlimit(1)); %upper curve
xsec2o = linspace(fillet_out_xlimit(2),fillet_out_xlimit(1)); %upper fillet
xsec2i = linspace(fillet_in_xlimit(2),fillet_in_xlimit(1)); %upper fillet
xsec3o = flange_xlimit(2)*ones(1,length(xsec1o)); %upper flange
xsec3i = flange_xlimit(1)*ones(1,length(xsec1i)); %upper flange
xsec4o = -xsec3o; %lower flange
xsec4i = -xsec3i; %lower flange
xsec5o = -sort(xsec2o); %lower fillet
xsec5i = -sort(xsec2i); %lower fillet
xsec6o = -sort(xsec1o); %lower curve
xsec6i = -sort(xsec1i); %lower curve

outerx=[xsec1o xsec2o xsec3o xsec4o xsec5o xsec6o];
%left side
curve1=subs(-curve_out_y,x,xsec1o);
fillet1=subs(-fillet_out_y,x,xsec2o);
flange2=linspace(flange_ylimit(1),flange_ylimit(2));
fillet2=subs(-subs(fillet_out_y,x,-x),x,xsec5o);
curve2=subs(-subs(curve_out_y,x,-x),x,xsec6o);
%right side
curve3=subs(curve_out_y,x,xsec1o);
fillet3=subs(fillet_out_y,x,xsec2o);
flange1=sort(-flange2);
fillet4=subs(subs(fillet_out_y,x,-x),x,xsec5o);
curve4=subs(subs(curve_out_y,x,-x),x,xsec6o);

leftoutery = [curve1 fillet1 -sort(-flange1) flange1 fillet2 curve2];
rightoutery = [curve3 fillet3 flange2 -sort(-flange2) fillet4 curve4];
plot(outerx,leftoutery,'r');
plot(outerx,rightoutery,'b');

innerx=[xsec1i xsec2i xsec3i xsec4i xsec5i xsec6i];
%left side
curve1=subs(-curve_in_y,x,xsec1i);
fillet1=subs(-fillet_in_y,x,xsec2i);
fillet2=subs(-subs(fillet_in_y,x,-x),x,xsec5i);
curve2=subs(-subs(curve_in_y,x,-x),x,xsec6i);
%right side
curve3=subs(curve_in_y,x,xsec1i);
fillet3=subs(fillet_in_y,x,xsec2i);
fillet4=subs(subs(fillet_in_y,x,-x),x,xsec5i);
```

```
curve4=subs(subs(curve_in_y,x,-x),x,xsec6i);

leftinnery = [curve1 fillet1 -sort(-flange1) flange1 fillet2 curve2];
rightinnery = [curve3 fillet3 flange2 -sort(-flange2) fillet4 curve4];

plot(innerx,leftinnery,'r');
plot(innerx,rightinnery,'b');

axis tight; axis equal;
title('Boom Cross-Section Geometry');
xlabel('Y'); ylabel('X');

% 3-D plot of Boom Prototype
hold off; fig = fig+1; figure(fig); hold on;

Xtop=abs([topouterx;topouterx]);
Xbot=abs([botouterx;botouterx]);
Y=abs([outery;outery]);
Z=abs([zeros(1,length(outery));L*ones(1,length(outery))]);

surf(Z,Xtop,Y);
surf(Z,Xbot,Y);
colormap(winter);
shading flat;
lighting none;
xlabel('Z'); ylabel('X'); xlabel('Y');

view(60,20);
axis equal;
```

A.2. inertia.m

```
%Calculates the expanded and flattened width and thickness of the boom.
%Calculates the cross-sectional area of the boom prototype.
%Calculates the area moment of inertia for a parameterized boom.
%
% (c) Copyright 2004, Sadie K. Michael. All Rights Reserved.
%
% Last Modified: 07/31/2004

%Parameters
%all dimensions are defined in inches
R=2;          % R: shape radius
r=0.75*R;     % r: fillet radius
a=r;          % a: center offset
```

```
b=0.5*R;      % b: flange width
t=0.01;       % t: profile thickness
ba=0.75*b;    % ba: flange bond width
ta=0;         % ta: flange adhesive thickness
L=720;        % L: boom length

% Ec: Elastic Modulus of composite boom material (psi)
Ec=9.7e6;          %YLA T300 (1K)/RS-3 Plain weave fabric laminate
% rhoc: density of composite boom material (lbm/in3)
rhoc =0.0553;      %YLA T300 (1K)/RS-3 Plain weave fabric laminate

% Ea: Elastic Modulus of adhesive (psi)
Ea=0;          %no adhesive assumed
% rhoa: density of adhesive (lbm/in3)
rhoa =0;       %no adhesive

% d=tanget point between curve and fillet
din = R*(r-a)/(R+r);
dout = (R+t)*(r-t-a)/(R+r);

%coordinate axes
syms x y

%Part Curves
curve_in = (x-(a+ta/2))^2 + y^2 - R^2;
curve_in_xlimit = [din+a, R+a]+ta/2;
curve_in_ylimit = [-sqrt(R^2-din^2), sqrt(R^2-din^2)];

curve_out = (x-(a+ta/2))^2 + y^2 - (R+t)^2;
curve_out_xlimit = [dout+a, R+t+a]+ta/2;
curve_out_ylimit = [-sqrt((R+t)^2-dout^2), sqrt((R+t)^2-dout^2)];

fillet_in = (x-(r+ta/2))^2 + (y-sqrt((R+r)^2-(r-a)^2))^2 - r^2;
fillet_in_xlimit = [0, din+a]+ta/2;
fillet_in_ylimit = [sqrt(R^2-din^2), sqrt((R+r)^2-(r-a)^2)];

fillet_out = (x-(r+ta/2))^2 + (y-sqrt((R+r)^2-(r-a)^2))^2 - (r-t)^2;
fillet_out_xlimit = [t, dout+a]+ta/2;
fillet_out_ylimit = [sqrt((R+t)^2-dout^2), sqrt((R+r)^2-(r-a)^2)];

flange_xlimit = [0,t]+ta/2;
flange_ylimit = [sqrt((R+r)^2-(r-a)^2), sqrt((R+r)^2-(r-a)^2)+b];

adhesive_xlimit = [0 ta/2];
adhesive_ylimit = [(sqrt((R+r)^2-(r-a)^2)+b)-ba, sqrt((R+r)^2-(r-a)^2)+b];
```

```
curve_out_x = solve(curve_out,x); curve_out_x = curve_out_x(1);
fillet_out_x = solve(fillet_out,x); fillet_out_x = fillet_out_x(2);

curve_in_x = solve(curve_in,x); curve_in_x = curve_in_x(1);
fillet_in_x = solve(fillet_in,x); fillet_in_x = fillet_in_x(2);

curve_out_y = solve(curve_out,y); curve_out_y = curve_out_y(1);
fillet_out_y = solve(fillet_out,y); fillet_out_y = fillet_out_y(2);

curve_in_y = solve(curve_in,y); curve_in_y = curve_in_y(1);
fillet_in_y = solve(fillet_in,y); fillet_in_y = fillet_in_y(2);

%Expanded and Flattened Parameters
%flattened width, w
phiR = acos((r+ta/2-1/2*(curve_in_xlimit(1)+curve_out_xlimit(1)))/(r-t/2));
phir = acos((1/2*(curve_in_xlimit(1)+curve_out_xlimit(1))-(a+ta/2))/(R+t/2));
w = 2*b + 2*(r-t/2)*phir + 2*(R+t/2)*phiR

%flattened thickness, H
H=2*t+ta

%expanded width, c
c = 2*flange_ylimit(2)

%expanded thickness, h
h = 2*curve_out_xlimit(2)

%Cross-sectional area calculation
area_top_outer = 2*(int(curve_out_x,y,0,curve_out_ylimit(2)) + …
      int(fillet_out_x,y,fillet_out_ylimit(1),fillet_out_ylimit(2)) + ...
      int(flange_xlimit(2),y,flange_ylimit(1),flange_ylimit(2)));

area_top_inner = 2*(int(curve_in_x,y,0,curve_in_ylimit(2)) + …
      int(fillet_in_x,y,fillet_in_ylimit(1),fillet_in_ylimit(2)) + ...
      int(flange_xlimit(1),y,flange_ylimit(1),flange_ylimit(2)));

area_composite = double(2*(area_top_outer - area_top_inner));
area_adhesive = 2*ta*ba;

area_total = area_composite + area_adhesive

%Area moment of inertia calculation: Ix=int(y^2*dA)=int(y^2*x*dy)
%Inertia of composite part is outer curve - inner curve
Ix_outer = 2*(2*int(y^2*flange_xlimit(2),y,flange_ylimit(1),flange_ylimit(2)) + ...
      2*int(y^2*fillet_out_x,y,fillet_out_ylimit(1),fillet_out_ylimit(2)) + ...
```

```
    2*int(y^2*curve_out_x,y,0,curve_out_ylimit(2)));

Ix_inner = 2*(2*int(y^2*flange_xlimit(1),y,flange_ylimit(1),flange_ylimit(2)) + ...
    2*int(y^2*fillet_in_x,y,fillet_in_ylimit(1),fillet_in_ylimit(2)) + ...
    2*int(y^2*curve_in_x,y,0,curve_in_ylimit(2)));

Ix_composite = double(Ix_outer - Ix_inner)

Ix_bond = 1/12*ta*ba^3; %assuming rectangular bonds
adhesive_yoffset = adhesive_ylimit(1) + ba/2;

Ix_adhesive = Ix_bond + 1/2*area_adhesive*(adhesive_yoffset)^2; %|| axis theorem

EIx = Ec*Ix_composite + Ea*2*Ix_adhesive

%Area moment of inertia calculation: Iy=int(x^2*dA)=int(x^2*y*dx)
%Inertia of composite part is outer curve - inner curve
Iy_outer = 2*(2*int(x^2*curve_out_y,x,curve_out_xlimit(1),curve_out_xlimit(2)) +...
    2*int(x^2*fillet_out_y,x,fillet_out_xlimit(1),fillet_out_xlimit(2)) + ...
    2*int(x^2*flange_ylimit(2),x,-flange_xlimit(2),flange_xlimit(2)));

Iy_inner = 2*(2*int(x^2*curve_in_y,x,curve_in_xlimit(1),curve_in_xlimit(2)) + ...
    2*int(x^2*fillet_in_y,x,fillet_in_xlimit(1),fillet_in_xlimit(2)) + ...
    2*int(x^2*flange_ylimit(2),x,-flange_xlimit(1),flange_xlimit(1)));

Iy_composite = double(Iy_outer- Iy_inner)

Iy_bond = 1/12*ta^3*ba; %assuming rectangular bonds
adhesive_xoffset = 0;

Iy_adhesive = Iy_bond+1/2*area_adhesive*(adhesive_xoffset)^2; %|| axis theorem

EIy = Ec*Iy_composite + Ea*2*Iy_adhesive

%Boom mass estimates
mass_composite = area_composite*rhoc;
mass_adhesive = area_adhesive*rhoa;
massperlength =mass_composite + mass_adhesive
mass_total = massperlength*L
```

A.3. tradeoffs.m

```
% Creates trade-off plots for lenticular boom cross-section
%  for a given material & thickness to determine achievable inertia
% Creates inertia vs. shape radius plot for varying r/R with a given b/R
```

```
% Creates inertia vs. shape radius plot for varying b/R with a given r/R
% Creates inertia vs. center offset plot for fixed b/R and r/R ratios
% Creates inertia vs. inertia plot for varying b/R and r/R for fixed R
%
% (c) Copyright 2004, Sadie K. Michael. All Rights Reserved.
%
% Last Modified: 08/01/2004

fig = 0; %figure count

syms R r b;

%R: shape radius
%r: fillet radius
%b: flange width
t = 0.01; %in, assumed constant profile thickness
%NOTE:
%a: center offset is assumed to be equal to fillet radius

%Material properties
%YLA, T300(1K)/RS-3
E = 9.7e6;     %psi, tensile elastic modulus

%Simplified Area and Inertia Equations
Area = 2*t*(2*b+pi*(r+R));

Ix = 1/3*t*b^3+4*t*b*(R+r+b/2)^2+pi*R.^3*t+…
      4*r.^3*t*(pi/4*(2*R.^2+3*r.^2+4*r.*R)/r.^2-2*(r+R)./r);

Iy = 4*R.^3*t*(pi/2*(r./R)^2+pi/4+2*r./R+(r./R)^3*(3*pi/4-2));

%Trade-off for varying r/R ratio, constant b/R ratio assumed
r_R = [0.5, 0.75, 1]; %ratio of r to R

rnew = R.*r_R;
bnewr = 0.5*R; %in, assumed

Rv = linspace(1,4);

Ixr_Rv = zeros(length(Rv),length(rnew));
Ixb = subs(Ix,b,bnewr);

for k=1:1:length(rnew)
   Ixr_R(k) = subs(Ixb,r,rnew(k));
   Ixr_Rv(:,k) = subs(Ixr_R(k),R,Rv)';
end
```

```
Iyr_Rv = zeros(length(Rv),length(rnew));
Iyb = subs(Iy,b,bnewr);

for k=1:1:length(rnew)
   Iyr_R(k) = subs(Iyb,r,rnew(k));
   Iyr_Rv(:,k) = subs(Iyr_R(k),R,Rv)';
end

hold off; fig=fig+1; figure(fig); hold on;
plot(Rv,Ixr_Rv,':',Rv,Iyr_Rv);
legend('Ix, r=0.5*R','Ix, r=0.75*R','Ix, r=R',...
   'Iy, r=0.5*R','Iy, r=0.75*R','Iy, r=R',0);
title('I vs. R for b=0.5*R');
xlabel('Shape radius, in'); ylabel('Area moment of inertia, in^4');

%Trade-off with varying b/R ratio and constant r/R
rnewb = 0.75*R; %assumed

b_R = [0.1, 0.3, 0.5, 0.7, 0.9]; %ratio of b to R

bnew = R.*b_R;

Ixb_Rv = zeros(length(Rv),length(bnew));
Ixr = subs(Ix,r,rnewb);

for k=1:1:length(bnew)
   Ixb_R(k) = subs(Ixr,b,bnew(k));
   Ixb_Rv(:,k) = subs(Ixb_R(k),R,Rv)';
end

Iyb_R = subs(Iy,r,rnewb);
Iyb_Rv = subs(Iyb_R,R,Rv);

hold off; fig=fig+1; figure(fig); hold on;
plot(Rv,Ixb_Rv,':',Rv,Iyb_Rv);
legend('Ix, b=0.1*R','Ix, b=0.3*R','Ix, b=0.5*R','Ix, b=0.7*R',…
      'Ix, b=0.9*R','Iy, all b values',0);
title('I vs. R for different b/R values (r=0.75*R)');
xlabel('Shape radius, in'); ylabel('Area moment of inertia, in^4');

%Trade-off plot of constant R, varying r/R and b/R inertias

clear rnew bnew Rv

Rv = 2;
```

```
rnew = [0.25,0.5,0.75,1].*Rv;
bnew = [0.1,0.3,0.5,0.7,0.9].*Rv;

Ixrb = zeros(length(rnew)*length(bnew),1);
Iyrb = zeros(length(rnew)*length(bnew),1);

Ixrb = zeros(length(bnew),length(rnew))';
Iyrb = zeros(length(bnew),length(rnew))';

for k = 1:1:length(bnew)
   for m = 1:1:length(rnew)
      Ixrb(m,k) = double(subs(Ix,{R,r,b},{Rv,rnew(m),bnew(k)}));
      Iyrb(m,k) = double(subs(Iy,{R,r,b},{Rv,rnew(m),bnew(k)}));
   end
end

hold off; fig=fig+1; figure(fig); hold on;
plot(Ixrb,Iyrb,Ixrb',Iyrb')
legend('b=0.1R','b=0.3R','b=0.5R','b=0.7R','b=0.9R',…
     'r=0.25R','r=0.5R','r=0.75R','r=R',0);
xlabel('Area moment of inertia about x-axis, in^4');
ylabel('Area moment of inertia about y-axis, in^4');

clear R r a b t ba ta;

%Plot of varying center offset
%Comparison of approximate and actual inertia and area formulae

%Parameters
%all dimensions are defined in inches
R=2;              % R: shape radius
r=0.75*R;         % r: fillet radius
a=linspace(0,r);  % a: center offset
b=0.5*R;          % b: flange width
t=0.01;           % t: profile thickness
ba=0.75*b;        % ba: flange bond width
ta=0;             % ta: flange adhesive thickness

%Actual boom inertia solution

% d=tanget point between curve and fillet
din = R*(r-a)/(R+r);
dout = (R+t)*(r-t-a)/(R+r);

%coordinate axes
syms x y
```

```
%Part Curves
curve_in = (x-(a+ta/2)).^2 + y^2 - R^2;
curve_in_xlimit = [din+a, R+a]+ta/2;
curve_in_ylimit = [-sqrt(R^2-din.^2), sqrt(R^2-din.^2)];

curve_out = (x-(a+ta/2)).^2 + y^2 - (R+t)^2;
curve_out_xlimit = [dout+a, R+t+a]+ta/2;
curve_out_ylimit = [-sqrt((R+t)^2-dout.^2), sqrt((R+t)^2-dout.^2)];

fillet_in = (x-(r+ta/2))^2 + (y-sqrt((R+r)^2-(r-a).^2)).^2 - r^2;
fillet_in_xlimit = [0, din+a]+ta/2;
fillet_in_ylimit = [sqrt(R^2-din.^2), sqrt((R+r)^2-(r-a).^2)];

fillet_out = (x-(r+ta/2))^2 + (y-sqrt((R+r)^2-(r-a).^2)).^2 - (r-t)^2;
fillet_out_xlimit = [t, dout+a]+ta/2;
fillet_out_ylimit = [sqrt((R+t)^2-dout.^2), sqrt((R+r)^2-(r-a).^2)];

flange_xlimit = [0,t]+ta/2;
flange_ylimit = [sqrt((R+r)^2-(r-a).^2), sqrt((R+r)^2-(r-a).^2)+b];

%Inertias: Ix=int(y^2*dA) and Iy=int(x^2*dA)

Ix_act = zeros(length(a),1);
Iy_act = zeros(length(a),1);
area_act = zeros(length(a),1);

for k=1:1:length(a)

curve_out_x = solve(curve_out(k),x); curve_out_x = curve_out_x(1);
fillet_out_x = solve(fillet_out(k),x); fillet_out_x = fillet_out_x(2);

curve_in_x = solve(curve_in(k),x); curve_in_x = curve_in_x(1);
fillet_in_x = solve(fillet_in(k),x); fillet_in_x = fillet_in_x(2);

Ix_outer =
2*(2*int(y^2*flange_xlimit(2),y,flange_ylimit(k),flange_ylimit(length(a)+k)) + ...
2*int(y^2*fillet_out_x,y,fillet_out_ylimit(k),fillet_out_ylimit(length(a)+k)) + ...
2*int(y^2*curve_out_x,y,0,curve_out_ylimit(length(a)+k)));

Ix_inner =
2*(2*int(y^2*flange_xlimit(1),y,flange_ylimit(k),flange_ylimit(length(a)+k)) + ...
2*int(y^2*fillet_in_x,y,fillet_in_ylimit(k),fillet_in_ylimit(length(a)+k)) + ...
2*int(y^2*curve_in_x,y,0,curve_in_ylimit(length(a)+k)));

Ix_act(k) = double(Ix_outer - Ix_inner);
```

```
curve_out_y = solve(curve_out(k),y); curve_out_y = curve_out_y(1);
fillet_out_y = solve(fillet_out(k),y); fillet_out_y = fillet_out_y(2);

curve_in_y = solve(curve_in(k),y); curve_in_y = curve_in_y(1);
fillet_in_y = solve(fillet_in(k),y); fillet_in_y = fillet_in_y(2);

Iy_outer =
2*(2*int(x^2*curve_out_y,x,curve_out_xlimit(k),curve_out_xlimit(length(a)+k)) +...
2*int(x^2*fillet_out_y,x,fillet_out_xlimit(1),fillet_out_xlimit(1+k)) + ...
2*int(x^2*flange_ylimit(length(a)+k),x,-flange_xlimit(2),flange_xlimit(2)));

Iy_inner =
2*(2*int(x^2*curve_in_y,x,curve_in_xlimit(k),curve_in_xlimit(length(a)+k)) + ...
2*int(x^2*fillet_in_y,x,fillet_in_xlimit(1),fillet_in_xlimit(1+k)) + ...
2*int(x^2*flange_ylimit(length(a)+k),x,-flange_xlimit(1),flange_xlimit(1)));

Iy_act(k) = double(Iy_outer- Iy_inner);

area_top_outer = 2*(int(curve_out_x,y,0,curve_out_ylimit(length(a)+k)) + ...
      int(fillet_out_x,y,fillet_out_ylimit(k),fillet_out_ylimit(length(a)+k)) + ...
      int(flange_xlimit(2),y,flange_ylimit(k),flange_ylimit(length(a)+k)));

area_top_inner = 2*(int(curve_in_x,y,0,curve_in_ylimit(length(a)+k)) + ...
      int(fillet_in_x,y,fillet_in_ylimit(k),fillet_in_ylimit(length(a)+k)) + ...
      int(flange_xlimit(1),y,flange_ylimit(k),flange_ylimit(length(a)+k)));

area_act(k) = double(2*(area_top_outer - area_top_inner));

end

Ix_approxv = Ix_approx*ones(length(a),1);
Iy_approxv = Iy_approx*ones(length(a),1);
hold off; fig=fig+1; figure(fig); hold on;
plot(a,Ix_act,a,Ix_approxv,'--',a,Iy_act,a,Iy_approxv,'--');
legend('Ix actual','Ix approximate','Iy actual','Iy approximate',0);
xlabel('Center Offset, a, in'); ylabel('Area Moment of Inertia, I, in^4');

errorx = abs(Ix_act-Ix_approx)./Ix_act * 100;
errory = abs(Iy_act-Iy_approx)./Iy_act * 100;
```

A.4. boomdesign.m

```
% Calculates the required boom stiffness properties for the extendable boom.
% Calculates and plots natural frequency versus boom deployed length.
```

```
%
% (c) Copyright 2004, Sadie K. Michael. All Rights Reserved.
%
% Last Modified: 08/01/2004

fig = 0; %figure count

%desired boom properties
L = 60*12     %inches, length of the boom (60 ft)
v = 2.4/12     %ft/sec, SRMS loaded velocity
      %Ref: "The Shuttle Remote Manipulator System - The Canadarm" (10.28.03)
      %http://www.ewh.ieee.org/reg/7/millennium/canadarm/canadarm_technical.html
dt = 1          %sec, time for acceleration calculation
a = v/dt        %ft/sec2, loaded acceleration assuming dv/dt

H = 0.02;      %in, boom prototype flattened thickness
w = 13;        %in, boom prototype flattened width

dens=1.53*(1e2)^3/1e3*3.61273e-5;     %lbm/in3, YLA T300(1K) RS-3 material
mblbm=dens*H*w                        %lbm/in, based on material density
mb=mblbm/32.174                       %slugs/in, distributed mass

mtlbm = 15/0.4536                     %lbm, tip mass
mt = 15/0.4536/32.174                 %slugs, tip mass (15 kg)

P = mt*a       %lb, tip load under SRMS acceleration
f = mb*a       %lb/in, distributed force along the boom under SRMS acceleration

%Solution to d2u/dx2 with boundary conditions u(z=0) = 0 and du/dz|z=0 = 0
%d2u/dz2 = -(P*(L-z)+0.5*f*(L-z)^2)/EI

syms z
%deflection as function of z position (deployed length)
EIu = -1/24*(f*z^4 - 4*(P+f*L)*z^3 + 6*(2*P*L + f*L^2)*z^2)

%Calculation of expected EI for given maximum deflection at tip when fully
deployed
%d2u/dz2 = (Pz*(L-z)-0.5*fz*(L-z)^2)/EIy
%Since Iy < Ix, Iy is limiting factor for determining desired stiffness

umax = -4     %inches, deflection in z-direction
EItip = subs(EIu,z,L)
EIy = EItip./umax       %lb-in2

%Plot u(z) when desired EI is achieved
hold off; fig = fig+1; figure(fig); hold on;
```

```
ezplot(EIu/EIy,[0 L]);
title('Boom Deflection Throughout Deployment');
xlabel('Boom Length in z-Direction, in');
ylabel('Boom Deflection in Z-Direction, in');

%Plot E vs. I for desired deflection under loaded acceleration
hold off; fig = fig+1; figure(fig); hold on;
ezplot(EIy/z,[0,5]);
title('Boom Stiffness versus Area Moment of Inertia');
xlabel('Area Moment of Inertia, in^4'); ylabel('Modulus of Elasticity, lb/in^2');

%Dyanmics: natural frequency calculation
f1 = 1.732/2/pi*sqrt(EIy*a*12/(P*L^3+0.236*f*L^4))

inertia    %calls inertia.m program to calculate the inertias of the boom prototype

%frequency calculations for the x and y directions
fx = 1.732/2/pi*sqrt(Ec*Ix_composite*a*12/(P*L^3+0.236*f*L^4))
fy = 1.732/2/pi*sqrt(Ec*Iy_composite*a*12/(P*L^3+0.236*f*L^4))

zvec = linspace(1,720);
ffx = 1.732/2/pi*sqrt(Ec*Ix_composite*a*12./(P.*zvec.^3+0.236*f.*zvec.^4));
ffy = 1.732/2/pi*sqrt(Ec*Iy_composite*a*12./(P.*zvec.^3+0.236*f.*zvec.^4));

%Plot f vs. z for desired deflection under loaded acceleration
hold off; fig = fig+1; figure(fig); hold on;

plot(zvec,ffx,'r'); plot(zvec,ffy,'b'); legend('fx','fy');
title('Boom Natural Frequency vs. Boom Deployed Length');
xlabel('deployed length, in'); ylabel('natural frequency, Hz');
```

Appendix B: Mathematica Computer Code

(*SRMSDB.nb

Calculates the Forward Kinematics of the SRMS-Deployable Boom Robotic Manipulator using the D-H Link Frame Convention

Last Modified 06/24/04 *)

```
 Off[General::spell,General::spell1];

(* INPUT DATA SET FOR SRMSDB ROBOT *)

(* NUMBER OF DEGREES OF FREEDOM *)
dof = 7;

(* D-H PARAMETERS FOR SRMSDB ARM
 JOINT TYPE [revolute=1, prismatic=0] *)
alpha[0]=0;     a[0]=0;   d[1]=0;    t[1]=t[1]; jtype[1]=1;
alpha[1]=90°;   a[1]=0;   d[2]=0;    t[2]=t[2]; jtype[2]=1;
alpha[2]=0;     a[2]=a2;  d[3]=0;    t[3]=t[3]; jtype[3]=1;
alpha[3]=0;     a[3]=a3;  d[4]=0;    t[4]=t[4]; jtype[4]=1;
alpha[4]=-90°;  a[4]=a4;  d[5]=0;    t[5]=t[5]; jtype[5]=1;
alpha[5]=-90°;  a[5]=0;   d[6]=d6;   t[6]=t[6]; jtype[6]=1;
alpha[6]=-90°;  a[6]=0;   d[7]=d[7]; t[7]=0;    jtype[7]=0;

(* TOOL TIP POSITION IN LAST LINK FRAME *)
pNT = {{0},{0},{0}};

(* Parameter Length Values (inches) *)
mechwidth = 6;(*in, assumed*)
translength = 24; (*in, assumed*)
pa2 = 251.1;  pa3=278.0;  pa4=19.6;  pd6=32.9+mechwidth; (*in*)

(* Depolyable Boom Limits (inches) *)
d7min=translength; d7max=720;

(* NASA "Home" Configuration - Stored in Orbiter Payload Bay -
(angles in radians) *)
t1h=0; t2h=ArcTan[-4.9/251.05]; t3h=-(t2h+t4h);
t4h=ArcTan[4.9/-277.95]; t5h=90*Degree //N; t6h=0; d7h=d7min;
qh={t1h,t2h,t3h,t4h,t5h,t6h,d7h};

(* Joint Variable Limits (mechanical stop) *)
t1mmin=-180°+t1h;     t2mmin=-2°+t2h;       t3mmin=-161°+t3h;
t4mmin=-121.4°+t4h;   t5mmin=-121.3°+t5h;   t6mmin=-447°+t6h;
d7mmin=d7min;
t1mmax=180°+t1h;   t2mmax=145°+t2h;   t3mmax=2.4°+t3h;
t4mmax=121.4°+t4h; t5mmax=121.3°+t5h; t6mmax=447°+t6h;
d7mmax=d7max;

qmlimitsl={t1mmin,t2mmin,t3mmin,t4mmin,t5mmin,t6mmin,d7mmin};
qmlimitsu={t1mmax,t2mmax,t3mmax,t4mmax,t5mmax,t6mmax,d7mmax};
```

```
(* Local Transformation Matrices *)

For[i=1,i≤dof,i++,
  {R[i]={{Cos[t[i]],-Sin[t[i]],0},
     {Sin[t[i]]*Cos[alpha[i-1]],Cos[t[i]]*Cos[alpha[i-1]],
       -Sin[alpha[i-1]]},{Sin[t[i]]*Sin[alpha[i-1]],
       Cos[t[i]]*Sin[alpha[i-1]],Cos[alpha[i-1]]}},
    p[i]={{a[i-1]},{-Sin[alpha[i-1]]*d[i]},{Cos[alpha[i-1]]*d[i]}}}];

(*Transformation of SRMS base frame {0}
   to Orbiter Body Axis System (OBAS)*)
Rb={{-1, 0, 0},{0, 1, 0},{0,0,-1}};
pb={{xb},{yb},{zb}};
pxb=-679.5; pyb=-108.0;pzb=-444.77;

(*Transformation of SRMS base frame {0}
   to Orbiter Rotation Axis System (ORAS)*)
Rr={{1, 0, 0},{0, -1, 0},{0,0,-1}};
pr={{xr},{yr},{zr}};
pxr=679.5; pyr=108.0;pzr=-444.77;


(* Forward Kinematics *)

W[0]=IdentityMatrix[3];
x[0]={{0},{0},{0}};
For[k=1,k≤dof,k++,
  {W[k]=W[k-1].R[k],
   dx[k]=W[k-1].p[k],
   x[k]=x[k-1]+dx[k]} ];

W[dof]=Simplify[W[dof]];
p0T=x[dof]+W[dof].pNT;
p0T=Simplify[p0T];
(*assume RNT=Identity*)
R0T=W[dof];

Print["FORWARD KINEMATICS:"];

For[i=1,i≤3,i++,
  Print["p0T[",i,"] = ",p0T[[i]]]
  ];
For[i=1,i≤3,i++,
  For[j=1,j≤3,j++,
   Print["R0T[",i,",",j,"] = ",R0T[[i,j]]] ] ];

Print["Boom Tip Position in OBAS Reference Frame:"];
pbT = Simplify[Rb.p0T+pb];

For[i=1,i≤3,i++,
  Print["pbT[",i,"] = ",pbT[[i]]] ];

Print["Boom Tip Orientation in ORAS Reference Frame:"];
RrT=Simplify[Rr.R0T];

For[i=1,i≤3,i++,
  For[j=1,j≤3,j++,
   Print["RrT[",i,",",j,"] = ",RrT[[i,j]]] ] ];


(* Forward Kinematics Test - Check Configurations *)
p = Flatten[p0T //.{a2→pa2, a3→pa3, a4→pa4, d6→pd6}];
```

```
R = R0T //.{a2→pa2, a3→pa3, a4→pa4, d6→pd6};
pb = Flatten[pbT //.{a2→pa2, a3→pa3, a4→pa4,
d6→pd6,xb→pxb,yb→pyb,zb→pzb}];
Rr = RrT;

(* "Home" Configuration *)
qfk=qh;
qdeg=qfk/Degree;
qdeg[[7]]=qfk[[7]];
Print["Configuration A:"];
Print[ " q1 = ",Table[qdeg]];
Print[" p0T_A = ",MatrixForm[p
//.{t[1]→qfk[[1]],t[2]→qfk[[2]],t[3]→qfk[[3]],t[4]→qfk[[4]],t[5]→qf
k[[5]],t[6]→qfk[[6]],d[7]→qfk[[7]]}],"   R0T_A = ",MatrixForm[R
//.{t[1]→qfk[[1]],t[2]→qfk[[2]],t[3]→qfk[[3]],t[4]→qfk[[4]],t[5]→qf
k[[5]],t[6]→qfk[[6]],d[7]→qfk[[7]]}]];
Print[" pbT_A = ",MatrixForm[pb
//.{t[1]→qfk[[1]],t[2]→qfk[[2]],t[3]→qfk[[3]],t[4]→qfk[[4]],t[5]→qf
k[[5]],t[6]→qfk[[6]],d[7]→qfk[[7]]}],"   RrT_A = ",MatrixForm[Rr
//.{t[1]→qfk[[1]],t[2]→qfk[[2]],t[3]→qfk[[3]],t[4]→qfk[[4]],t[5]→qf
k[[5]],t[6]→qfk[[6]],d[7]→qfk[[7]]}]];

(* Maximum Manipulator Length *)
qfk={0,90°,0,0,-90°,0,d7max};
qdeg=qfk/Degree;
qdeg[[7]]=qfk[[7]];
Print["Configuration B: "];
Print[" qB = ",Table[qdeg]];
Print[" p0T_B = ",MatrixForm[p
//.{t[1]→qfk[[1]],t[2]→qfk[[2]],t[3]→qfk[[3]],t[4]→qfk[[4]],t[5]→qf
k[[5]],t[6]→qfk[[6]],d[7]→qfk[[7]]}],"   R0T_B = ",MatrixForm[R
//.{t[1]→qfk[[1]],t[2]→qfk[[2]],t[3]→qfk[[3]],t[4]→qfk[[4]],t[5]→qf
k[[5]],t[6]→qfk[[6]],d[7]→qfk[[7]]}]];
Print[" pbT_B = ",MatrixForm[pb
//.{t[1]→qfk[[1]],t[2]→qfk[[2]],t[3]→qfk[[3]],t[4]→qfk[[4]],t[5]→qf
k[[5]],t[6]→qfk[[6]],d[7]→qfk[[7]]}],"   RrT_B = ",MatrixForm[Rr
//.{t[1]→qfk[[1]],t[2]→qfk[[2]],t[3]→qfk[[3]],t[4]→qfk[[4]],t[5]→qf
k[[5]],t[6]→qfk[[6]],d[7]→qfk[[7]]}]];

(* All joint variables at zero values *)
qfk={0,0,0,0,0,0,d7min};
qdeg=qfk/Degree;
qdeg[[7]]=qfk[[7]];
Print["Configuration C:"];
Print[" qC = ",Table[qdeg]];
Print[" p0T_C = ",MatrixForm[p
//.{t[1]→qfk[[1]],t[2]→qfk[[2]],t[3]→qfk[[3]],t[4]→qfk[[4]],t[5]→qf
k[[5]],t[6]→qfk[[6]],d[7]→qfk[[7]]}],"   R0T_C = ",MatrixForm[R
//.{t[1]→qfk[[1]],t[2]→qfk[[2]],t[3]→qfk[[3]],t[4]→qfk[[4]],t[5]→qf
k[[5]],t[6]→qfk[[6]],d[7]→qfk[[7]]}]];
Print[" pbT_C = ",MatrixForm[pb
//.{t[1]→qfk[[1]],t[2]→qfk[[2]],t[3]→qfk[[3]],t[4]→qfk[[4]],t[5]→qf
k[[5]],t[6]→qfk[[6]],d[7]→qfk[[7]]}],"   RrT_C = ",MatrixForm[Rr
//.{t[1]→qfk[[1]],t[2]→qfk[[2]],t[3]→qfk[[3]],t[4]→qfk[[4]],t[5]→qf
k[[5]],t[6]→qfk[[6]],d[7]→qfk[[7]]}]];
```

References

[1] Columbia Accident Investigation Board, *Columbia Accident Investigation Board Report* [online report], Vol. 1, August 2003, URL: http://www.caib.us/news/report/pdf/vol1/full/caib_report_volume1.pdf [cited 2 Sept. 2003].

[2] Hill, P. S., "Orbiter Inspection and Repair Summary [online presentation]," Introduction to Space Shuttle Return to Flight Planning Media Workshop, Johnson Space Center, Houston, TX, 16-18 September 2003, URL: http://spaceflight.nasa.gov/shuttle/rtf/hill/inspect_repair_sep9_summary_covey.ppt [cited 17 September 2003].

[3] National Aeronautics and Space Administration, *NASA's Implementation Plan for Space Shuttle Return to Flight and Beyond* [online report], Vol. 1, Rev. 2, 26 April 2004, URL: http://www.nasa.gov/pdf/58541main_RTF_rev2.pdf [cited 30 April 2004].

[4] National Aeronautics and Space Administration, *System Description and Design Data – Payload Deployment and Retrieval System*, NSTS 07700, Vol. XIV, Appendix 8, Rev. K, 2000.

[5] Bowden, M., "Deployment Devices," *Space Vehicle Mechanisms: Elements of Successful Design*, edited by P. L. Conley, John Wiley & Sons, New York, 1998. pp. 495-542.

[6] Pellegrino, S., "Deployable Structures in Engineering," *Deployable Structures*, edited by S. Pellegrino, Springer Wien New York, Itlay, 2001, pp. 1-35.

[7] Astro Aerospace, "Inflatable Sunshield in Space (ISIS) TELESCOPIC MAST™ [online datasheet]," URL: http://www.astro-aerospace.com/datasheets_papers/DS-410forweb.pdf [cited 28 October 2003].

[8] Astro Aerospace, "Telescopic Mast Model 7301 [online datasheet]," URL: http://www.astro-aerospace.com/datasheets_papers/DS-401forweb.pdf [cited 28 October 2003].

[9] Astro Aerospace, "Self-Deployed AstroMast® [online datasheet]," URL: http://www.astro-aerospace.com/datasheets_papers/DS-307forweb.pdf [cited 24 October 2003].

[10] Astro Aerospace, "Canister AstroMast® [online datasheet]," URL: http://www.astro-aerospace.com/datasheets_papers/DS-303forweb.pdf [cited 28 October 2003].

[11] AEC-ABLE Engineering Company, Inc., "Automatically Deployable: Able Booms," [technical brochure].

[12] AEC-ABLE Engineering Company, "ADAM Articulated Boom System [online datasheet]," URL: http://www.aec-able.com/Booms/adam.html [cited 5 November 2003].

[13] AEC-ABLE Engineering Company, "CoilABLE Booms: Heritage Linear Deployment Technology [online datasheet]," URL: http://www.aec-able.com/Booms/Resources/Coilable%20PDS.pdf [cited 5 November 2003].

[14] National Aeronautics and Space Administration, "Tubular Spacecraft Booms (Extendible, Reel Stored)," *NASA Space Vehicle Design Criteria (Guidance and Control)*, NASA SP-8065, 1971.

[15] Herbeck, L., Eiden, M., Leipold, M, Sickinger, C., and Unckenbold, W., "Deployment and Test of Deployable Ultra-Lightweight CFRP-Booms for a Solar Sail," *European Conference on Spacecraft Structures, Materials and Mechanical Testing*, ESTEC, Noordwijk, November 2000, URL: http://www.sm.bs.dlr.de/strukturtechnologie/Projekte/CFRP-Booms/pdf/ESTEC_00.pdf [cited 10 July 2003].

[16] Herbeck, L., Sickinger, C., Eiden, M., and Leipold, M, "Solar Sail Hardware Developments," *European Conference on Spacecraft Structures, Materials and Mechanical Testing*, Toulouse, France, 2002.

[17] Leipold, M., Eiden, M., Garner, C. E., Herbeck, L., Kassing, D., Niederstadt, T., Krüger, T., Pagel, G., Rezazad, M., Rozemeijer, H., Seboldt, W., Schöppinger, C., Sickinger, C., and Unckenbold, W., "Solar Sail Technology Development and Demonstration," In Jahrbuch 2000, Deutsche Gesellschaft für Luft- und Raumfahrt (DGLR), Leipzig, Sep. 2000, http://www.sm.bs.dlr.de/strukturtechnologie/Projekte/CFRP-Booms/pdf/DGLR_00%20Leipold%20et%20al.pdf [cited 10 July 2003].

[18] Sickinger, C., and Herbeck, L., "Deployment Strategies, Analysis and Tests for the CFRP Booms of a Solar Sail," *European Conference on Spacecraft Structures, Materials and Mechanical Testing, CNES*, Toulouse, France, December 2002.

[19] Aguirre-Martinez, M., Bowen, D. H., Davidson, R., Lee, R. J., and Thorpe, T., "The Development of a Continuous Manufacturing Method for a Deployable Satellite Mast in CFRP," *British Plastics Congress*, Sept. 1986, pp. 107-110.

[20] National Aeronautics and Space Administration, *Space Shuttle System Payload Accommodations*, NSTS 07700, Vol. XIV, Rev. L, 2001.

[21] National Aeronautics and Space Administration, *System Description and Design Data – Contamination Environment*, NSTS 07700, Vol. XIV, Appendix 1, Rev. L, 2000.

[22] National Aeronautics and Space Administration, *System Description and Design Data – Thermal*, NSTS 07700, Vol. XIV, Appendix 2, Rev. K, 2000.

[23] National Aeronautics and Space Administration, *System Description and Design Data – Electrical Power and Avionics*, NSTS 07700, Vol. XIV, Appendix 3, Rev. L, 2001.

[24] National Aeronautics and Space Administration, *System Description and Design Data – Ground Operations*, NSTS 07700, Vol. XIV, Appendix 5, Rev. L, 2002.

[25] National Aeronautics and Space Administration, *System Description and Design Data – Mission Planning and Flight Design*, NSTS 07700, Vol. XIV, Appendix 6, Rev. K, 2001.

[26] National Aeronautics and Space Administration, *System Description and Design Data – Extravehicular Activities*, NSTS 07700, Vol. XIV, Appendix 7 (Formerly JSC 10615), Rev. K, 2000.

[27] National Aeronautics and Space Administration, *System Description and Design Data – Intravehicular Activities*, NSTS 07700, Vol. XIV, Appendix 9, Rev. L, 2003.

[28] National Aeronautics and Space Administration, Space Shuttle Program Office, *Shuttle/Payload Standard Integration Plan for Deployable/Retrievable-Type Payloads*, NSTS 21000-SIP-DRP, Rev. D, 2002.

[29] National Aeronautics and Space Administration, *System Description and Design Data – Structures and Mechanics*, NSTS 07700, Vol. XIV, Appendix 4, Rev. L, 2001.

[30] National Aeronautics and Space Administration, *Space Shuttle Program Payload Bay Payload User's Guide: Basic*, NSTS 21492, 2000.

[31] National Aeronautics and Space Administration, *Guidelines for the Preparation of Payload Flight Safety Data Packages and Hazard Reports for Payloads Using the Space Shuttle*, JSC 26943, 1995.

[32] National Aeronautics and Space Administration, *Interpretations of NSTS/ISS Payload Safety Requirements*, NSTS/ISS 18798, Rev. B, 1997.

[33] National Aeronautics and Space Administration, *Shuttle Orbiter Failure Modes and Fault Tolerances for Interface Services*, NSTS 16979, Part I, Rev. C, 1991.

[34] National Aeronautics and Space Administration, *Safety Policy and Requirements for Payloads Using the Space Transportation System*, NSTS 1700.7B, 1989.

[35] DeVault, G. M., Smith, W. K., Harris, B. P., Rotter, H. A., Serna, R., Miller, C. R., and Gurevich, G. E., "Space Shuttle Integration," *Spacecraft Thermal Control Handbook – Volume 1: Fundamental Technologies*, edited by D. G. Gilmore, The Aerospace Press, El Segundo, CA, 2002.

[36] MD Robotics, "The Shuttle Remote Manipulator System – The Canadarm" [online data sheet], URL: http://ewh.ieee.org/reg/7/millennium/canadarm/canadarm_technical.html [cited 28 October 2003].

[37] Marchel, O., "Space qualification program for CFRP-prepregs used for design of deployable booms as a main structural part of a Solar Sail," AMTT European Major Research Infrastructure Contract No. HPRI-CT-1999-00024, AMTT-User II-23.

[38] Craig, J. J., *Introduction to Robotics: Mechanics and Control*, 2nd ed., Addison-Wesley, Reading, MA, 1989, pp. 76-77.

[39] Sciavicco, L. and Siciliano, B., *Modelling and Control of Robot Manipulators*, 2nd ed., Springer-Verlag, London, 2000.

[40] Shahinpoor, M., *A Robot Engineering Textbook*, Harper & Row, New York, 1987.

[41] Murray, R. N., Li, Z., and Sastry, S. S., *A Mathematical Introduction to Robotic Manipulation*, CRC Press, Boca Raton, 1994.

[42] National Aeronautics and Space Administration, "Space Shuttle Coordinate System," *NSTS 1988 News Reference Manual* [online reference], URL: http://science.ksc.nasa.gov/shuttle/technology/sts-newsref/sts_coord.html [cited 5 November 2003].

[43] Modarres, M., Kaminskiy, M., and Krivtsov, V., *Reliability Engineering and Risk Analysis: A Practical Guide*, Marcel Dekker, New York, 1999.

[44] Davion Systems, "Risk Management," *Risk Information and Assessment System*, URL: http://www.davion.com/services/risk_management.html [cited 7 June 2004].

[45] YLA, Inc. Advanced Composite Materials, "T300(1K)/RS-3 Plain Weave Fabric Laminate Physical and Ambient Mechanical Properties," *RS-3: 350°F Service, Toughened Polycyanate Resin*, Product Bulletin, PBR03-01whf, 2000.

[46] YLA, Inc. Advanced Composite Materials, *RS-3: 350°F Service, Toughened Polycyanate Resin*, Technical Bulletin, TBR03-00whf, 2000.

[47] Karnovsky, I. A and Lebed, O. I., *Formulas for Structural Dynamics: Tables, Graphs and Solutions*, McGraw-Hill, New York, 2001.

[48] Young, W. C., *Roark's Formulas for Stress and Strain*, 6th ed. McGraw-Hill, New York, 1989, pp. 714-715.

[49] ADMC, "Aerospace—degradation and failure mechanisms," URL: http://www.admc.aeat.co.uk/CDKB/Sectors/Aerospace/InService.asp [cited 8 June 2004].

[50] Mallick, P. K, *Fiber-Reinforced Composites*, 2nd ed., Marcel Dekker, New York, 1993, pp. 3-4.

[51] Fanucci, J. P., Gorman, J. J., and Nykvist, W., "Pultrusion Technology: Large Composites Structures are Appearing on the Horizon," *SAMPE Journal*, Vol. 37, No. 1, 2001, pp. 18-24.

[52] Iqbal, K., and Pellegrino, S., "Bi-Stable Composite Shells," AIAA 2000-1385.

[53] Pellegrino, S., "Bi-Stable Structures," *Deployable Structures*, edited by S. Pellegrino, Springer Wien New York, Itlay, 2001, pp. 99-111.

[54] Pellegrino, S., "Elastic Folding of Shell Structures," *Deployable Structures*, edited by S. Pellegrino, Springer Wien New York, Itlay, 2001, pp. 77-98.

[55] ADMC, "Design Approach – Aerospace Industry," URL: http://www.admc.aeat.co.uk/CDKB/Sectors/Aerospace/Approach.asp [cited 8 June 2004].

[56] Bickler, D., "Quasi-Fractal Lenticular Booms," *NASA Tech Briefs*, NPO-20815, URL: http://www.nasatech.com/Briefs/Aug01/NPO20815.html [cited 20 June 2003].

[57] Composite Technology Development, "Elastic Memory Composite (EMC) Material," *Products* [online description], URL: http://www.ctd-materials.com/products/emc.htm [cited 15 October 2003].

[58] Fortescue, P., Stark, J., and Swinerd, G. (eds.), *Spacecraft Systems Engineering*, 3rd ed., Wiley, UK, 2003.

[59] Gilmore, D. G. (ed.), *Spacecraft Thermal Control Handbook, Volume I: Fundamental Technologies*, 2nd ed., Aerospace Press, El Segundo, CA, 2002.

[60] Hazelton, C. S., Gall, K. R., Abrahamson, E. R., Denis, R. J., and Lake, M. S., "Development of a Prototype Elastic Memory Composite STEM for Large

Space Structures," AIAA 2003-1977, *44th Structures, Structural Dynamics, and Materials Conference*, 7-10 April 2003, Norfolk, VA.

[61] Hecht, H., *Systems Reliability and Failure Prevention*, Artech House, Boston, 2004.

[62] Hibbeler, R. C., *Mechanics of Materials*, 4th ed., Prentice Hall, Upper Saddle River, NJ, 2000.

[63] Hyer, M. W., *Stress Analysis of Fiber-Reinforced Composite Materials*, WCB McGraw-Hill, Boston, 1998.

[64] MD Robotics, "Description of the Shuttle Remote Manipulator System," URL: http://www.mdrobotics.ca/descrms.htm [cited 5 December 2003].

[65] Morris, W. D., and White, N. H., "Analysis of Shuttle Orbiter Reliability and Maintainability Data for Conceptual Studies," *AIAA*, 1996.

[66] National Aeronautics and Space Administration, "Space Shuttle Orbiter Systems: Thermal Protection System," *NSTS 1988 News Reference Manual* [online reference], URL: http://science.ksc.nasa.gov/shuttle/technology/sts-newsref/sts_sys.html [cited 2 December 2003].

[67] Paté-Cornell, M. E., and Fischbeck, P. S., "Risk Management for the Tiles of the Space Shuttle," *Interfaces*, Vol. 24, No. 1, 1994, pp. 64-86.

[68] Pilkey, Walter D., *Mechanics of Structures: Variational and Computational Methods*, CRC Press, Boca Raton, 1994.

[69] Umland, J. W., and Eisen, H., "SRTM On-Orbit Structural Dynamics," *42nd AIAA/ASME/ASCE/AHS/ASC Structures, Structural Dynamics, and Materials Conference and Exhibit*, 16-19 April 2001, Seattle, WA, AIAA 2001-1588, pp.1-11.